

## Pharmacological and Cell-Specific Genetic PI3K $\alpha$ Inhibition Worsens Cardiac Remodeling After Myocardial Infarction

Xueyi Chen<sup>1,3</sup>, Pavel Zhabyeyev<sup>1,3</sup>, Abul K. Azad<sup>1</sup>, Bart Vanhaesebroeck<sup>4</sup>,  
Chad E. Grueter<sup>5</sup>, Allan G. Murray<sup>1</sup>, Zamaneh Kassiri<sup>2,3</sup>,  
and Gavin Y. Oudit<sup>1,3,\*</sup>

<sup>1</sup>Department of Medicine, <sup>2</sup>Department of Physiology, <sup>3</sup>Mazankowski Alberta Heart Institute, University of Alberta, Edmonton, Canada; <sup>4</sup>Cancer Institute, University College London, London, UK. <sup>5</sup>Division of Cardiovascular Medicine, Department of Internal Medicine, Francois M. Abboud Cardiovascular Research Center, Fraternal Order of Eagles Diabetes Research Center, University of Iowa, Iowa City, IA, USA.

**Running title:** PI3K $\alpha$  inhibition worsens heart disease

**\*Corresponding Author:** Gavin Y. Oudit, MD, PhD, FRCP(C), Division of Cardiology, Department of Medicine, Mazankowski Alberta Heart Institute, University of Alberta, Edmonton, Alberta, T6G 2R3, Canada; Phone: (780)-407-8569, Fax: (780)-492-9753. Email: gavin.oudit@ualberta.ca.

**Category:** Research Article

**Word Count:** 9157 words; 8 Figures, 4 Supplemental Tables, and 7 Supplemental Figures.

## **Abstract**

**Background:** PI3K $\alpha$  (Phosphoinositide 3-kinase  $\alpha$ ) regulates multiple downstream signaling pathways controlling cell survival, growth, and proliferation and is an attractive therapeutic target in cancer and obesity. The clinically-approved PI3K $\alpha$  inhibitor, BYL719, is in further clinical trials for cancer and overgrowth syndrome. However, the potential impact of PI3K $\alpha$  inhibition on the heart and following myocardial infarction (MI) is unclear. We aim to determine whether PI3K $\alpha$  inhibition affects cardiac physiology and post-MI remodeling and to elucidate the underlying molecular mechanisms.

**Methods and Results:** Wildtype (WT) 12-wk old male mice receiving BYL719 (daily, p.o.) for 10 days showed reduction in left ventricular longitudinal strain with normal ejection fraction, weight loss, mild cardiac atrophy, body composition alteration, and prolonged QT<sub>C</sub> interval. RNASeq analysis showed gene expression changes in multiple pathways including extracellular matrix remodeling and signaling complexes. After MI, both p110 $\alpha$  and phospho-Akt protein levels were increased in human and mouse hearts. Pharmacological PI3K $\alpha$  inhibition aggravated cardiac dysfunction and resulted in adverse post-MI remodeling, with increased apoptosis, elevated inflammation, suppressed hypertrophy, decreased coronary blood vessel density, and inhibited Akt/GSK3 $\beta$ /eNOS signaling. Selective genetic ablation of PI3K $\alpha$  in endothelial cells was associated with worsened post-MI cardiac function and reduced coronary blood vessel density. *In vitro*, BYL719 suppressed Akt/eNOS activation, cell viability, proliferation, and angiogenic sprouting in coronary and human umbilical vein endothelial cells. Cardiomyocyte-specific genetic PI3K $\alpha$  ablation resulted in mild cardiac systolic dysfunction at baseline. After MI, cardiac function markedly deteriorated with increased mortality concordant with greater

apoptosis and reduced hypertrophy. In isolated adult mouse cardiomyocytes, BYL719 decreased hypoxia-associated activation of Akt/GSK3 $\beta$  signaling and cell survival.

**Conclusions:** PI3K $\alpha$  is required for cell survival (endothelial cells and cardiomyocytes) hypertrophic response, and angiogenesis to maintain cardiac function after MI. Therefore, PI3K $\alpha$  inhibition that is used as anti-cancer treatment, can be cardiotoxic, especially after MI.

**Keywords:** angiogenesis / myocardial infarction / myocardial remodeling / signaling / PI3K $\alpha$

## 1. Introduction

The phosphoinositide 3-kinases (PI3Ks) are a family of conserved lipid kinases that regulate critical intracellular signaling responsible for hypertrophy, survival, proliferation, and metabolism [1, 2]. PI3K $\alpha$  is the functionally dominant PI3K isoform in many cell types and a key regulator in a wide range of cellular processes. The catalytic conversion of phosphatidylinositol-3,4-bisphosphate (PtdIns(3,4)P<sub>2</sub> or PIP<sub>2</sub>) to phosphatidylinositol-3,4,5-trisphosphate (PtdIns(3,4,5)P<sub>3</sub> or PIP<sub>3</sub>) leads to membrane recruitment of Akt, allowing the phosphorylation of an effector kinase, Akt, at Thr308 by PDK1. Subsequently, Akt phosphorylates downstream effectors and regulates various pathways, including glycogen synthase kinase 3 $\beta$  (GSK3 $\beta$ ) and endothelial nitric oxide synthase (eNOS). PI3K $\alpha$  signaling mediates cell survival, growth, electrophysiology and metabolism in different cell types [3-6].

Due to the widespread expression and diverse roles of PI3K $\alpha$ , the aberrations in PI3K $\alpha$  signaling are associated with a broad spectrum of human diseases including cancer. Gain-of-function mutations of *PIK3CA*, the gene that encodes the p110 $\alpha$  (catalytic subunit of PI3K $\alpha$ ), are frequent in many human tumors such as lung, head and neck, breast, endometrial, and cervical cancer [7]. In addition, disruptions of PI3K $\alpha$  signaling contribute to obesity, diabetes, and heart failure [8-10]. Currently, several PI3K $\alpha$  inhibitors are in clinical trials as cancer treatment [11]. One of them, BYL719 (Alpelisib), has demonstrated dose- and time-dependent PI3K $\alpha$  inhibition in both animal and human studies [12-15] and is therapeutic in *PIK3CA*-related solid tumors and overgrowth syndrome in recent clinical trials [14-16].

Heart disease is the leading cause of death followed by cancer [17] and both are frequently present in the same patient. Following myocardial infarction (MI), cardiac repair and remodeling, which are the result of complex interactions of cardiomyocytes and vascular endothelial cells, define cardiac recovery and patient outcomes [18]. We and others have identified PI3K $\alpha$  as a regulator of physiological hypertrophy, insulin signaling, ion channel activity, and contractility in cardiomyocytes [4, 19-21] while maintaining vascular function and tone [2, 3]. However, cell-specific role of PI3K $\alpha$  on post-MI cardiac remodeling has not been elucidated and the increased use of PI3K $\alpha$  inhibitors in clinical practice as novel cancer therapies may result in cardiotoxicity due to inhibition of PI3K $\alpha$  in both cardiomyocytes and endothelial cells [22, 23]. Indeed, very little is known about the potential cardiotoxicity with PI3K $\alpha$  inhibition.

In the present study, we showed that BYL719 administration in mice is associated with reduced global left ventricular longitudinal strain, prolonged QT interval, and altered gene expression profile. In mice receiving BYL719, post-MI vascular density was reduced, hypertrophy was suppressed, and myocardial apoptosis was increased. We also examined cell-specific effects of the loss of PI3K $\alpha$  activity in post-MI cardiac remodeling by studying post-MI remodeling in endothelial-specific (p110 $\alpha^{EC}$ ) and cardiomyocyte-specific (p110 $\alpha^{CM}$ ) PI3K $\alpha$  knockouts. We found that in endothelial cells, PI3K $\alpha$  controls endothelial survival, proliferation, and angiogenesis, while in adult cardiomyocytes, PI3K $\alpha$  is important for cell survival. Our study highlights the potential cardio-oncology issues associated with this new class of cancer therapy.

## 2. Methods

Detailed methods used in the present study and all other supporting data are available in the Data Supplement.

### 2.1 Animal Models

All animal studies were conducted according to the Canadian Council for Animal Care guidelines and approved by Animal Care and Use Committee at University of Alberta. Wild type (WT) C57BL/6 mice were purchased from Jackson Laboratory. BYL719 (50 mg/Kg/day, *p.o.*, Chemietek) or vehicle was given to 11- to 12-week-old WT mice in the morning for 10 days. Inducible endothelial-specific PI3K $\alpha$ -knockout mice (p110 $\alpha$ <sup>EC</sup>) were generated by crossing p110 $\alpha$ <sup>flx/flx</sup> mice (*PIK3CA* gene with floxed 18 and 19 exons) [3] with tamoxifen-induced and Tie2 promoter-controlled Cre expression mice (Tie2-MerCreMer). Tamoxifen (80 mg/kg/day, Sigma-Aldrich) was given to 10-week-old mice by intraperitoneal injection for 5 days to induce endothelial-specific, floxed-exon deletion in p110 $\alpha$ ; this method has been previously shown to spare hematopoietic cells from targeted gene deletion [24, 25]. Cardiomyocyte-specific PI3K $\alpha$ -knockout mice (p110 $\alpha$ <sup>CM</sup>) were generated by crossing p110 $\alpha$ <sup>flx/flx</sup> with  $\alpha$ MHC-driven Cre expressing mice [4]. Homozygous littermates (p110 $\alpha$ <sup>flx/flx</sup>) of p110 $\alpha$ <sup>EC</sup> and p110 $\alpha$ <sup>CM</sup> mice were used as control. All mice were on the C57BL/6 background. Only male mice were used in the experiments.

The pharmacological inhibition of PI3K $\alpha$  was achieved by gavage with BYL719 (50 mg/kg by) daily for 10 days (Figure 1A). The dosing was based on studies that confirmed the therapeutic effects on PI3K $\alpha$ -driven tumors in mice (osteosarcoma, lung cancer, and squamous cell carcinomas).[26-28] Blood glucose measured after overnight fasting

without glucose challenge. Myocardial infarction was achieved by permanently ligating the proximal left anterior descending artery (LAD) of 12-week-old mice after they received 3 doses of BYL719 [29]. Surgery was performed by a technician who was blinded to the mouse strains and treatment. Tissue collection was performed on mice anesthetized with ketamine (100 mg/kg) and xylazine (10 mg/kg).

## **2.2 Human Explanted Hearts**

Human cardiac specimens from non-failing control (NFC) and failing post-MI hearts were obtained as part of the Human Organ Procurement and Exchange program (HOPE) and Human Explanted Heart Program (HELP) respectively, approved by the Mazankowski Alberta Heart Institute and the Institutional Ethics Committee at University of Alberta [30].

## **2.3 Body Composition Measurement, Echocardiography and Electrocardiogram**

Body composition was measured in live, conscious mice using a NMR-MRI scanner (EchoMRI) [31]. Non-invasive transthoracic echocardiography was performed on mice anesthetized with 1.5% isoflurane using Vevo 3100 (Visualsonics). Conventional measurements and speckle-tracking strain analysis was carried out as previously described including the fractional area change (FAC) as a measure of RV systolic function [25]. Non-invasive electrocardiogram in lead I configuration was carried out as described [20, 25].

## **2.4 Endothelial Cell Culture, Flow Cytometry, and Bead Angiogenesis Assay**

Human umbilical vein endothelial cells (HUVEC) and human coronary artery endothelial cells (HCAEC, ATCC) were used between passage 3 to 7. BYL719 was used at indicated doses. Recombinant human vascular endothelial growth factor (VEGF<sub>165</sub>, PeproTech) was added to stimulate endothelial cell responses at 50 ng/ml. Cell survival was examined on overnight vehicle- or BYL719-treated cell using flow cytometry (Attune NxT, Invitrogen) with annexin V and propidium iodide staining (Invitrogen). *In vitro* 3 dimensional (3D spheroid) angiogenesis assays were performed on HUVEC and HCAEC as previously described [25].

## **2.5 Adult Murine Cardiomyocyte Isolation, Culture, and Stretching**

Adult murine ventricular cardiomyocytes were isolated from 2% isoflurane anesthetized mice. Plated cardiomyocytes were cultured with vehicle, BYL719, or PI3K $\gamma$  inhibitor-AS252424 for 1 hour under normoxia (20% O<sub>2</sub>, 2% CO<sub>2</sub>) or hypoxia (1% O<sub>2</sub>, 2% CO<sub>2</sub>) before protein collection. Cyclical mechanical stretch of cardiomyocytes was achieved using Flexcell FX-5000 Tension System (Flexcell International Corp) at 1 Hz and 5% elongation for 3 hours in serum-free culture medium under hypoxic atmosphere [25]. Then, cells were collected for morphologic study.

## **2.6 Immunofluorescence and Immunoblotting**

Immunofluorescence staining was performed using established protocols [25]. Antibodies against CD31, Ly6B, CD68, Ki67, and BrdU were used. Intravital perfusion with fluorescein-conjugated lectin (Vectorlabs) was performed to identify the functional



vasculature. Wheat Germ Agglutinin (WGA) or phalloidin staining was performed to identify cardiomyocytes. Fragmented DNA of apoptotic cells was detected using the DeadEnd Fluorometric Terminal Deoxynucleotidyl Transferase-mediated dUTP Nick-End Labeling (TUNEL) System. Immunoblotting for various proteins was performed on left ventricular homogenates or cultured cell lysates as before [24, 25].

## 2.7 RNA Sequencing Analysis

RNA isolation and RNA sequencing were performed as previously described.[32] Total RNAs from left ventricles (6 hearts/group) were extracted. Altered genes were defined by the boundary conditions:  $p_{adj} < 0.1$  and expression level of at least 750 TPM (transcripts per million) for either WT-vehicle or WT-BYL group (750 is 1% of 75,000 TPM, which was a maximal expression level in the dataset). Data were analyzed using WebGestalt, Protein ANalysis THrough Evolutionary Relationships (PANTHER) classification system (Pantherdb.org), and Ingenuity Pathway Analysis.

## 2.8 Statistical Analysis

Statistical analyses were carried out using SPSS Statistics 24 software, and statistical significance was defined as  $p < 0.05$  (two-sided). Continuous data were presented in scatter plots with mean  $\pm$  SEM. The differences between the two independent groups were evaluated using independent t-test or Mann-Whitney U test after normality examination. Paired t-test was carried out for two paired groups. One-way ANOVA or Kruskal-Wallis test with pairwise comparisons was used in studies with more than two groups based on the normality of the data. Two-way ANOVA was used to compare the

differences between groups with two independent variables. Repeated measures ANOVA was carried out in data with multiple measures. Categorical data were compared using Fisher exact test. Survival data were presented as the Kaplan-Meier plots, and the log-rank test was used to evaluate the statistical significance.

### **3. Results**

#### **3.1 Inhibition of PI3K $\alpha$ with BYL719 results in adverse systemic changes and altered myocardial gene expression**

BYL719 resulted in weight loss, leading to a decrease in body weight, and transiently increased blood glucose, but not fasting glucose (Figure 1A-1C). The mice displayed an increase in fat mass with a corresponding decrease in lean mass over the 10-day treatment period, associated with reduced heart and left ventricular weight (Figure 1D and 1E). Despite the preserved ejection fraction in BYL719-treated mice, stroke volume and global longitudinal strain were reduced (Table S1 and Figure 1F). The QT<sub>c</sub> interval was prolonged without alterations in the heart rate, PR interval, or QRS duration (Figure 1G and Figure S1).

To investigate the effect of pharmacological inhibition of PI3K $\alpha$  at the molecular level in the heart, we performed gene profiling of the LV tissue from mice treated with placebo or BYL719 (Data Supplement Bulk-RNAseq). A total of 292 genes were changed after BYL719 exposure, with log<sub>2</sub> FC (Fold Change) for the most genes in the approximate range of -2 to 2 (Figure 1H; heatmap of the most changed genes, Figure S2A; list of top 10 affected genes, Table S1; principle component analysis plot, Figure S3). Gene set enrichment analysis showed multiple changes in categories of biological regulation,

metabolic processes, response to stimulus (Figure S2B); membrane and nucleus, protein-containing complex, (Figure S2C); protein binding, ion binding, and nucleotide binding (Figure S2D). Kyoto Encyclopedia of Genes and Genomes (KEGG) pathway analysis showed downregulation of pathways related to structural integrity (extracellular matrix (ECM)-receptor interaction, focal adhesion) metabolism of glucose and proteins (protein digestion and absorption, AGE-RAGE signaling), and electrical activity (Figure 1I) and upregulation of metabolic pathways responsible for degradation of ketones, fatty acids, and several amino acids (Figure 1J). Taken together, these results demonstrate that PI3K $\alpha$  inhibition with BYL719 results in mild adverse systemic effects, altered myocardial gene expression and early cardiac dysfunction.

### **3.2 PI3K $\alpha$ in human and murine post MI hearts**

Left ventricular specimens from post-MI patients showed markedly increased levels of p110 $\alpha$ , the catalytic subunit of PI3K $\alpha$ , in the infarct and peri-infarct regions. This increase correlated with enhanced Akt phosphorylation in these regions compared with non-failing human hearts (Figure 2A). We observed similar changes in PI3K $\alpha$ /Akt signaling in post-MI murine hearts (Figure 2A) showing a conserved response in humans and mice. These changes suggest that the PI3K $\alpha$  pathway is upregulated in response to MI and may have an adaptive role. To investigate this possibility, we induced MI by LAD ligation in mice treated with either vehicle or BYL719 (Figure 2B). BYL719 treatment decreased post-MI survival due to increase in non-rupture related deaths (Figure 2C). Echocardiographic analyses showed exacerbation of systolic dysfunction in BYL719 versus vehicle-treated post-MI mice, characterized by decreased ejection fraction, enlarged left ventricular

chamber, and worsened wall motion index (Figure 2D and Table S2). Interestingly, right ventricular fractional area change, a measure of RV systolic function, was also further compromised in the post-MI setting in response to BYL719 (Figure 2D and Table S2).

Because myocardial apoptosis determines the severity of myocardial ischemic injury, we evaluated apoptosis using TUNEL staining. One-day post-MI, BYL719-treatment increased myocardial apoptosis and elevated inflammatory cell infiltration compared with vehicle-treated controls (Figure 3A and 3B). In addition, BYL719 treatment suppressed post-MI cardiomyocyte hypertrophy and reduced coronary vascular density in the peri-infarct area without affecting cardiomyocyte size or vascular density of sham-operated groups (Figure 3C and 3D). Phosphorylation of myocardial Akt (Thr308), GSK3 $\beta$  (Ser9), and eNOS (Ser1177) were reduced in BYL719-treated mice in comparison with vehicle-treated day 7 post-MI (Figure 3E), but levels of p110 $\alpha$ , phospho-Akt at Ser473, and phospho-ERK were not altered (Figure S4). These results indicate that systemic PI3K $\alpha$  inhibition is detrimental in the post-MI setting by curtailing protective signaling pathways, resulting in increased apoptosis, impaired hypertrophy, and reduced vascular density.

### 3.3 Endothelial-specific PI3K $\alpha$ Ablation Worsens Post-MI Remodeling

We next examined the cell-specific role of PI3K $\alpha$  signaling in endothelial cells and cardiomyocytes in myocardial ischemic injury. We used mice with endothelial-specific PI3K $\alpha$  ablation (p110 $\alpha$ <sup>EC</sup>) (Figure 4A) [25, 33, 34]. Successful ablation in endothelial cells was confirmed by the presence of truncated *PIK3CA* in the DNA extracted from lungs of p110 $\alpha$ <sup>EC</sup> mice (Figure S5A). Mice with endothelial-PI3K $\alpha$  ablation showed comparable

body weight, heart weight, and myocardial levels of p110 $\alpha$ , phospho-Akt, and phospho-eNOS compared to p110 $\alpha^{\text{flx/flx}}$  littermate controls at baseline (Figure S5B-C). Systolic function and global longitudinal strain were similar in p110 $\alpha^{\text{EC}}$  and p110 $\alpha^{\text{flx/flx}}$  hearts (Figure 4B, Figure S5D, and Table S3).

Following MI, deterioration in systolic function worsened at 7-day and 4-week post-MI in p110 $\alpha^{\text{EC}}$  hearts compared with sham; however, post-MI survival was similar (Figure 4B, Figure S5E-F, and Table S3). Inflammatory cell infiltration was increased post-MI in p110 $\alpha^{\text{EC}}$  hearts compared with controls (Figure S5G) without altering the increase in cardiomyocyte size post-MI (Figure S5H). Since endothelial survival and angiogenesis is critical in post-infarct recovery, and PI3K $\alpha$  is highly expressed in endothelial cells, we performed immunostaining to examine apoptosis, proliferation, and vascular density. We detected a higher number of apoptotic endothelial cells at day 1, decreased number of proliferating endothelial cells at day 3, lower vascular density, and reduced functional vasculature at day 7 post-MI in p110 $\alpha^{\text{EC}}$  mice (Figure 4C-4E). Whole-heart phospho-Akt levels were lower post-MI in p110 $\alpha^{\text{EC}}$  hearts (Figure 4F). These results indicate that endothelial PI3K $\alpha$  is required in the infarct and peri-infarct regions of the heart to maintain cardiac function by supporting endothelial survival, proliferation, and angiogenesis.

### 3.4 Inhibition of PI3K $\alpha$ Impairs Angiogenesis

To further delineate the impact of PI3K $\alpha$  inhibition on endothelial cells, we examined the effects of BYL719 on human umbilical vein endothelial cells (HUVEC), commonly used primary endothelial cells, and human coronary artery endothelial cells (HCAEC), human coronary primary endothelial cells. We first tested the effect of BYL719 on primary

endothelial cells in response to VEGF. BYL719 concentration range 10-500 nmol/L was selected because 500 nmol/L is the lowest concentration in the plasma of patients with continuous BYL719 treatment [14]. In HUVEC without VEGF stimulation, BYL719 suppressed Akt activity without affecting phospho-eNOS or p110 $\alpha$  protein levels (Figure 5A) while VEGF-induced Akt phosphorylation decreased in response to BYL719 treatment in a dose-dependent manner (Figure 5B). Meanwhile, VEGF-induced eNOS phosphorylation was only partially suppressed by 500 nmol/L BYL719 (Figure 5B). In HCAEC and in the absence of VEGF, 100 nmol/L and 500 nmol/L exerted a small inhibition of Akt/eNOS signaling (Figure 5C) while in response to VEGF stimulation, BYL719 at 100 nmol/L and 500 nmol/L abolished VEGF-induced Akt activation, with partial inhibitory effect on eNOS phosphorylation (Figure 5D).

BYL719 inhibition in HUVEC decreased the number of viable cells, increased apoptosis, and reduced proliferation (Figure 6A and 6B). The majority of HUVEC underwent cell death through apoptosis, not necrosis. BYL719 treatment reduced angiogenic sprouting illustrated by reduced number of sprouts and cumulative sprout length (Figure 6C). In HCAEC, both 100 nmol/L and 500 nmol/L BYL719 decreased cell viability, increased apoptosis, and decreased cell proliferation (Figure 6D and 6E) with survival analyses of HCAECs showing cell death patterns similar to HUVEC. Angiogenic sprouting (number of sprouts and cumulative sprout length) was inhibited by BYL719 (Figure 6F) in HCAEC. Collectively, these results suggest that endothelial PI3K $\alpha$  activity is required to maintain Akt/eNOS signaling in ECs, survival, proliferation, and angiogenesis.

### 3.5 Cardiomyocyte PI3K $\alpha$ Protects Against Ischemic Injury by Inhibiting Apoptosis and Supporting Hypertrophy

We next investigated the role of PI3K $\alpha$  in the cardiomyocytes during MI was investigated using mice with cardiomyocyte-specific p110 $\alpha$  ablation (p110 $\alpha^{\text{CM}}$ ) (Figure S6A). The p110 $\alpha^{\text{CM}}$  mice express truncated *PIK3CA* gene (Figure S6B). These mice had unchanged body weight and displayed reduced heart weight and left ventricular weight compared to p110 $\alpha^{\text{flx/flx}}$  littermates (Figure 7A), similar to the findings from BYL719-treated WT mice. p110 $\alpha^{\text{CM}}$  hearts showed marked reduction in p110 $\alpha$  and basal phospho-GSK3 $\beta$  levels without differences in basal phospho-Akt level (Figure S6C). Cardiomyocyte-specific PI3K $\alpha$  deficiency exacerbated post-MI systolic dysfunction, enlargement of the left ventricle, and increased mortality due to cardiac rupture (Figure 7B, 7C, and Table S4). Although p110 $\alpha^{\text{CM}}$  hearts showed no apoptosis at baseline, the number of apoptotic cells detected in p110 $\alpha^{\text{CM}}$  hearts at day 1 post-MI was considerably larger than in p110 $\alpha^{\text{flx/flx}}$  (Figure 7D). p110 $\alpha^{\text{CM}}$  hearts also displayed an increase in inflammatory responses after MI as shown by increased infiltration by neutrophils and macrophages (Figure S6D). Post-MI myocardial hypertrophy and vascular density in the non-infarct area was compromised in p110 $\alpha^{\text{CM}}$  hearts (Figure 7E and Figure S6E). Furthermore, Akt phosphorylation was lower in p110 $\alpha^{\text{CM}}$  hearts after MI (Figure 7F). These results suggest that (i) under normal physiological conditions, cardiomyocyte PI3K $\alpha$  plays a role in maintaining normal cardiac function and (ii) in the post-MI setting, cardiomyocyte PI3K $\alpha$  controls cell survival and hypertrophy.

To elucidate acute effects of the PI3K $\alpha$  activity on cardiomyocyte survival, adult mouse cardiomyocytes were isolated from WT mice, and treated with BYL719 in normoxic

and hypoxic conditions. While BYL719 had no effect on Akt activity under normoxic condition, it inhibited hypoxia-induced Akt activation and GSK3 $\beta$  phosphorylation in a dose-dependent manner (Figure 8A). This effect could not be attributed to potential role of PI3K $\gamma$  since using AS252424, a specific inhibitor of PI3K $\gamma$ , caused further inhibition of Akt phosphorylation without a differential effect on GSK3 $\beta$  phosphorylation (Figure S7). These results confirm that lowered GSK3 $\beta$  phosphorylation in the p110 $\alpha^{\text{CM}}$  hearts and in cells treated with BYL719 is directly link to decrease in PI3K $\alpha$  signaling. Subjecting cultured isolated cardiomyocytes to 3-hr mechanical stretching under hypoxia to simulate *in vivo* conditions revealed increased cardiomyocyte apoptosis (Figure 8B). BYL719 treatment also blunted the hypoxia-triggered increase in F/G-actin ratio (Figure 8C), a key control mechanism for PI3K $\alpha$  [9], rendering cells more vulnerable to biomechanical stress. Taken together, PI3K $\alpha$  activity plays a role in post-MI hypertrophy, cytoskeletal response to biomechanical stress, and cell survival by protecting against hypoxia-induced apoptosis.

#### **4. Discussion**

Cardiovascular disease (CVD) and cancer are the two leading causes of death worldwide [35, 36] and are closely linked illustrated by cancer patients having a higher incidence of ischemic heart disease, and vice versa [37, 38], which has been attributed to shared risk factors and, importantly, the consequence of cancer therapy having detrimental effects on the cardiovascular system [22, 23, 39, 40]. Since PI3K $\alpha$  is emerging as a major target for cancer therapies [12-16], knowledge of PI3K $\alpha$  function in healthy and post-MI hearts is critical for optimization of treatment of ischemic heart disease and cancer care.



Activation of the PI3K $\alpha$ /Akt signaling pathway contributes to cancer development and progression as PI3K $\alpha$  activity is frequently activated in a variety of common human tumors [7]. Use of PI3K $\alpha$ -specific inhibitors, such as alpelisib (BYL719) and serabelisib, has achieved initial success on advanced solid tumors especially in combination with standard anti-cancer therapy [14, 15, 41, 42]. The major toxic effects of PI3K $\alpha$  inhibitors reported in clinical trials are hyperglycemia, cutaneous reactions, and gastrointestinal discomfort [43]. In this study, we used the dose of 50 mg/kg because it produces robust anti-tumor response in mouse models [12, 26-28] comparable to the antitumor effects and burden of hyperglycemia seen in humans [14, 44]. In our study, we found that BYL719 also leads to transient hyperglycemia associated with lean mass reduction and fat mass increase, which are associated with poor outcomes in CVD [31, 45]. Treatment with BYL719 also resulted in reduced cardiac size, prolonged QT<sub>c</sub> interval, and compromised LV global longitudinal strain. Both prolonged QT<sub>c</sub> interval and lower global longitudinal strain have been associated with a higher risk of cardiovascular morbidity and mortality in patients [46, 47]. BYL719-mediated prolongation of QT<sub>c</sub> interval is due to the inhibition of the late sodium current in cardiomyocytes, which increases the risk of ventricular arrhythmias [11, 20]. BYL719 also resulted in transcriptome changes in the heart characterized by (i) disruptions in pathways responsible for metabolism of glucose, fatty acids, and amino acids; (ii) downregulation of the pathways responsible for structural integrity (ECM-receptor interactions and focal adhesion); and (iii) disruptions in excitability. Taken together, our study demonstrates that the systemic (e.g., hyperglycemia) and cardiac-specific effects of PI3K $\alpha$  inhibition predispose the heart to greater cardiovascular risks.

We found that the PI3K $\alpha$  inhibitor, BYL719, has detrimental effects on cardiac health and post-MI cardiac repair, suggesting that both endothelial and cardiomyocyte PI3K $\alpha$  plays an important role in cardiac recovery after MI (Figure 8D). In both human and murine hearts, p110 $\alpha$  and Akt phosphorylation were upregulated after MI suggesting that PI3K $\alpha$ /Akt signaling is required for compensatory post-MI ventricular remodeling and revascularization (Figure 8D, green paths). Pharmacological inhibition of PI3K $\alpha$  (Figure 8D, red paths) inhibits both cardiomyocyte and endothelial PI3K $\alpha$  leading to increased apoptotic cell death, decreased cardiomyocyte hypertrophy, and diminished angiogenesis. Reduced number of cardiomyocytes, disrupted compensatory hypertrophy, and diminished re-vascularization resulted in exacerbated cardiac dysfunction and a tendency to increased mortality after MI. Importantly, post-MI biventricular dysfunction was exacerbated by inhibition of PI3K $\alpha$  signaling. Our findings are corroborated by the increased risk of heart failure in patients treated with sunitinib, a tyrosine kinase inhibitor with antitumor and antiangiogenic activities [48] and are likely to translate to other types of chemotherapy such as anthracycline where cell protective signaling plays a dominant role [31, 49].

Endothelial PI3K $\alpha$  signaling is required to maintain vascular function under physiologic conditions with endothelial cells under unstressed physiologic conditions. Post-MI, endothelial-specific PI3K $\alpha$  ablation resulted in (i) unchanged mortality, (ii) increased apoptosis and inflammation, (iii) reduced angiogenesis in infarct and peri-infarct areas, and (iv) worsened cardiac dysfunction. Reduced angiogenesis in response to PI3K $\alpha$  inhibition was also observed *in vitro* and was mediated via Akt/eNOS signaling consistent with a key role of eNOS in increasing capillary density post-MI and attenuating

heart failure [50, 51]. We observed that the cardiomyocyte PI3K $\alpha$  is required to maintain heart weight, and normal cardiac function. Cardiomyocyte-specific PI3K $\alpha$  ablation lead to considerable increase in mortality and was associated with enhanced myocardial apoptosis and inflammation, suppressed adaptive hypertrophy, reduced angiogenesis in non-infarct area, and worsened cardiac dysfunction. The cardioprotective effects seen with increased cardiac PI3K $\alpha$  activity further corroborate our results [52].

*Clinical implications of PI3K $\alpha$  inhibition.* Our results suggest (i) a therapeutic potential of upregulation of cardiac PI3K $\alpha$  to enhance post-MI cardiac repair by improving cell survival and angiogenesis; (ii) a concern of cardiotoxicity of PI3K $\alpha$  inhibitors in healthy and MI hearts. Patients receiving these drugs in clinical trials need close monitoring especially in patients with preexisting cardiovascular disease. Further research is needed into the development of strategies to counteract cardiotoxic effects of PI3K $\alpha$  inhibition for healthy and MI hearts.

### **Funding**

This work was supported by operating grants from the Canadian Institutes for Health Research (CIHR) and Heart and Stroke Foundation to GY Oudit. Ms. Xueyi Chen was funded by Li Ka Shing Sino-Canadian Exchange Program.

### **Author contributions**

XC performed experiments, analyzed data, drafted the manuscript; PZ, CEG performed experiments, analyzed data, revised the manuscript; AKA performed experiments,

analyzed data; BV, AGM, ZK, revised manuscript; GYO, revised manuscript, funding, supervision.

## **Disclosures**

B.V. is a consultant for Karus Therapeutics (Oxford, UK), iOnctura (Geneva, Switzerland) and Venthera (Palo Alto, CA, USA) and has received speaker fees from Gilead Sciences (Foster City, US). The other authors have no competing interests.

## **References**

- [1] B. Vanhaesebroeck, L. Stephens, P. Hawkins, PI3K signalling: the path to discovery and understanding, *Nature reviews. Molecular cell biology* 13(3) (2012) 195-203.
- [2] G.Y. Oudit, H. Sun, B.G. Kerfant, M.A. Crackower, J.M. Penninger, P.H. Backx, The role of phosphoinositide-3 kinase and PTEN in cardiovascular physiology and disease, *Journal of molecular and cellular cardiology* 37(2) (2004) 449-71.
- [3] M. Graupera, J. Guillermet-Guibert, L.C. Foukas, L.K. Phng, R.J. Cain, A. Salpekar, et al., Angiogenesis selectively requires the p110 $\alpha$  isoform of PI3K to control endothelial cell migration, *Nature* 453(7195) (2008) 662-6.
- [4] B.A. McLean, P. Zhabyeyev, V.B. Patel, R. Basu, N. Parajuli, J. DesAulniers, et al., PI3K $\alpha$  is essential for the recovery from Cre/tamoxifen cardiotoxicity and in myocardial insulin signalling but is not required for normal myocardial contractility in the adult heart, *Cardiovascular research* 105(3) (2015) 292-303.
- [5] B.A. McLean, P.C. Kienesberger, W. Wang, G. Masson, P. Zhabyeyev, J.R. Dyck, et al., Enhanced recovery from ischemia-reperfusion injury in PI3K $\alpha$  dominant negative hearts:

investigating the role of alternate PI3K isoforms, increased glucose oxidation and MAPK signaling, *Journal of molecular and cellular cardiology* 54 (2013) 9-18.

[6] K.C. Yang, Y.T. Tseng, J.M. Nerbonne, Exercise training and PI3K $\alpha$ -induced electrical remodeling is independent of cellular hypertrophy and Akt signaling, *Journal of molecular and cellular cardiology* 53(4) (2012) 532-41.

[7] P. Liu, H. Cheng, T.M. Roberts, J.J. Zhao, Targeting the phosphoinositide 3-kinase pathway in cancer, *Nature reviews. Drug discovery* 8(8) (2009) 627-44.

[8] X. Huang, G. Liu, J. Guo, Z. Su, The PI3K/AKT pathway in obesity and type 2 diabetes, *International journal of biological sciences* 14(11) (2018) 1483-1496.

[9] V.B. Patel, P. Zhabyeyev, X. Chen, F. Wang, M. Paul, D. Fan, et al., PI3K $\alpha$ -regulated gelsolin activity is a critical determinant of cardiac cytoskeletal remodeling and heart disease, *Nature communications* 9(1) (2018) 5390.

[10] R.R. Madsen, B. Vanhaesebroeck, R.K. Semple, Cancer-Associated PIK3CA Mutations in Overgrowth Disorders, *Trends in molecular medicine* 24(10) (2018) 856-870.

[11] C. Sadasivan, P. Zhabyeyev, D. Labib, J.A. White, D.I. Paterson, G.Y. Oudit, Cardiovascular toxicity of PI3K $\alpha$  inhibitors, *Clin Sci (Lond)* 134(19) (2020) 2595-2622.

[12] C. Fritsch, A. Huang, C. Chatenay-Rivauday, C. Schnell, A. Reddy, M. Liu, et al., Characterization of the novel and specific PI3K $\alpha$  inhibitor NVP-BYL719 and development of the patient stratification strategy for clinical trials, *Molecular cancer therapeutics* 13(5) (2014) 1117-29.

[13] A. Mizrachi, Y. Shamay, J. Shah, S. Brook, J. Soong, V.K. Rajasekhar, et al., Tumour-specific PI3K inhibition via nanoparticle-targeted delivery in head and neck squamous cell carcinoma, *Nature communications* 8 (2017) 14292.

[14] D. Juric, J. Rodon, J. Tabernero, F. Janku, H.A. Burris, J.H.M. Schellens, et al., Phosphatidylinositol 3-Kinase  $\alpha$ -Selective Inhibition With Alpelisib (BYL719) in PIK3CA-

Altered Solid Tumors: Results From the First-in-Human Study, *Journal of clinical oncology* : official journal of the American Society of Clinical Oncology 36(13) (2018) 1291-1299.

[15] F. Andre, E. Ciruelos, G. Rubovszky, M. Campone, S. Loibl, H.S. Rugo, et al., Alpelisib for PIK3CA-Mutated, Hormone Receptor-Positive Advanced Breast Cancer, *The New England journal of medicine* 380(20) (2019) 1929-1940.

[16] Q. Venot, T. Blanc, S.H. Rabia, L. Berteloot, S. Ladraa, J.P. Duong, et al., Targeted therapy in patients with PIK3CA-related overgrowth syndrome, *Nature* 558(7711) (2018) 540-546.

[17] G.B.D.C.o.D. Collaborators, Global, regional, and national age-sex specific mortality for 264 causes of death, 1980-2016: a systematic analysis for the Global Burden of Disease Study 2016, *Lancet (London, England)* 390(10100) (2017) 1151-1210.

[18] S.D. Prabhu, N.G. Frangogiannis, The Biological Basis for Cardiac Repair After Myocardial Infarction: From Inflammation to Fibrosis, *Circ Res* 119(1) (2016) 91-112.

[19] J.R. McMullen, T. Shioi, L. Zhang, O. Tarnavski, M.C. Sherwood, P.M. Kang, et al., Phosphoinositide 3-kinase(p110 $\alpha$ ) plays a critical role for the induction of physiological, but not pathological, cardiac hypertrophy, *Proceedings of the National Academy of Sciences of the United States of America* 100(21) (2003) 12355-60.

[20] P. Zhabyeyev, B. McLean, X. Chen, B. Vanhaesebroeck, G.Y. Oudit, Inhibition of PI3Kinase- $\alpha$  is pro-arrhythmic and associated with enhanced late Na(+) current, contractility, and Ca(2+) release in murine hearts, *Journal of molecular and cellular cardiology* 132 (2019) 98-109.

[21] M.A. Crackower, G.Y. Oudit, I. Kozieradzki, R. Sarao, H. Sun, T. Sasaki, et al., Regulation of myocardial contractility and cell size by distinct PI3K-PTEN signaling pathways, *Cell* 110(6) (2002) 737-49.

[22] U. Campia, J.J. Moslehi, L. Amiri-Kordestani, A. Barac, J.A. Beckman, D.D. Chism, et al., Cardio-Oncology: Vascular and Metabolic Perspectives: A Scientific Statement From the American Heart Association, *Circulation* 139(13) (2019) e579-e602.

- [23] C.G. Lenneman, D.B. Sawyer, Cardio-Oncology: An Update on Cardiotoxicity of Cancer-Related Treatment, *Circ Res* 118(6) (2016) 1008-20.
- [24] M. Shen, M. Hu, P.W.M. Fedak, G.Y. Oudit, Z. Kassiri, Cell-Specific Functions of ADAM17 Regulate the Progression of Thoracic Aortic Aneurysm, *Circ Res* 123(3) (2018) 372-388.
- [25] X. Chen, P. Zhabyeyev, A.K. Azad, W. Wang, R.A. Minerath, J. DesAulniers, et al., Endothelial and cardiomyocyte PI3Kbeta divergently regulate cardiac remodelling in response to ischaemic injury, *Cardiovascular research* 115(8) (2019) 1343-1356.
- [26] E. Castellano, C. Sheridan, M.Z. Thin, E. Nye, B. Spencer-Dene, M.E. Diefenbacher, et al., Requirement for interaction of PI3-kinase p110alpha with RAS in lung tumor maintenance, *Cancer cell* 24(5) (2013) 617-30.
- [27] B. Gobin, M.B. Huin, F. Lamoureux, B. Ory, C. Charrier, R. Lanel, et al., BYL719, a new alpha-specific PI3K inhibitor: single administration and in combination with conventional chemotherapy for the treatment of osteosarcoma, *International journal of cancer* 136(4) (2015) 784-96.
- [28] M. Elkabets, E. Pazarentzos, D. Juric, Q. Sheng, R.A. Pelosof, S. Brook, et al., AXL mediates resistance to PI3Kalpha inhibition by activating the EGFR/PKC/mTOR axis in head and neck and esophageal squamous cell carcinomas, *Cancer cell* 27(4) (2015) 533-46.
- [29] W. Wang, S.M. McKinnie, V.B. Patel, G. Haddad, Z. Wang, P. Zhabyeyev, et al., Loss of Apelin exacerbates myocardial infarction adverse remodeling and ischemia-reperfusion injury: therapeutic potential of synthetic Apelin analogues, *Journal of the American Heart Association* 2(4) (2013) e000249.
- [30] M. Litvinukova, C. Talavera-Lopez, H. Maatz, D. Reichart, C.L. Worth, E.L. Lindberg, et al., Cells of the adult human heart, *Nature* doi: 10.1038/s41586-020-2797-4. (2020).
- [31] B.A. McLean, V.B. Patel, P. Zhabyeyev, X. Chen, R. Basu, F. Wang, et al., PI3Kalpha Pathway Inhibition With Doxorubicin Treatment Results in Distinct Biventricular Atrophy and

Remodeling With Right Ventricular Dysfunction, *Journal of the American Heart Association* 8(9) (2019) e010961.

[32] D.D. Hall, J.M. Ponce, B. Chen, K.M. Spitler, A. Alexia, G.Y. Oudit, et al., Ectopic expression of Cdk8 induces eccentric hypertrophy and heart failure, *JCI insight* 2(15) (2017) e92476.

[33] J. Guillermet-Guibert, K. Bjorklof, A. Salpekar, C. Gonella, F. Ramadani, A. Bilancio, et al., The p110beta isoform of phosphoinositide 3-kinase signals downstream of G protein-coupled receptors and is functionally redundant with p110gamma, *Proceedings of the National Academy of Sciences of the United States of America* 105(24) (2008) 8292-7.

[34] W. Wang, M. Shen, C. Fischer, R. Basu, S. Hazra, P. Couvineau, et al., Apelin protects against abdominal aortic aneurysm and the therapeutic role of neutral endopeptidase resistant apelin analogs, *Proceedings of the National Academy of Sciences of the United States of America* 116(26) (2019) 13006-13015.

[35] C.W. Duarte, V. Lindner, S.A. Francis, D. Schoormans, Visualization of Cancer and Cardiovascular Disease Co-Occurrence With Network Methods, *JCO clinical cancer informatics* 1 (2017) 1-12.

[36] L. Vincent, D. Leedy, S.C. Masri, R.K. Cheng, Cardiovascular Disease and Cancer: Is There Increasing Overlap?, *Current oncology reports* 21(6) (2019) 47.

[37] B. Zoller, J. Ji, J. Sundquist, K. Sundquist, Risk of coronary heart disease in patients with cancer: a nationwide follow-up study from Sweden, *European journal of cancer (Oxford, England : 1990)* 48(1) (2012) 121-8.

[38] T. Hasin, Y. Gerber, S.A. Weston, R. Jiang, J.M. Killian, S.M. Manemann, et al., Heart Failure After Myocardial Infarction Is Associated With Increased Risk of Cancer, *Journal of the American College of Cardiology* 68(3) (2016) 265-271.

[39] R.J. Koene, A.E. Prizment, A. Blaes, S.H. Konety, Shared Risk Factors in Cardiovascular Disease and Cancer, *Circulation* 133(11) (2016) 1104-14.



- [40] W.C. Meijers, M. Maglione, S.J.L. Bakker, R. Oberhuber, L.M. Kieneker, S. de Jong, et al., Heart Failure Stimulates Tumor Growth by Circulating Factors, *Circulation* 138(7) (2018) 678-691.
- [41] I.A. Mayer, A. Prat, D. Egle, S. Blau, J.A.P. Fidalgo, M. Gnant, et al., A Phase II Randomized Study of Neoadjuvant Letrozole Plus Alpelisib for Hormone Receptor-Positive, Human Epidermal Growth Factor Receptor 2-Negative Breast Cancer (NEO-ORB), *Clinical cancer research : an official journal of the American Association for Cancer Research* 25(10) (2019) 2975-2987.
- [42] D. Juric, F. Janku, J. Rodon, H.A. Burris, I.A. Mayer, M. Schuler, et al., Alpelisib Plus Fulvestrant in PIK3CA-Altered and PIK3CA-Wild-Type Estrogen Receptor-Positive Advanced Breast Cancer: A Phase 1b Clinical Trial, *JAMA oncology* 5(2) (2019) e184475.
- [43] A. Esposito, G. Viale, G. Curigliano, Safety, Tolerability, and Management of Toxic Effects of Phosphatidylinositol 3-Kinase Inhibitor Treatment in Patients With Cancer: A Review, *JAMA oncology* (2019).
- [44] Y. Ando, S. Iwasa, S. Takahashi, H. Saka, T. Kakizume, K. Natsume, et al., Phase I study of alpelisib (BYL719), an alpha-specific PI3K inhibitor, in Japanese patients with advanced solid tumors, *Cancer Sci* 110(3) (2019) 1021-1031.
- [45] P. Srikanthan, T.B. Horwich, C.H. Tseng, Relation of Muscle Mass and Fat Mass to Cardiovascular Disease Mortality, *The American journal of cardiology* 117(8) (2016) 1355-60.
- [46] J.B. Nielsen, C. Graff, P.V. Rasmussen, A. Pietersen, B. Lind, M.S. Olesen, et al., Risk prediction of cardiovascular death based on the QTc interval: evaluating age and gender differences in a large primary care population, *European heart journal* 35(20) (2014) 1335-44.
- [47] T. Biering-Sorensen, S.R. Biering-Sorensen, F.J. Olsen, M. Sengelov, P.G. Jorgensen, R. Mogelvang, et al., Global Longitudinal Strain by Echocardiography Predicts Long-Term Risk of Cardiovascular Morbidity and Mortality in a Low-Risk General Population: The Copenhagen City Heart Study, *Circulation. Cardiovascular imaging* 10(3) (2017).

- [48] C.J. Richards, Y. Je, F.A. Schutz, D.Y. Heng, S.M. Dallabrida, J.J. Moslehi, et al., Incidence and risk of congestive heart failure in patients with renal and nonrenal cell carcinoma treated with sunitinib, *Journal of clinical oncology : official journal of the American Society of Clinical Oncology* 29(25) (2011) 3450-6.
- [49] J. Li, P.Y. Wang, N.A. Long, J. Zhuang, D.A. Springer, J. Zou, et al., p53 prevents doxorubicin cardiotoxicity independently of its prototypical tumor suppressor activities, *Proceedings of the National Academy of Sciences of the United States of America* 116(39) (2019) 19626-19634.
- [50] S.P. Jones, J.J. Greer, R. van Haperen, D.J. Duncker, R. de Crom, D.J. Lefer, Endothelial nitric oxide synthase overexpression attenuates congestive heart failure in mice, *Proceedings of the National Academy of Sciences of the United States of America* 100(8) (2003) 4891-6.
- [51] L. Chen, Y. Zhang, L. Tao, Z. Yang, L. Wang, Mesenchymal Stem Cells with eNOS Over-Expression Enhance Cardiac Repair in Rats with Myocardial Infarction, *Cardiovasc Drugs Ther* 31(1) (2017) 9-18.
- [52] K.C. Yang, P.Y. Jay, J.R. McMullen, J.M. Nerbonne, Enhanced cardiac PI3K $\alpha$  signalling mitigates arrhythmogenic electrical remodelling in pathological hypertrophy and heart failure, *Cardiovascular research* 93(2) (2012) 252-62.

## **Figure Legends**

**Figure 1. Systemic effects and changes in the transcriptome with BYL719 treatment.** **A.** Schematic of experimental design for 10-day BYL719 administration in WT mice. **B.** Time course of body weight changes during BYL treatment (left: n=10-11 mice/group) and body weight after 10-day treatment with vehicle or BYL719 (right: n=17-18 mice/group). **C.** Blood glucose level in mice treated with vehicle or BYL719 (n=9-13 mice/group) at 3 and 10 days. **D.** Alteration of body composition in mice after 10-day treatment with vehicle or BYL719 (n=9 mice/group). **E.** Heart weight and left ventricular weight in mice after 10-day treatment with vehicle or BYL719 (n=16 mice/group). **F.** Representative M-mode images, ejection fraction (EF) (n=10 mice/group), and left ventricular longitudinal strain analysis (n=7 mice/group) in mice after 10-day treatment with vehicle or BYL719. **G.** QTc interval in mice treated with BYL719 on Day 0 (before administration), Day 3, and Day 10 (n=11 mice). **H.** Volcano plot of gene expression changes due 10-day treatment with BYL719. Blue symbols: altered genes defined by the boundary conditions ( $p < 0.1$  and expression levels for WT-vehicle or WT-BYL of at least 1% of maximal expression level, 75,000 TPM). Grey symbols: genes that did not satisfy boundary conditions. **I.** Over-representation analysis of upregulated genes within KEGG (Kyoto Encyclopedia of Genes and Genomes) pathways displayed as an enrichment ratio (x axis). **J.** Over-representation analysis of downregulated genes within KEGG pathways displayed as an enrichment ratio (X-axis). Data are presented as mean $\pm$ SEM; statistical significance is calculated using repeated measures ANOVA with pairwise test in B and G; independent t-test in B, D, E, and F; one-way ANOVA in C. \* $p < 0.05$  vs WT-Vehicle

group in B and D-F, vs fasting in C, and vs day 0 in F; # $p < 0.05$  vs WT-Vehicle (1 h post treatment) in C.

**Figure 2. Alterations in PI3K $\alpha$  pathway in human and murine hearts post MI and the effect of BYL719 on post-MI mortality and cardiac function.** **A.** Protein levels of p110 $\alpha$  and phosphorylation levels of Akt in control (non-failing control (NFC) or Sham) and post-MI hearts (n=4-5 hearts/group). **B.** Schematic of experimental design for testing the effect of BYL719 treatment on post-MI remodeling. **C.** Kaplan-Meier survival curve (left) and distribution of causes of death (right) in post-MI mice treated with vehicle or BYL719 (n=26 mice/group) ( $p = 0.065$ ). **D.** Echocardiographic assessment of cardiac function at 7 days post MI: representative M-mode images, left ventricular ejection fraction (EF), right ventricular fractional area change (FAC), left ventricular end-systolic volume (LVESV), left ventricular end-diastolic volume (LVEDV), and wall motion score index (WMSI) in mice treated with vehicle or BYL719 (n=10-14 mice/group). Data are presented as mean $\pm$ SEM; statistical significance is calculated using one-way ANOVA in A, log-rank test and fisher exact test in C, and two-way ANOVA with pairwise test in D; \* $p < 0.05$  vs NFC or sham, # $p < 0.05$  vs WT-Vehicle 7-day MI.

**Figure 3. BYL719 and post-MI ventricular remodeling.** **A.** Apoptosis: terminal deoxynucleotidyl transferase-mediated dUTP nick-end labeling (TUNEL, green) and DAPI (blue) staining of the sections of 1-day post-MI hearts; representative images (left) and quantification (right, n=5 hearts/group). **B.** Inflammation: immunofluorescence staining for neutrophils (anti-Ly6B, red; top: representative images, left, and

quantification, right) and macrophages (anti-CD68, red; bottom: representative images, left, and quantification, right); DAPI (blue); n=5 hearts/group. **C.** Cellular hypertrophy: wheat germ agglutinin (WGA) staining (green) to outline cardiomyocyte; DAPI (blue); representative images (left) and quantification (right, n=5 hearts/ group). **D.** Vascularization: endothelial cell immunofluorescence staining (anti-CD31, red); DAPI (blue); representative images (left) and quantification (right, n=5 hearts/group). **E.** Western blots and quantifications of phosphorylation levels of Akt-T308, GSK3 $\beta$ -S9, and eNOS-S1177 in left ventricular lysates (n=4-5 hearts/group). Data are presented as mean $\pm$ SEM; statistical significance is calculated using two-way ANOVA with pairwise comparison in A, C, and D, independent t-test in B, and one-way ANOVA in E; \*p<0.05 vs sham, #p<0.05 vs WT-Vehicle MI.

**Figure 4. Endothelial PI3K $\alpha$  is required for preservation of cardiac function and angiogenesis after MI.** **A.** Schematic of experimental design for testing the role of endothelial PI3K $\alpha$  in post-MI remodeling using conditional knock-out (p110 $\alpha^{EC}$ ) and control (p110 $\alpha^{flx/flx}$  littermates) mice. **B.** Echocardiographic assessment of cardiac function at 7 days post MI: representative M-mode images, ejection fraction (EF), left ventricular end-systolic volume (LVESV), left ventricular end-diastolic volume (LVEDV), and wall motion score index (WMSI) (n=10 mice/group). **C.** Endothelial apoptosis: immunofluorescence staining of endothelial cells (ECs) (CD31, red), TUNEL (green), and DAPI (blue): representative images (left, white arrows indicate red-green co-localization) and quantification (right, n=5 hearts/group). **D.** Endothelial proliferation: immunofluorescence staining for ECs (CD31, green), immunofluorescence staining of

proliferating ECs (Ki67, red), and DAPI (blue): representative images (left, white arrows indicate red-green co-localization) and quantification (right, n=5 hearts/group). **E.** Vascularization: immunofluorescence staining of ECs (CD31, red; top), lectin (green; middle) *in vivo* perfusion, and quantifications (bottom, n = 5 hearts/group). **F.** Western blots and quantification of Akt phosphorylation in 7-day post-MI hearts (n=4-7 hearts/group). Data are presented as mean $\pm$ SEM; statistical significance is calculated using two-way ANOVA with pairwise comparisons in B-E, and independent t-test in F; \*p<0.05 vs sham in B and E, vs infarct in C and D, vs indicated group in F, #p<0.05 vs p110 $\alpha$ <sup>flx/flx</sup> within the same treatment.

**Figure 5. PI3K $\alpha$  activity is required to maintain Akt/eNOS signaling in endothelial cells.** **A.** Inhibition of PI3K $\alpha$  by BYL719 and Akt/eNOS signaling in cultured human umbilical vein endothelial cells (HUVEC) (no VEGF; n=3 independent experiments). **B.** Effect of inhibition of PI3K $\alpha$  by BYL719 on vascular endothelial growth factor (VEGF)-induced Akt/eNOS activation in HUVEC (n=3 independent experiments). **C.** Inhibition of PI3K $\alpha$  by BYL719 and Akt/eNOS signaling in human coronary artery endothelial cells (HCAEC) (no VEGF, n=4 independent experiments). **D.** Effect of inhibition of PI3K $\alpha$  by BYL719 on VEGF-stimulated Akt/eNOS signaling in HCAEC (n=4 independent experiments). Data are presented as mean $\pm$ SEM; statistical significance is calculated using one-way ANOVA; \*p<0.05 vs vehicle without VEGF, #p<0.05 vs vehicle with VEGF.

**Figure 6. PI3K $\alpha$  activity is required for endothelial cell survival, proliferation, and angiogenesis.** **A.** Effect of BYL719 (500 nmol/L) on cell survival of HUVEC: flow

cytometry images and quantification of staining with annexin V and propidium iodide (n=6 independent experiments). **B.** Effect of BYL719 (500 nmol/L) on proliferation rate of HUVEC: BrdU (red) and DAPI (blue) staining (n=8 independent experiments). **C.** Effects of BYL719 (500 nmol/L) on angiogenic sprouting in HUVEC (n=4 independent experiments). **D.** Effect of BYL719 (500 nmol/L) on cell survival of HCAEC: flow cytometry images and quantification of staining with annexin V and propidium iodide (n=5 independent experiments). **E.** Effects of BYL719 (500 nmol/L) on proliferation rate of HCAEC: BrdU (red) and DAPI (blue) staining (n=6 independent experiments). **F.** Effects of BYL719 (500 nmol/L) on angiogenic sprouting in HCAEC (n=4 independent experiments). Data are presented as mean $\pm$ SEM; statistical significance is calculated using independent t-test in A-C, one-way ANOVA in D-F; \*p<0.05 vs vehicle.

**Figure 7. Role of cardiomyocyte PI3K $\alpha$  at baseline and in post-MI cardiac remodeling.** **A.** Body weight, heart weight, and left ventricular weight in cardiomyocyte-specific knockout (p110 $\alpha$ <sup>CM</sup>) and control (littermates, p110 $\alpha$ <sup>flx/flx</sup>) mice (n=9-14 mice/group). **B.** Echocardiographic assessment of cardiac function at 7 days post MI: representative M-mode images, left ventricular ejection fraction (EF), right ventricular fractional area change (FAC), left ventricular end-systolic volume (LVESV), and left ventricular end-diastolic volume (LVEDV) (n=10 mice/group). **C.** Kaplan-Meier survival analysis for survival rate (top) and cardiac rupture incidence (bottom) (n=13-30 mice/group). **D.** Apoptosis: TUNEL (green) and DAPI (blue) staining: representative images (left) and quantification (right, n=4 hearts/group). **E.** Cellular hypertrophy: WGA (green) staining to outline cardiomyocytes: representative images (left) and quantification

(right, n=5 hearts/group). **F.** Western blots and quantification for Akt in left ventricle lysates from post-MI p110 $\alpha^{CM}$  and p110 $\alpha^{flx/flx}$  hearts (n=4-5 hearts/group). Data are presented as mean $\pm$ SEM; statistical significance is calculated using independent t-test in A and F, two-way ANOVA with pairwise comparison in B, D, and E, and log-rank test in C; \*p<0.05 vs p110 $\alpha^{flx/flx}$  in A, C, and F, vs sham in B, D, and E, #p<0.05 vs p110 $\alpha^{flx/flx}$  MI.

**Figure 8. Effects BYL719 on isolated adult mouse cardiomyocytes under hypoxia and schematic of the roles of PI3K $\alpha$  in cardiomyocytes and endothelial cells at baseline and post MI.** **A.** Western blots and quantification of Akt/GSK3 $\beta$  signaling in lysates from cardiomyocytes cultured under normoxic and hypoxic condition (n=6 hearts, 3 independent experiments). **B.** Representative images (left) and quantification of apoptotic cell death (right) of isolated cardiomyocyte under hypoxic condition with cyclic mechanical stretch (right, n=8 hearts, 4 independent experiments). **C.** Representative images of F-actin (green), G-actin (red), and DAPI (blue) staining (left) and quantification of F/G-actin ratio (right, n=8 hearts, 4 independent experiments). **D.** Schematic of the roles of PI3K $\alpha$  in cardiomyocytes and endothelial cells at baseline and post-MI: in cardiomyocyte, PI3K $\alpha$  regulates survival and adaptive hypertrophy; in endothelial cells, PI3K $\alpha$  regulates survival and angiogenesis to maintain vascular distribution in response to MI. Data are presented as mean $\pm$ SEM; statistical significance is calculated using one-way ANOVA in A and B, two-way ANOVA with pairwise comparison in C; \*p<0.05 vs normoxia in A and C, vs vehicle in B, #p<0.05 vs hypoxia-vehicle in A and C.



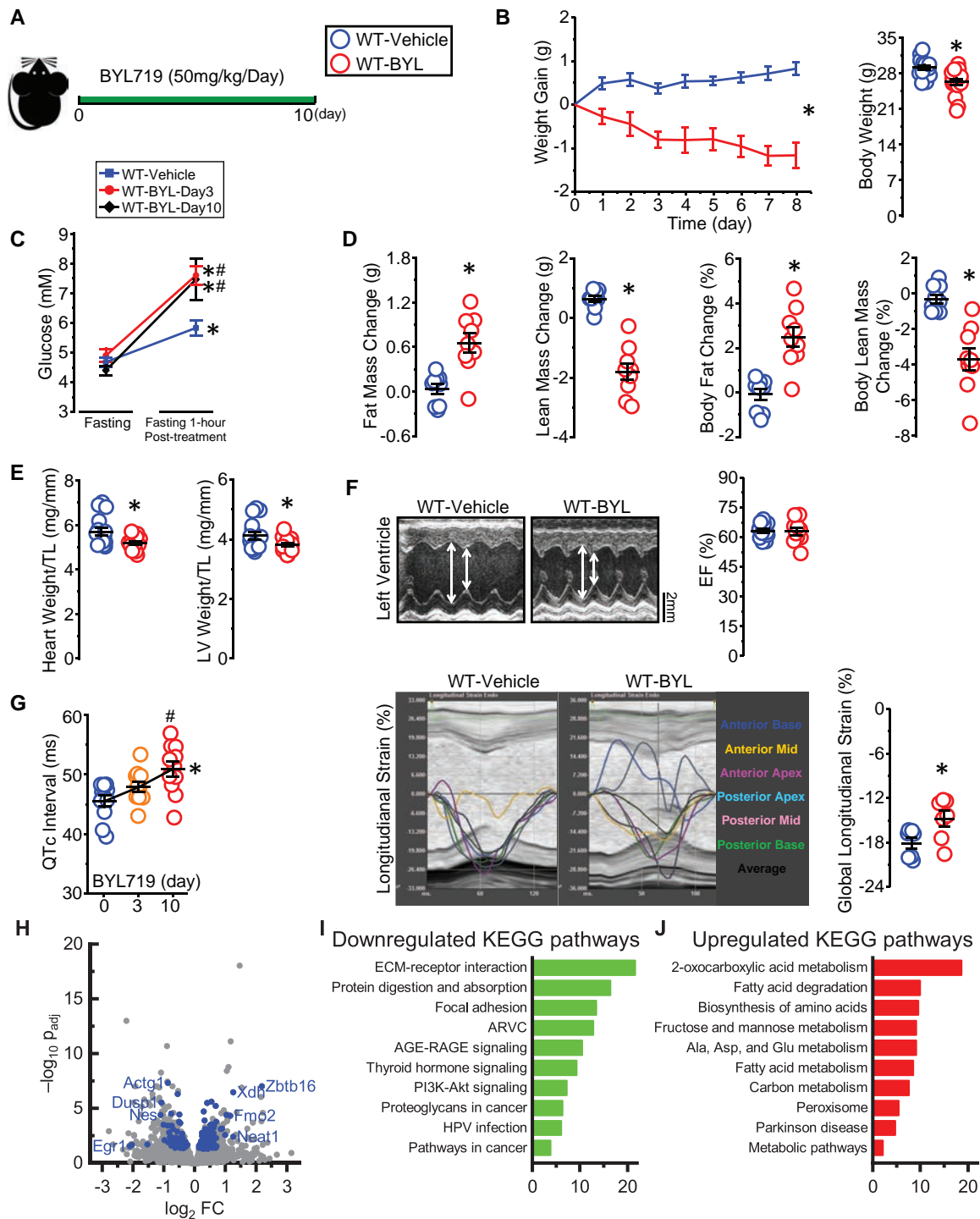


**Figure 1. Systemic effects and changes in the transcriptome after 10-day treatment with BYL719.**

(A) Schematic of experimental design for 10-day BYL719 administration in WT mice. (B) Time course of body weight changes during BYL treatment (left: n=10-11 mice/group) and body weight after 10-day treatment with vehicle or BYL719 (right: n=17-18 mice/group). (C) Blood glucose level in mice treated with vehicle or BYL719 (n=9-13 mice/group) at 3 and 10 days. (D) Alteration of body composition in mice after 10-day treatment with vehicle or BYL719 (n=9 mice/group). (E) Heart weight and left ventricular weight in mice after 10-day treatment with vehicle or BYL719 (n=16 mice/group). (F) Representative M-mode images, ejection fraction (EF) (n=10 mice/group), and left ventricular longitudinal strain analysis (n=7 mice/group) in mice after 10-day treatment with vehicle or BYL719. (G) QTc interval in mice treated with BYL719 on Day 0 (before administration), Day 3, and Day 10 (n=11 mice). (H) Volcano plot of gene expression changes due 10-day treatment with BYL719. Blue symbols: altered genes defined by the boundary conditions ( $p < 0.1$  and expression levels for WT-vehicle or WT-BYL of at least 1% of maximal expression level, 75,000 TPM). Grey symbols: genes that did not satisfy boundary conditions. (I) Over-representation analysis of upregulated genes within KEGG (Kyoto Encyclopedia of Genes and Genomes) pathways displayed as an enrichment ratio (X axis). (J) Over-representation analysis of downregulated genes within KEGG pathways displayed as an enrichment ratio (X axis). Data are presented as mean $\pm$ SEM; statistical significance is calculated using repeated measures ANOVA with pairwise test in B and G; independent t-test in B, D, E, and F; one-way ANOVA in C. \* $p < 0.05$  vs WT-Vehicle group in B and D-F, vs fasting in C, and vs day 0 in F; # $p < 0.05$  vs WT-Vehicle (1 h post treatment) in C.

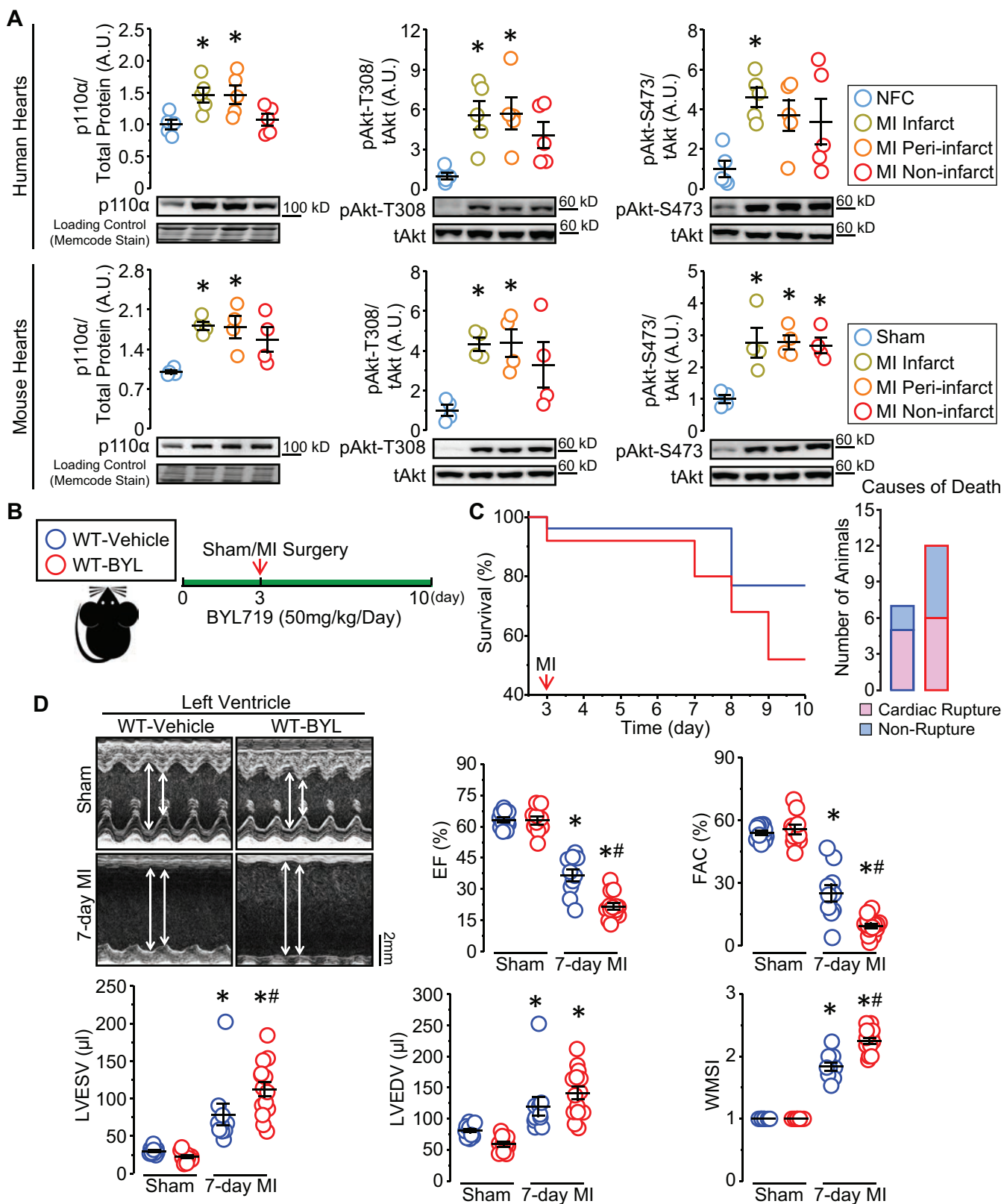


**Figure 2. Alterations in PI3K $\alpha$  pathway in human and murine hearts post MI and the effect of BYL719 on post-MI mortality and cardiac function. (A)** Protein levels of p110 $\alpha$  and phosphorylation levels of Akt in control (non-failing control (NFC) or Sham) and post-MI hearts (n=4-5 hearts/group). **(B)** Schematic of experimental design for testing the effect of BYL719 treatment on post-MI remodeling. **(C)** Kaplan-Meier survival curve (left) and distribution of causes of death (right) in post-MI mice treated with vehicle or BYL719 (n=25-26 mice/group) (p=0.065). **(D)** Echocardiographic assessment of cardiac function at 7 days post MI: representative M-mode images, left ventricular ejection fraction (EF), right ventricular fractional area change (FAC), left ventricular end-systolic volume (LVESV), left ventricular end-diastolic volume (LVEDV), and wall motion score index (WMSI) in mice treated with vehicle or BYL719 (n=10-14 mice/group). Data are presented as mean $\pm$ SEM; statistical significance is calculated using one-way ANOVA in A, log-rank test and fisher exact test in C, and two-way ANOVA with pairwise test in D; \*p<0.05 vs NFC or sham, #p<0.05 vs WT-Vehicle 7-day MI.

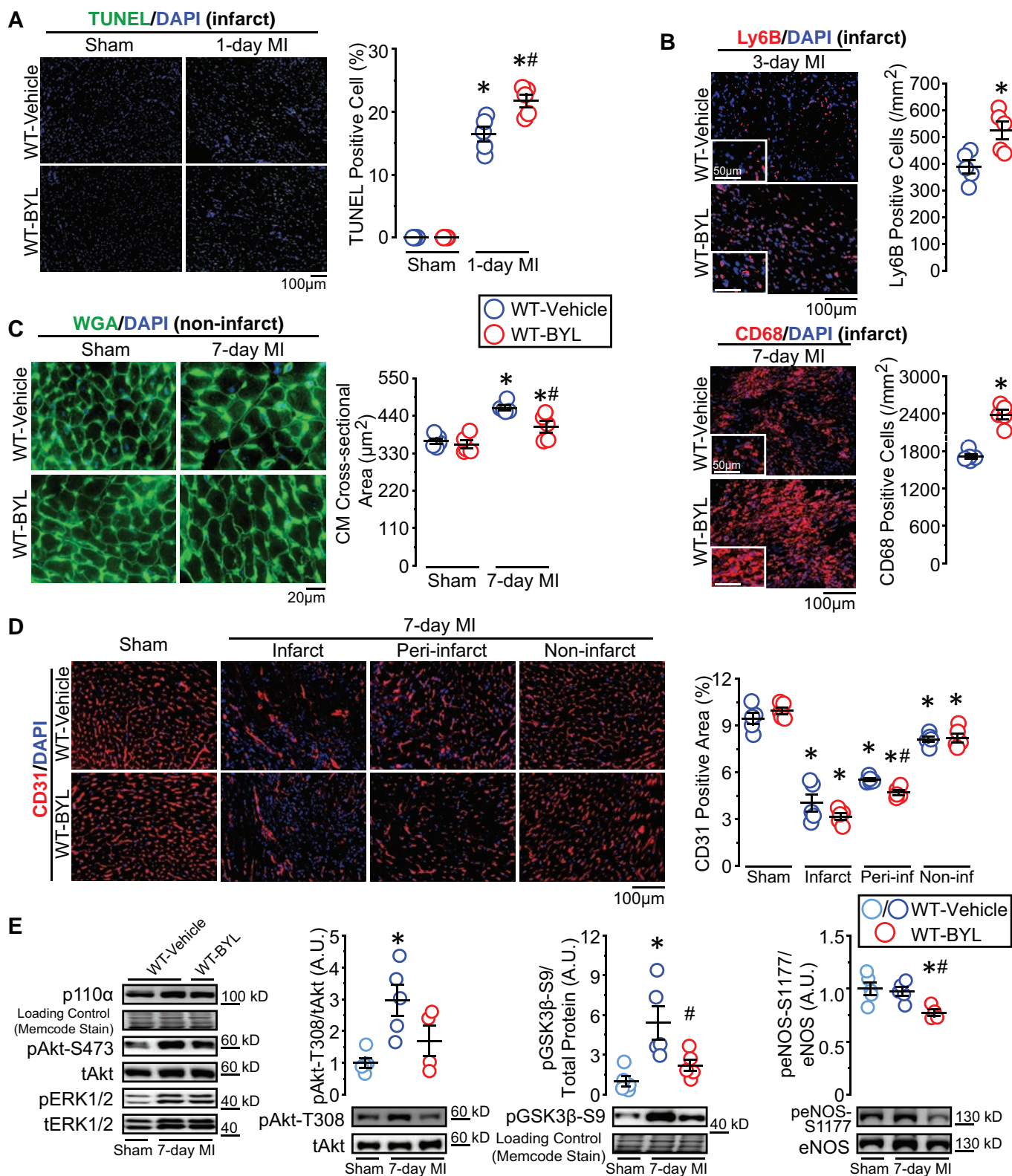


**Figure 3. BYL719 and post-MI ventricular remodeling.** (A) Apoptosis: terminal deoxynucleotidyl transferase-mediated dUTP nick-end labeling (TUNEL, green) and DAPI (blue) staining of the sections of 1-day post-MI hearts; representative images (left) and quantification (right, n=5 hearts/group). (B) Inflammation: immunofluorescence staining for neutrophils (anti-Ly6B, red; top: representative images, left, and quantification, right) and macrophages (anti-CD68, red; bottom: representative images, left, and quantification, right); DAPI (blue); n=5 hearts/group. (C) Cellular hypertrophy: wheat germ agglutinin (WGA) staining (green) to outline cardiomyocyte; DAPI (blue); representative images (left) and quantification (right, n=5 hearts/group). (D) Vascularization: endothelial cell immunofluorescence staining (anti-CD31, red); DAPI (blue); representative images (left) and quantification (right, n=5 hearts/group). (E) Western blots and quantifications of phosphorylation levels of Akt-T308, GSK3β-S9, and eNOS-S1177 in left ventricular lysates (n=4-5 hearts/group). Data are presented as mean±SEM; statistical significance is calculated using two-way ANOVA with pairwise comparison in A, C, and D, independent t-test in B, and one-way ANOVA in E; \*p<0.05 vs sham, #p<0.05 vs WT-Vehicle MI.

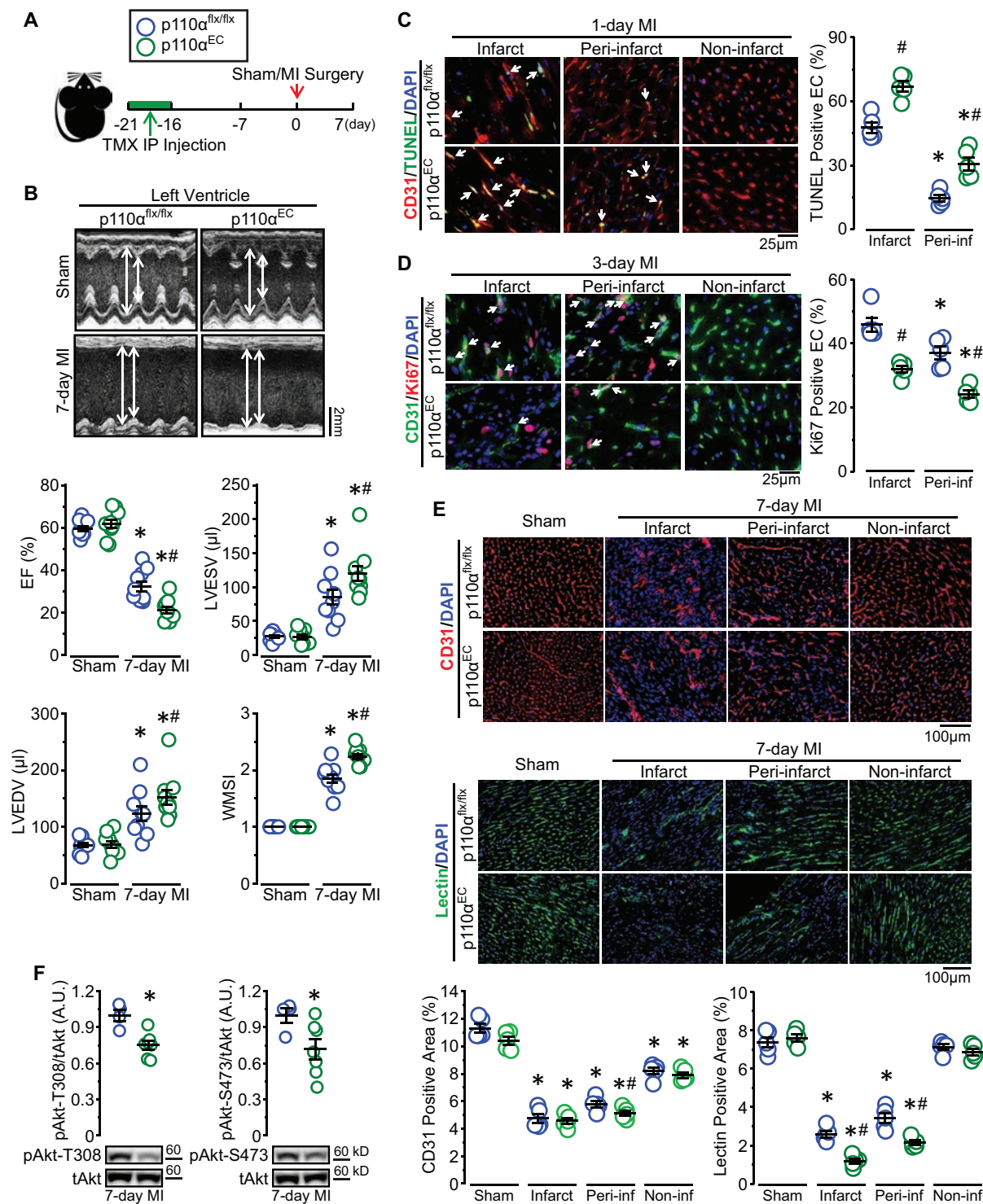


**Figure 4. Endothelial PI3K $\alpha$  is required for preservation of cardiac function and angiogenesis after MI.**

**(A)** Schematic of experimental design for testing the role of endothelial PI3K $\alpha$  in post-MI remodeling using conditional knock-out (p110 $\alpha^{EC}$ ) and control (p110 $\alpha^{flx/flx}$  littermates) mice. **(B)** Echocardiographic assessment of cardiac function at 7 days post MI: representative M-mode images, ejection fraction (EF), left ventricular end-systolic volume (LVESV), left ventricular end-diastolic volume (LVEDV), and wall motion score index (WMSI) (n=10 mice/group). **(C)** Endothelial apoptosis: immunofluorescence staining of endothelial cells (ECs) (CD31, red), TUNEL (green), and DAPI (blue): representative images (left, white arrows indicate red-green co-localization) and quantification (right, n=5 hearts/group). **(D)** Endothelial proliferation: immunofluorescence staining for ECs (CD31, green), immunofluorescence staining of proliferating ECs (Ki67, red), and DAPI (blue): representative images (left, white arrows indicate red-green co-localization) and quantification (right, n=5 hearts/group). **(E)** Vascularization: immunofluorescence staining of ECs (CD31, red; top), lectin (green; middle) *in vivo* perfusion, and quantifications (bottom, n=5 hearts/group). **(F)** Western blots and quantifications of Akt phosphorylation in 7-day post-MI hearts (n=4-7 hearts/group). Data are presented as mean $\pm$ SEM; statistical significance is calculated using two-way ANOVA with pairwise comparisons in B-E, and independent t-test in F; \*p<0.05 vs sham in B and E, vs infarct in C and D, vs indicated group in F, #p<0.05 vs p110 $\alpha^{flx/flx}$  within the same treatment.

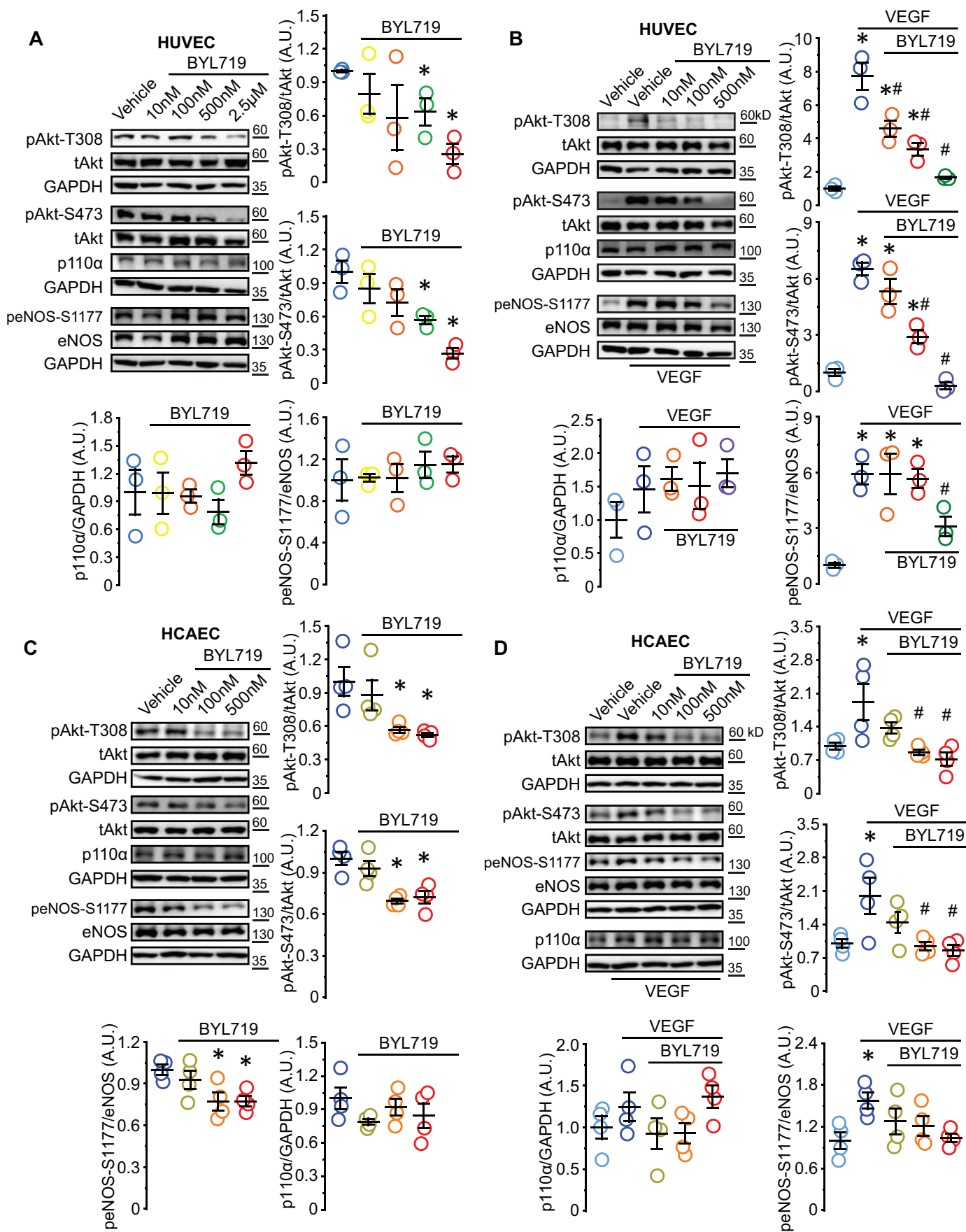


**Figure 5. PI3K $\alpha$  activity is required to maintain Akt/eNOS signaling in endothelial cells. (A)** Inhibition of PI3K $\alpha$  by BYL719 and Akt/eNOS signaling in cultured human umbilical vein endothelial cells (HUVEC) (no VEGF; n=3 independent experiments). **(B)** Effect of inhibition of PI3K $\alpha$  by BYL719 on vascular endothelial growth factor (VEGF)-induced Akt/eNOS activation in HUVEC (n=3 independent experiments). **(C)** Inhibition of PI3K $\alpha$  by BYL719 and Akt/eNOS signaling in human coronary artery endothelial cells (HCAEC) (no VEGF, n=4 independent experiments). **(D)** Effect of inhibition of PI3K $\alpha$  by BYL719 on VEGF-stimulated Akt/eNOS signaling in HCAEC (n=4 independent experiments). Data are presented as mean $\pm$ SEM; statistical significance is calculated using one-way ANOVA; \*p<0.05 vs vehicle without VEGF, #p<0.05 vs vehicle with VEGF.

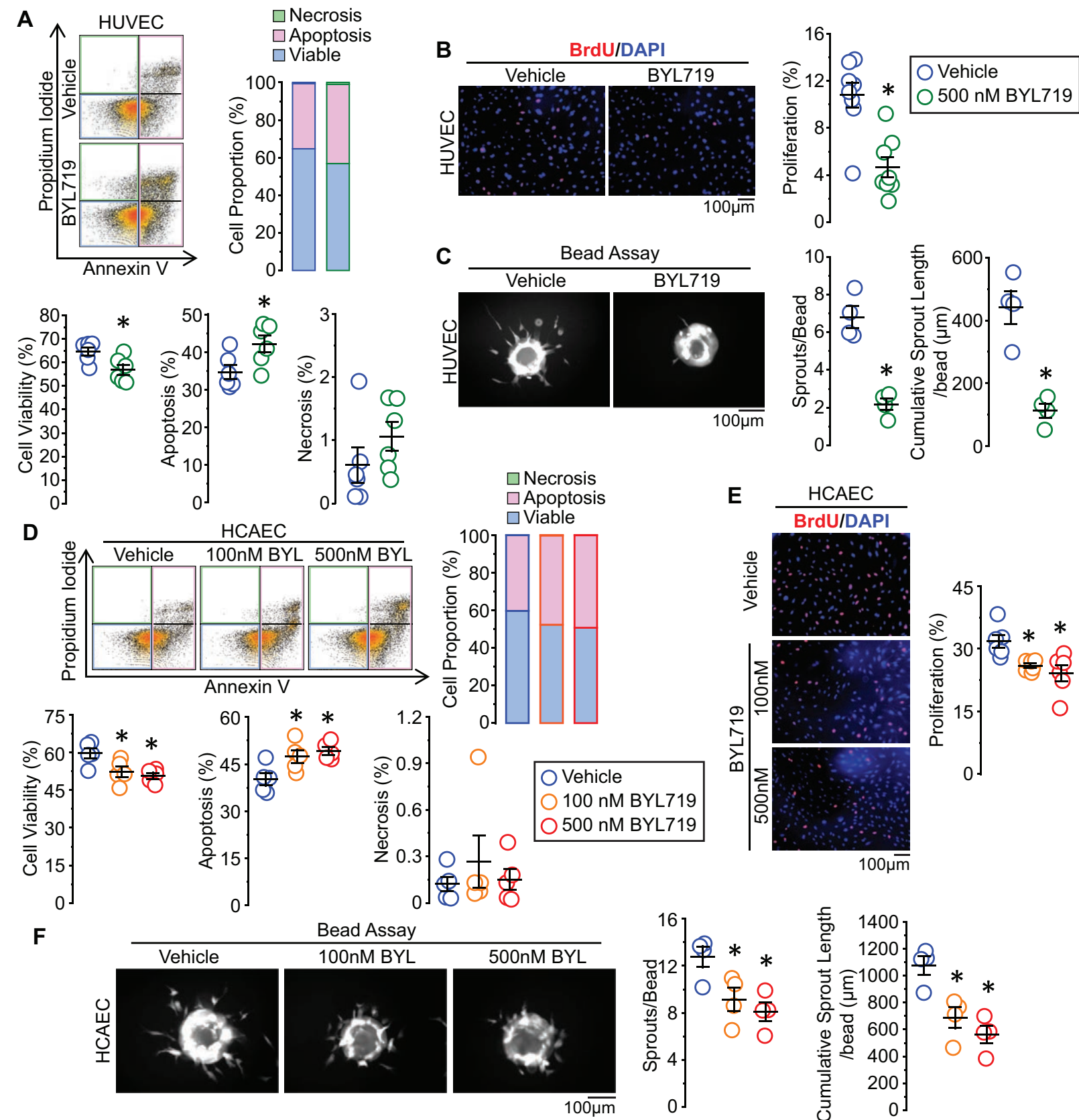


**Figure 6. PI3K $\alpha$  activity is required for endothelial cell survival, proliferation, and angiogenesis. (A)** Effect of BYL719 (500 nmol/L) on cell survival of HUVEC: flow cytometry images and quantification of staining with annexin V and propidium iodide (n=6 independent experiments). **(B)** Effect of BYL719 (500 nmol/L) on proliferation rate of HUVEC: BrdU (red) and DAPI (blue) staining (n=8 independent experiments). **(C)** Effects of BYL719 (500 nmol/L) on angiogenic sprouting in HUVECs (n=4 independent experiments). **(D)** Effect of BYL719 (500 nmol/L) on cell survival of HCAEC: flow cytometry images and quantification of staining with annexin V and propidium iodide (n=5 independent experiments). **(E)** Effects of BYL719 (500 nmol/L) on proliferation rate of HCAEC: BrdU (red) and DAPI (blue) staining (n=6 independent experiments). **(F)** Effects of BYL719 (500 nmol/L) on angiogenic sprouting in HCAEC (n=4 independent experiments). Data are presented as mean $\pm$ SEM; statistical significance is calculated using independent t-test in A-C, one-way ANOVA in D-F; \*p<0.05 vs vehicle.

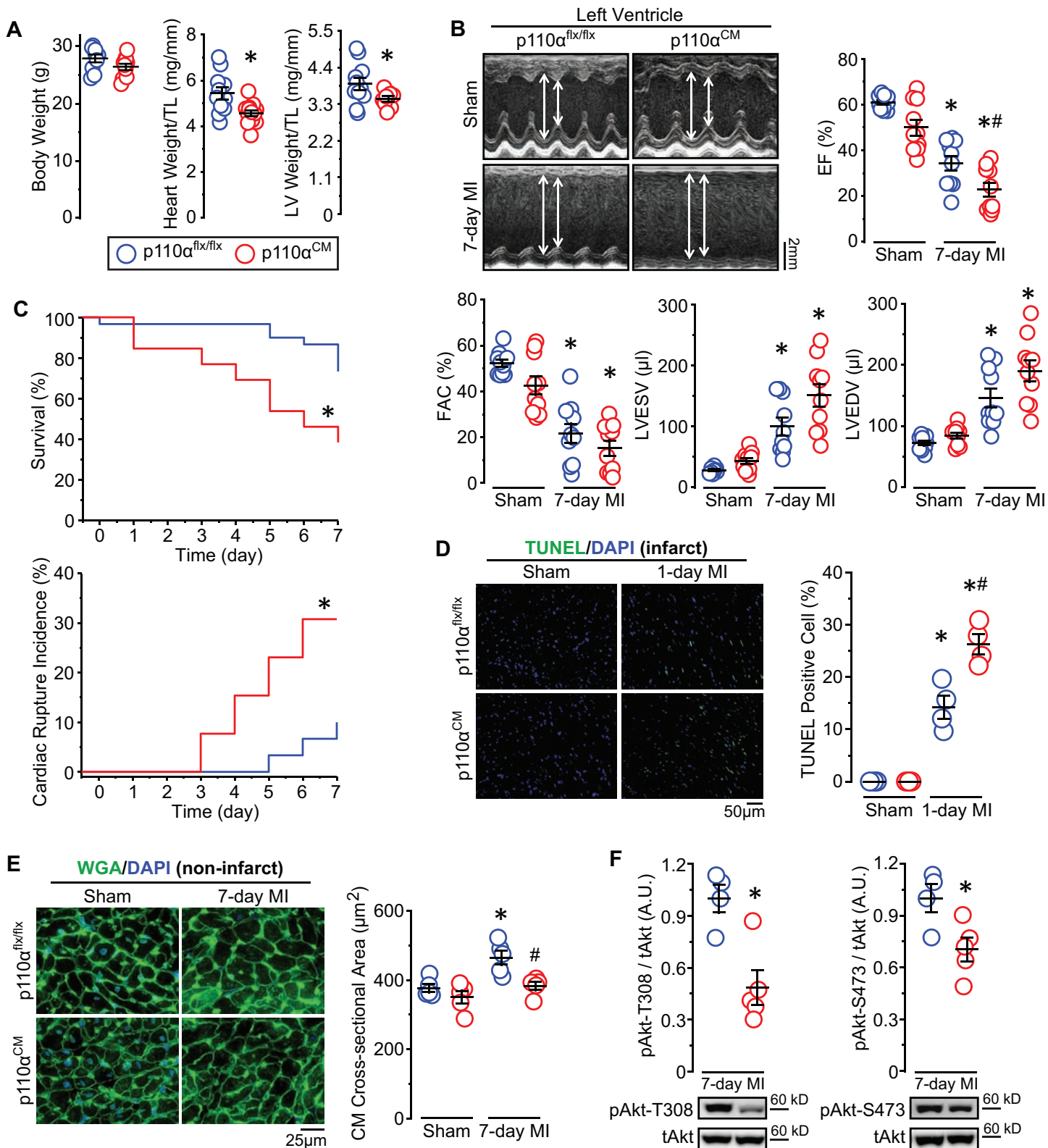


**Figure 7. Role of cardiomyocyte PI3K $\alpha$  at baseline and in post-MI cardiac remodeling.** (A) Body weight, heart weight, and left ventricular weight in cardiomyocyte-specific knockout ( $p110\alpha^{CM}$ ) and control (littermates,  $p110\alpha^{flx/flx}$ ) mice ( $n=9-14$  mice/group). (B) Echocardiographic assessment of cardiac function at 7 days post MI: representative M-mode images, left ventricular ejection fraction (EF), right ventricular fractional area change (FAC), left ventricular end-systolic volume (LVESV), and left ventricular end-diastolic volume (LVEDV) ( $n=10$  mice/group). (C) Kaplan-Meier survival analysis for survival rate (top) and cardiac rupture incidence (bottom) ( $n=13-30$  mice/group). (D) Apoptosis: TUNEL (green) and DAPI (blue) staining: representative images (left) and quantification (right,  $n=4$  hearts/group). (E) Cellular hypertrophy: WGA (green) staining to outline cardiomyocytes: representative images (left) and quantification (right,  $n=5$  hearts/group). (F) Western blots and quantification for Akt in left ventricle lysates from post-MI  $p110\alpha^{CM}$  and  $p110\alpha^{flx/flx}$  hearts ( $n=4-5$  hearts/group). Data are presented as mean  $\pm$  SEM; statistical significance is calculated using independent t-test in A and F, two-way ANOVA with pairwise comparison in B, D, and E, and log-rank test in C; \* $p < 0.05$  vs  $p110\alpha^{flx/flx}$  in A, C, and F, vs sham in B, D, and E, # $p < 0.05$  vs  $p110\alpha^{flx/flx}$  MI.

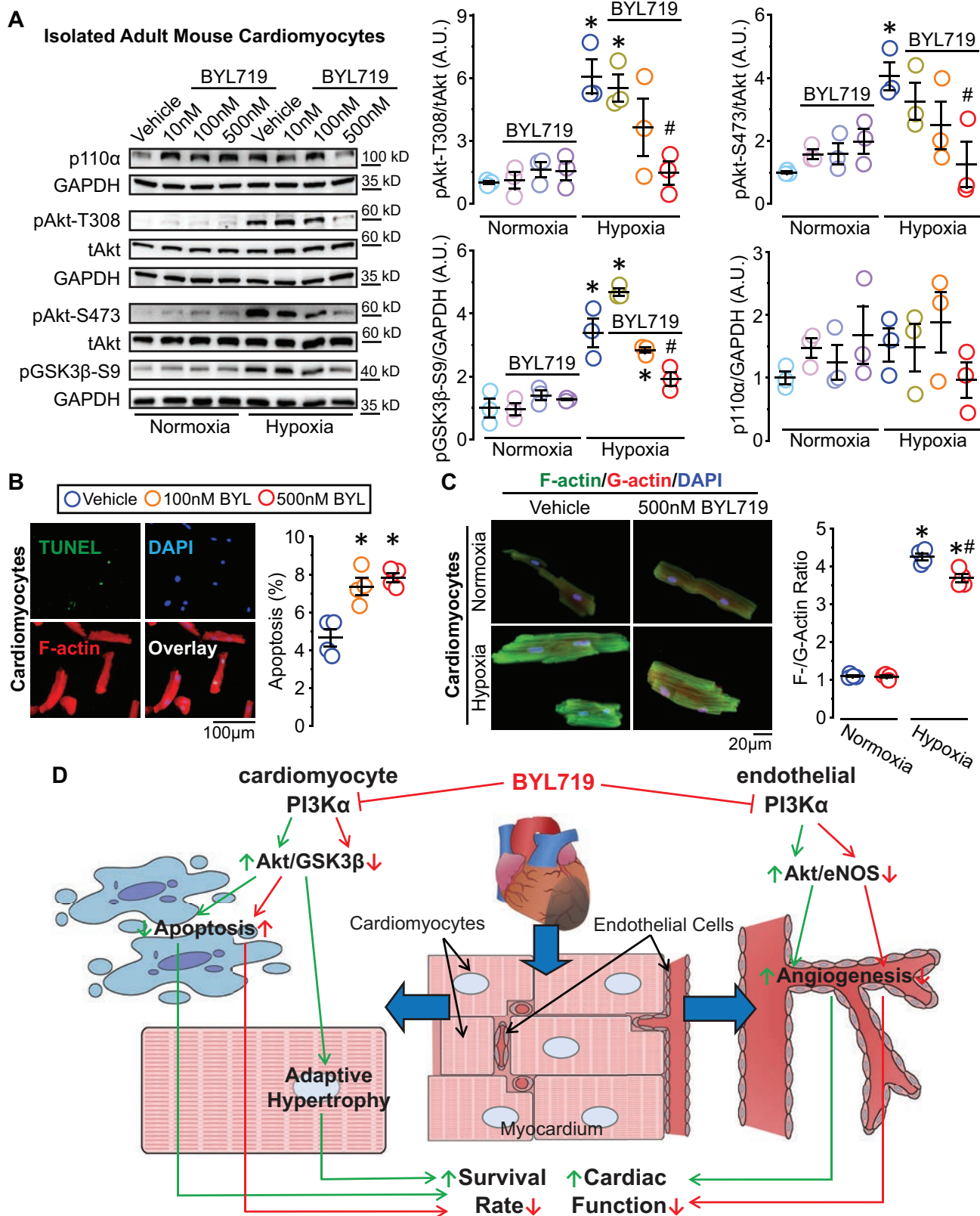


**Figure 8. Effects BYL719 on isolated adult mouse cardiomyocytes under hypoxia and schematic of the roles of PI3K $\alpha$  in cardiomyocytes and endothelial cells at baseline and post MI. (A)** Western blots and quantification of Akt/GSK3 $\beta$  signaling on lysates from cardiomyocytes cultured under normoxic and hypoxic condition (n=6 hearts, 3 independent experiments). **(B)** Representative images (left) and quantification of apoptotic cell death (right) of isolated cardiomyocyte under hypoxic condition with cyclic mechanical stretch (right, n=8 hearts, 4 independent experiments). **(C)** Representative images of F-actin (green), G-actin (red), and DAPI (blue) staining (left) and quantification of F/G-actin ratio (right, n=8 hearts, 4 independent experiments). **(D)** Schematic of the roles of PI3K $\alpha$  in cardiomyocytes and endothelial cells at baseline and post-MI: in cardiomyocyte, PI3K $\alpha$  regulates survival and adaptive hypertrophy; in endothelial cells, PI3K $\alpha$  regulates survival and angiogenesis to maintain vascular distribution in response to MI. Data are presented as mean $\pm$ SEM; statistical significance is calculated using one-way ANOVA in A and B, two-way ANOVA with pairwise comparison in C; \*p<0.05 vs normoxia in A and C, vs vehicle in B, #p<0.05 vs hypoxia-vehicle in A and C.



## Supplemental Information

### Pharmacological and Genetic PI3K $\alpha$ Inhibition Worsens Cardiac Remodeling After Myocardial Infarction

Xueyi Chen<sup>1,3</sup>, Pavel Zhabyeyev<sup>1,3</sup>, Abul K. Azad<sup>1</sup>, Bart Vanhaesebroeck<sup>4</sup>,  
Chad E. Grueter<sup>5</sup>, Allan G. Murray<sup>1</sup>, Zamaneh Kassiri<sup>2,3</sup>,  
and Gavin Y. Oudit<sup>1,3,\*</sup>

<sup>1</sup>Department of Medicine, <sup>2</sup>Department of Physiology, <sup>3</sup>Mazankowski Alberta Heart Institute, University of Alberta, Edmonton, Canada; <sup>4</sup>University College London Cancer Institute, University College London, London, UK. <sup>5</sup>Division of Cardiovascular Medicine, Department of Internal Medicine, Francois M. Abboud Cardiovascular Research Center, Fraternal Order of Eagles Diabetes Research Center, University of Iowa, Iowa City, IA, USA.

**Running title:** PI3K $\alpha$  inhibition worsens myocardial healing after MI

**\*Corresponding Author:** Gavin Y. Oudit, MD, PhD, FRCP(C), Division of Cardiology, Department of Medicine, Mazankowski Alberta Heart Institute, University of Alberta, Edmonton, Alberta, T6G 2R3, Canada; Phone: (780)-407-8569, Fax: (780)-492-9753. Email: gavin.oudit@ualberta.ca.

## Supplemental Methods

### Animal Models and Human Explanted Hearts

Mice were bred and housed at University of Alberta, and all animal experiments were conducted in accordance with the Canadian Council for Animal Care guidelines and the Guide for the Care and Use of Laboratory Animals published by the US National Institutes of Health (revised 2011).

All mice in the study were on the C57/B6 background. Wild type (WT, C57BL/6) mice in experiments studying the effects of pharmacological PI3K $\alpha$  inhibition were purchased from Jackson Laboratory. BYL719 (Chemietek) or vehicle was given to 11- to 12-week-old WT mice in the morning for 10 day (50 mg/Kg/day, *p.o.*). Mouse strains used in the study included p110 $\alpha^{EC}$  and p110 $\alpha^{CM}$ . Mice with inducible endothelial-specific p110 $\alpha$  ablation (p110 $\alpha^{EC}$ ) were generated by crossbreeding p110 $\alpha^{flx/flx}$  mice as previously described, which display *PIK3CA* gene (encoding p110 $\alpha$ ) with floxed 18 and 19 exons [1], with tamoxifen-induced and Tie2 promoter-controlled Cre expression mice (Tie2<sup>MerCreMer</sup>). [2] Tamoxifen (Sigma-Aldrich, 80 mg/kg/day) was given to 10-week-old p110 $\alpha^{EC}$  and control littermates by intraperitoneal injection for 5 days to induce gene deletion in p110 $\alpha^{EC}$  mice, which has previously shown sparing hematopoietic cells from targeted gene deletion. [2] Animals were given two weeks to recover from tamoxifen toxicity and to allow sufficient cre-recombinase expression before experiments. Mice with cardiomyocyte-specific PI3K $\alpha$  ablation (p110 $\alpha^{CM}$ ) were generated by crossbreeding p110 $\alpha^{flx/flx}$  with  $\alpha$ MHC-driven Cre ( $\alpha$ MHC<sup>Cre</sup>) mice. [3, 4] Cre-recombinase deletes exons 18 and 19 from *PIK3CA*, producing a truncated p110 $\alpha$  protein which lacks catalytic

activity. Homozygous littermates p110 $\alpha^{flx/flx}$  from each strain were used as control. Only male mice were used in the experiments.

Myocardial infarction was achieved by permanently ligating the proximal left anterior descending artery (LAD) on WT mice after receiving 3 doses of BYL719 or vehicle and on about 12-week-old p110 $\alpha^{EC}$ , p110 $\alpha^{CM}$ , and control mice. The ligation of LAD or sham surgery was performed by a technician who was blinded to the mouse strains.[5] Briefly, left thoracotomy was performed on 1.5% isoflurane-anesthetized and intubated mice in the fourth intercostal space. After opening the pericardium and exposing the left ventricle, LAD was identified and encircled with a 7-0 silk. LAD was ligated in MI mice, while it was encircled only in sham-operated mice. Afterwards, the muscle and skin were closed in layers with a 6-0 silk suture. Animals were inspected at least twice daily before sacrificed, and survival data were recorded. Autopsy was carried out on each mouse found dead during the study. Mice were sacrificed with intraperitoneal injection of ketamine (100 mg/kg) and xylazine (10 mg/kg) cocktail, and the heart tissue were collected.

Human tissue from non-failing control hearts and failing post-MI hearts were collected as part of the Human Organ Procurement and Exchange program (HOPE) and Human Explanted Heart Program (HELP) respectively, which received ethical approval from the Mazankowski Alberta Heart Institute and the Institutional Ethics Committee.[5, 6] Informed and signed consents were obtained.

### **Echocardiography and Electrocardiogram**

Noninvasive transthoracic echocardiography was performed on mice anesthetized with 1.5% isoflurane in O<sub>2</sub> using Vevo 3100 (Visualsonics). Conventional measurements and speckle-tracking strain analysis was carried out. [5, 7] Global peak systolic strain was calculated as the average of 6 standard anatomical segments. Non-invasive electrocardiogram (ECG) was carried out to evaluate the electrical activity of the heart on mice anesthetized with 1.5% isoflurane in O<sub>2</sub> as described. [2]

### **Immunofluorescence**

Immunofluorescence staining was performed using established protocols[5]. Briefly, optimal cutting temperature compound (OCT)-embedded tissue sections and cultured cells were fixed with 4% paraformaldehyde and rehydrated in wash buffer. Then, permeabilization with 0.1% triton X-100 and blockage with 4% Bovine Serum Albumin were carried out in sequence. The sections were incubated overnight at 4°C with primary antibody, including anti-mouse Ly-6B.2 (AbD Serotec), anti-mouse CD68 (AbD Serotec), anti-CD31 (BD Pharmingen), anti-Ki67 (R&D), or anti-BrdU (Bio-Rad) followed by incubation with secondary antibody (Invitrogen) at 37°C for one hours. After mounting with DAPI media (Life Technologies), the slides were used for visualization and imaging by fluorescence microscopy (Olympus IX81). In addition, Wheat Germ Agglutinin (WGA, Invitrogen) or phalloidin (Invitrogen) staining was performed to identify cardiomyocytes. Fluorescein-conjugated Lectin (Vectorlabs) intravital perfusion was performed to identify the functional vasculature. [5] Fragmented DNA of apoptotic cells was detected using the DeadEnd Fluorometric Terminal Deoxynucleotidyl Transferase-

mediated dUTP Nick-End Labeling (TUNEL) System (Promega) according to instructions.

### **Endothelial Cell Culture, Flow cytometry, and Bead Angiogenesis Assay**

Human umbilical vein endothelial cells (HUVECs) and human coronary artery endothelial cells (HCAECs, ATCC) were used between passage 3 to 7. In vascular endothelial growth factor (VEGF) stimulation experiment, cells were starved in basal medium for 5 hours including 1-hour vehicle or BYL719 incubation prior to stimulation with 50 ng/ml recombinant human VEGF<sub>165</sub> (PeproTech) for 10 minutes. Studying the general effects of BYL719 on Akt signaling, cells were treated with vehicle or BYL719 for 5 hours before protein collection. Cell survival was examined on overnight vehicle- or BYL719-treated cell using flow cytometry (Attune NxT, Invitrogen) with annexin V and propidium iodide staining (Invitrogen).

*In vitro* angiogenesis bead assay of HUVECs/HCAECs was performed as described[5]. Images were captured using a fluorescent inverted microscope (Leica). The number of sprouts and the length of sprouts was analyzed using image analysis software (ImageJ), and at least 30 beads per independent experiment were analyzed.

### **Adult Cardiomyocyte Isolation, Culture, and Stretching**

Adult murine left ventricular cardiomyocytes were isolated from isoflurane (2%)-anesthetized mice; and the isolated cardiomyocytes were cultured and stretched as described. [8, 9] Briefly, after anesthetized and heparinized a mouse, the heart was excised and cannulated on a Langendorff perfusion apparatus. Then, a calcium-free

buffer was perfused in the heart, followed by collagenase digestion. The digested ventricles were teased into small pieces and gently pipetted with an increasing concentration of CaCl<sub>2</sub>. Plated cardiomyocytes were culture with vehicle or BYL719 for 1 hour under normoxia (2% CO<sub>2</sub>) or hypoxia (1% O<sub>2</sub>, 2% CO<sub>2</sub>) before protein collection. PI3K $\gamma$  inhibitor-AS252424 was used at 400 nmol/L. Cyclical mechanical stretch of cardiomyocytes was achieved using Flexcell FX-5000 Tension System (Flexcell International Corp) at 1Hz and 5% elongation for 3 hours in serum-free culture medium under hypoxic atmosphere. Then, cardiomyocytes were fixed in 4% paraformaldehyde and imaged under light microscope to assess the cell viability. TUNEL staining was performed to access apoptosis rate.

### **Immunoblotting**

Immunoblotting was performed as previously described[2]. Extracted proteins from tissue or cells were separated by 8% to 15% sodium dodecyl sulfate polyacrylamide gel electrophoresis, followed by electrotransfer to polyvinylidene difluoride membranes. Primary antibodies, including phospho-(Thr308)/phospho-(Ser473)/total Akt, phospho-(Thr202/Tyr204)/total p44/42 MAPK (Erk1/2), phospho-eNOS (Ser1177)/eNOS, PI3K p110 $\alpha$ , phospho-(Ser9)/total GSK3 $\beta$ , and GAPDH (Cell Signaling Technology), were used in the study. Blots were visualized and analyzed using ImageQuant LAS 4000 (GE Healthcare).

## Statistical Analysis

Statistical analyses were carried out using SPSS Statistics 24 software, and statistical significance was defined as  $p < 0.05$  (two-sided). Continuous data were presented in scatter plots with mean  $\pm$  SEM. The differences between two independent groups were evaluated using independent t-test or Mann-Whitney U test after normality examination. Paired t-test was carried out for two paired groups. One-way ANOVA or Kruskal-Wallis test with pairwise comparisons were used in studies with more than two groups based on the normality of the data. Two-way ANOVA was used to compare the differences between groups with two independent variables. Repeated measures ANOVA was carried out in data with multiple measures. Categorical data was compared using Fisher exact test. Survival data were presented as the Kaplan-Meier plots, and the log-rank test was used to evaluate the statistical significance.

## References

- [1] M. Graupera, J. Guillermet-Guibert, L.C. Foukas, L.K. Phng, R.J. Cain, A. Salpekar, et al., Angiogenesis selectively requires the p110 $\alpha$  isoform of PI3K to control endothelial cell migration, *Nature* 453(7195) (2008) 662-6.
- [2] X. Chen, P. Zhabyeyev, A.K. Azad, W. Wang, R.A. Minerath, J. DesAulniers, et al., Endothelial and cardiomyocyte PI3K $\beta$  divergently regulate cardiac remodelling in response to ischaemic injury, *Cardiovascular research* 115(8) (2019) 1343-1356.
- [3] J. Guillermet-Guibert, K. Bjorklof, A. Salpekar, C. Gonella, F. Ramadani, A. Bilancio, et al., The p110 $\beta$  isoform of phosphoinositide 3-kinase signals downstream of G protein-coupled receptors and is functionally redundant with p110 $\gamma$ , *Proceedings of the National Academy of Sciences of the United States of America* 105(24) (2008) 8292-7.

- [4] B.A. McLean, P. Zhabyeyev, V.B. Patel, R. Basu, N. Parajuli, J. DesAulniers, et al., PI3K $\alpha$  is essential for the recovery from Cre/tamoxifen cardiotoxicity and in myocardial insulin signalling but is not required for normal myocardial contractility in the adult heart, *Cardiovascular research* 105(3) (2015) 292-303.
- [5] W. Wang, S.M. McKinnie, V.B. Patel, G. Haddad, Z. Wang, P. Zhabyeyev, et al., Loss of Apelin exacerbates myocardial infarction adverse remodeling and ischemia-reperfusion injury: therapeutic potential of synthetic Apelin analogues, *Journal of the American Heart Association* 2(4) (2013) e000249.
- [6] M. Litvinukova, C. Talavera-Lopez, H. Maatz, D. Reichart, C.L. Worth, E.L. Lindberg, et al., Cells of the adult human heart, *Nature* doi: 10.1038/s41586-020-2797-4. (2020).
- [7] M. Bauer, S. Cheng, M. Jain, S. Ngoy, C. Theodoropoulos, A. Trujillo, et al., Echocardiographic speckle-tracking based strain imaging for rapid cardiovascular phenotyping in mice, *Circ Res* 108(8) (2011) 908-16.
- [8] D. Li, J. Wu, Y. Bai, X. Zhao, L. Liu, Isolation and culture of adult mouse cardiomyocytes for cell signaling and in vitro cardiac hypertrophy, *Journal of visualized experiments : JoVE* (87) (2014).
- [9] V.B. Patel, P. Zhabyeyev, X. Chen, F. Wang, M. Paul, D. Fan, et al., PI3K $\alpha$ -regulated gelsolin activity is a critical determinant of cardiac cytoskeletal remodeling and heart disease, *Nature communications* 9(1) (2018) 5390.



**Table S1. Ten the most affected genes in mice treated with BYL.**

Gene	log <sub>2</sub> FC	Protein / RNA	Function
Zbtb16	2.186	Zinc finger and BTB domain-containing protein 16	Nuclear protein involved in cell cycle progression and interacts with a histone deacetylase
Egr1	-2.093	Early Growth Response 1	cancer suppressor gene
Nr4a1	-2.025	Nuclear Receptor Subfamily 4 Group A Member 1	Translocation of the protein from the nucleus to mitochondria induces apoptosis
Errfi1	-1.533	ERBB Receptor Feedback Inhibitor 1	expression is upregulated with cell growth
Xdh	1.258	xanthine dehydrogenase	oxidative metabolism of purines
Neat1	1.256	Nuclear Paraspeckle Assembly Transcript 1	lncRNA (core structural component of the paraspeckle sub-organelles)
Fmo2	1.164	Flavin Containing Dimethyl-aniline Monooxygenase 2	catalyzes the N-oxidation of some primary alkylamines
Nes	-1.094	Nestin	intermediate filament protein (nerve cells)
Dusp1	-1.071	Dual Specificity Phosphatase 1	dephosphorylate MAP kinase MAPK1/ERK2
Pim3	1.040	Pim-3 Proto-Oncogene, Serine/Threonine Kinase	overexpressed in hematological and epithelial tumors

RNA-seq was performed on RNA extracted from the hearts of mice after 10-day vehicle or BYL719 treatment; FC, fold change. Genes with expression levels of at least 1% of maximal expression level in either WT-placebo or WT-BYL group and with  $p_{adj} < 0.1$  were selected for analysis.

**Table S2. Cardiac Function in Vehicle- and BYL719-treated Mice by Echocardiography**

Mean $\pm$ SEM	Sham		MI	
	WT-Vehicle	WT-BYL	WT-Vehicle	WT-BYL
Sample Size	11	10	10	14
HR (bpm)	446 $\pm$ 10	496 $\pm$ 17	420 $\pm$ 16	493 $\pm$ 16 #
EF (%)	63.21 $\pm$ 1.13	62.87 $\pm$ 1.88	36.64 $\pm$ 2.94 *	21.63 $\pm$ 1.56 *#
FAC (%)	53.75 $\pm$ 1.04	55.46 $\pm$ 2.42	24.95 $\pm$ 4.01 *	9.29 $\pm$ 1.14 *#
WMSI	1.00 $\pm$ 0.00	1.00 $\pm$ 0.00	1.83 $\pm$ 0.06 *	2.24 $\pm$ 0.05 *#
SV ( $\mu$ l)	51.54 $\pm$ 2.25	37.01 $\pm$ 2.19 #	41.37 $\pm$ 2.88 *	28.89 $\pm$ 1.12 *#
LVESV ( $\mu$ l)	29.86 $\pm$ 1.36	22.33 $\pm$ 2.19	78.69 $\pm$ 14.28 *	112.43 $\pm$ 9.80 *#
LVEDV ( $\mu$ l)	81.40 $\pm$ 2.97	59.35 $\pm$ 3.92	120.06 $\pm$ 15.31 *	141.32 $\pm$ 10.15 *
LVPWd (mm)	0.66 $\pm$ 0.02	0.68 $\pm$ 0.02	0.62 $\pm$ 0.03	0.37 $\pm$ 0.03 *#
E'/A'	1.14 $\pm$ 0.02	0.99 $\pm$ 0.06	0.91 $\pm$ 0.12	0.87 $\pm$ 0.07
LA Size (mm)	1.57 $\pm$ 0.05	1.57 $\pm$ 0.05	1.92 $\pm$ 0.11 *	1.97 $\pm$ 0.08 *

Echocardiography was performed on 10-day vehicle- or BYL719-treated mice which received sham or MI surgery on day-3 post-treatment. HR indicates heart rate; bpm, beats per minute; EF, ejection fraction; FAC, fractional area change; WMSI, wall motion score index; SV, stroke volume; LVESV, left ventricular end-systolic volume; LVEDV, left ventricular end-diastolic volume; LVPWd, end-diastolic left ventricular posterior wall thickness; LA size, left atrial size. \* $p$ <0.05 vs sham; # $p$ <0.05 vs WT-Vehicle in two-way ANOVA.

**Table S3. Cardiac Function in p110 $\alpha$ <sup>EC</sup> and littermate control Mice by echocardiography**

Mean $\pm$ SEM	Sham		MI	
	p110 $\alpha$ <sup>flx/flx</sup>	p110 $\alpha$ <sup>EC</sup>	p110 $\alpha$ <sup>flx/flx</sup>	p110 $\alpha$ <sup>EC</sup>
Sample Size	10	10	10	10
HR (bpm)	411 $\pm$ 10	428 $\pm$ 21	430 $\pm$ 16	420 $\pm$ 25
EF (%)	59.69 $\pm$ 1.17	61.98 $\pm$ 1.99	32.29 $\pm$ 2.34*	21.24 $\pm$ 1.56*#
FAC (%)	50.86 $\pm$ 2.37	51.93 $\pm$ 1.79	19.51 $\pm$ 3.14*	8.17 $\pm$ 1.78*#
WMSI	1.00	1.00	1.86 $\pm$ 0.07*	2.24 $\pm$ 0.05*#
SV ( $\mu$ l)	40.44 $\pm$ 2.52	42.17 $\pm$ 3.20	38.00 $\pm$ 2.47	31.90 $\pm$ 2.72*
LVESV ( $\mu$ l)	27.42 $\pm$ 1.86	26.79 $\pm$ 3.26	85.74 $\pm$ 10.94*	120.57 $\pm$ 10.93*#
LVEDV ( $\mu$ l)	67.86 $\pm$ 4.11	68.96 $\pm$ 5.98	123.73 $\pm$ 12.75*	152.47 $\pm$ 12.55*#
LVPWd (mm)	0.64 $\pm$ 0.04	0.65 $\pm$ 0.02	0.68 $\pm$ 0.04	0.58 $\pm$ 0.09
E'/A'	1.23 $\pm$ 0.05	1.26 $\pm$ 0.07	0.96 $\pm$ 0.09*	0.71 $\pm$ 0.02*#
LA Size (mm)	1.63 $\pm$ 0.08	1.72 $\pm$ 0.07	2.08 $\pm$ 0.13*	2.34 $\pm$ 0.17*

Echocardiography was performed on 7-day post-surgery p110 $\alpha$ <sup>EC</sup> and p110 $\alpha$ <sup>flx/flx</sup> mice. HR indicates heart rate; bpm, beats per minute; EF, ejection fraction; FAC, fractional area change; WMSI, wall motion score index; SV, stroke volume; LVESV, left ventricular end-systolic volume; LVEDV, left ventricular end-diastolic volume; LVPWd, end-diastolic left ventricular posterior wall thickness; LA size, left atrial size. \*p<0.05 vs sham; #p<0.05 vs WT-Vehicle in two-way ANOVA.

**Table S4. Cardiac Function in p110 $\alpha$ <sup>CM</sup> and littermate control mice by echocardiography**

Mean $\pm$ SEM	Sham		MI	
	p110 $\alpha$ <sup>flx/flx</sup>	p110 $\alpha$ <sup>CM</sup>	p110 $\alpha$ <sup>flx/flx</sup>	p110 $\alpha$ <sup>CM</sup>
Sample Size	10	10	10	10
HR (bpm)	440 $\pm$ 13.58	503 $\pm$ 15.25	446 $\pm$ 14.67	444 $\pm$ 15.25
EF (%)	60.84 $\pm$ 0.99	49.97 $\pm$ 3.48	34.22 $\pm$ 3.22 *	22.81 $\pm$ 2.70 *#
FAC (%)	52.26 $\pm$ 1.63	42.60 $\pm$ 4.05	21.61 $\pm$ 4.23 *	15.26 $\pm$ 3.32 *
SV ( $\mu$ l)	44.04 $\pm$ 2.61	41.11 $\pm$ 2.02	46.53 $\pm$ 3.22	39.10 $\pm$ 2.70
LVESV ( $\mu$ l)	28.16 $\pm$ 1.43	43.38 $\pm$ 4.95	99.70 $\pm$ 14.47 *	150.97 $\pm$ 18.54*#
LVEDV ( $\mu$ l)	72.20 $\pm$ 3.75	84.49 $\pm$ 4.78	146.23 $\pm$ 15.43 *	190.07 $\pm$ 17.44*#
LVPWd (mm)	0.65 $\pm$ 0.03	0.56 $\pm$ 0.02	0.63 $\pm$ 0.05	0.62 $\pm$ 0.02
E'/A'	1.19 $\pm$ 0.04	1.07 $\pm$ 0.05	0.81 $\pm$ 0.06 *	0.79 $\pm$ 0.07 *
LA Size (mm)	1.68 $\pm$ 0.06	1.76 $\pm$ 0.09	1.98 $\pm$ 0.16	2.28 $\pm$ 0.19

Echocardiography was performed on 7-day post-surgery p110 $\alpha$ <sup>CM</sup> and p110 $\alpha$ <sup>flx/flx</sup> mice. HR indicates heart rate; bpm, beats per minute; EF, ejection fraction; FAC, fractional area change; SV, stroke volume; LVESV, left ventricular end-systolic volume; LVEDV, left ventricular end-diastolic volume; LVPWd, end-diastolic left ventricular posterior wall thickness; LA size, left atrial size. \*P<0.05 vs sham; #P<0.05 vs WT-Vehicle in two-way ANOVA.

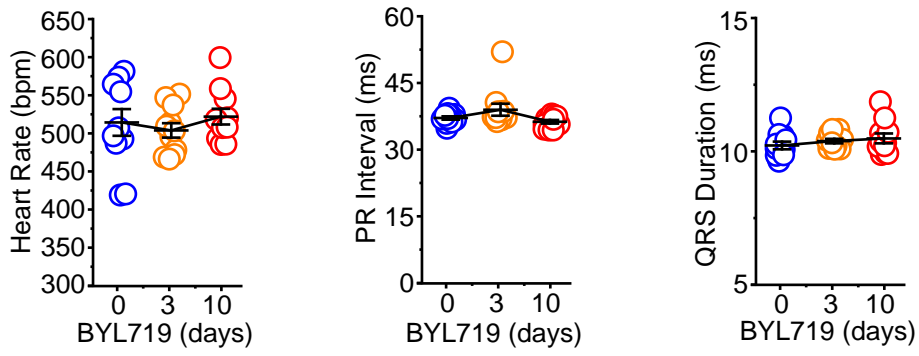


**Figure S1.** Heart rate, PR interval, and QRS duration in mice treated with BYL719 on Day 0 (before administration), Day 3, and Day 10 (n=11 mice). Data are presented as mean $\pm$ SEM.

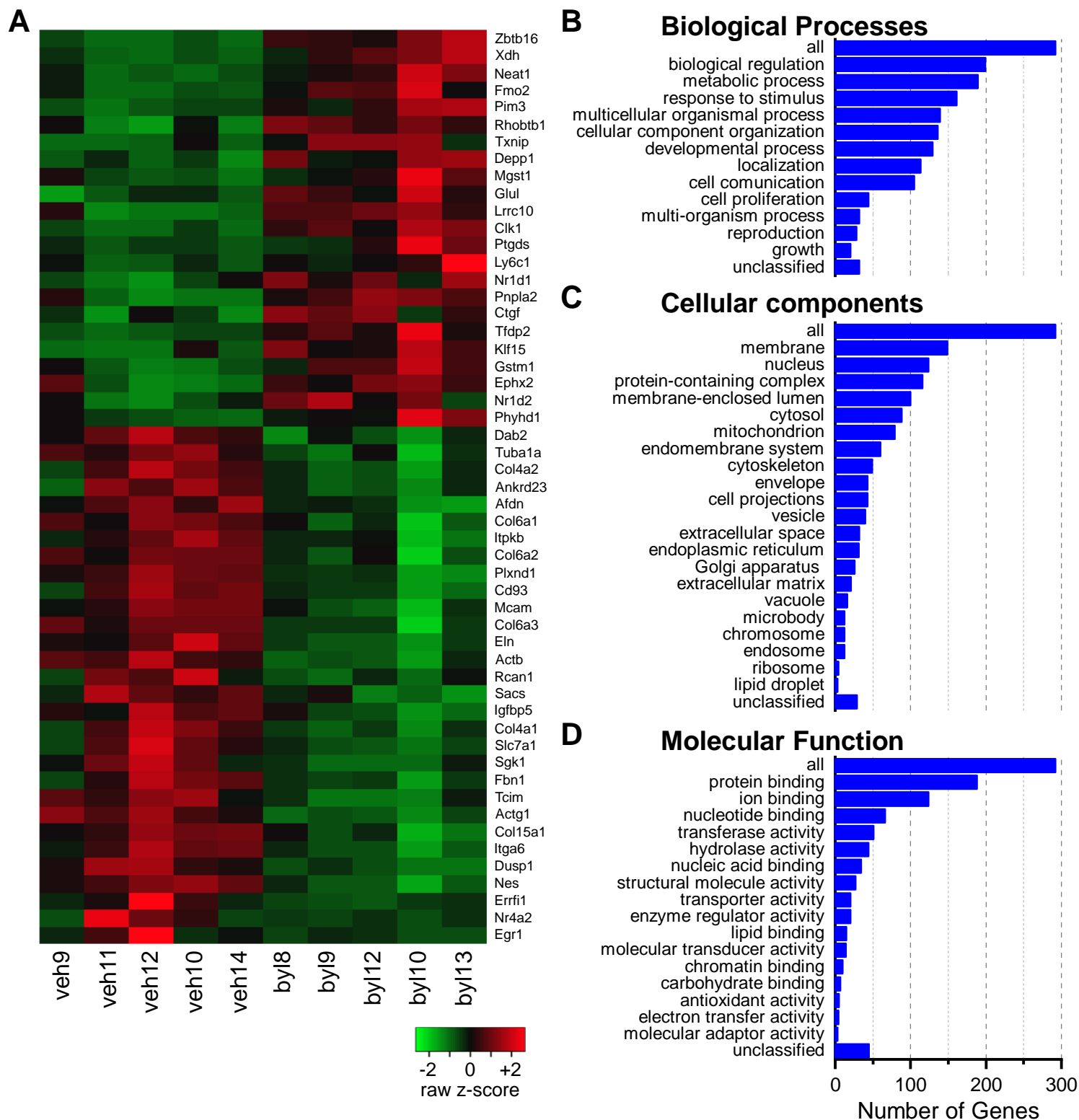


**Figure S2. Alteration in transcriptome of LV tissue after 10-day treatment with BYL719. (A)** Heatmap of differential expression in left ventricle: vehicle vs BYL719 (10-day treatment). **(B)** Number of altered genes (X axis) per biological process categories using Web Gestalt Gene Set Enrichment Analysis (Gene ontology). **(C)** Number of altered genes (X axis) per cellular components categories using Web Gestalt Gene Set Enrichment Analysis (Gene ontology). **(D)** Number of altered genes (X axis) per molecular function categories using Web Gestalt Gene Set Enrichment Analysis (Gene ontology).

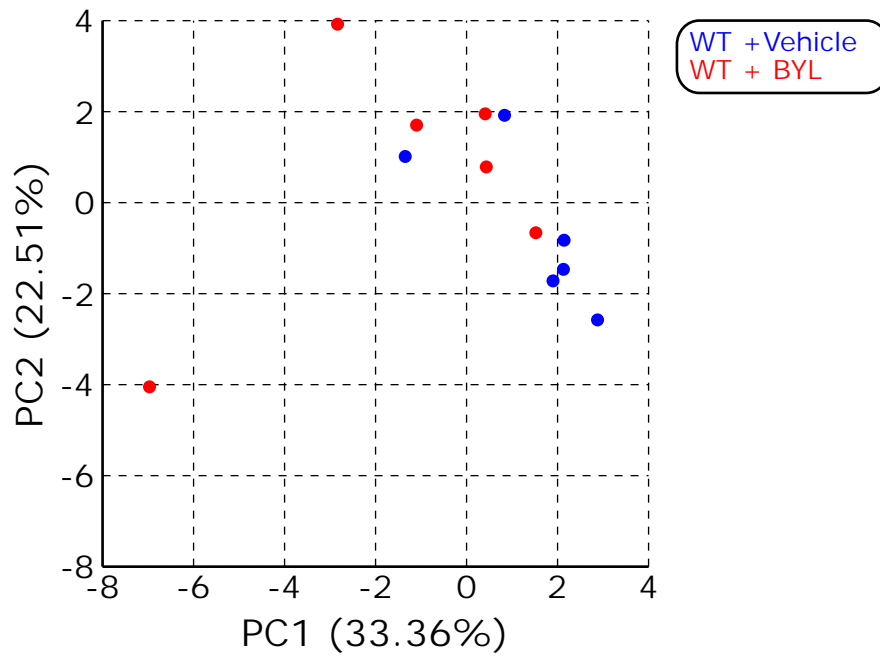


**Figure S3.** Primary Component Analysis (PCA) of RNA seq expression levels in the left ventricle of WT mice treated with vehicle or BYL719 for 10 days.

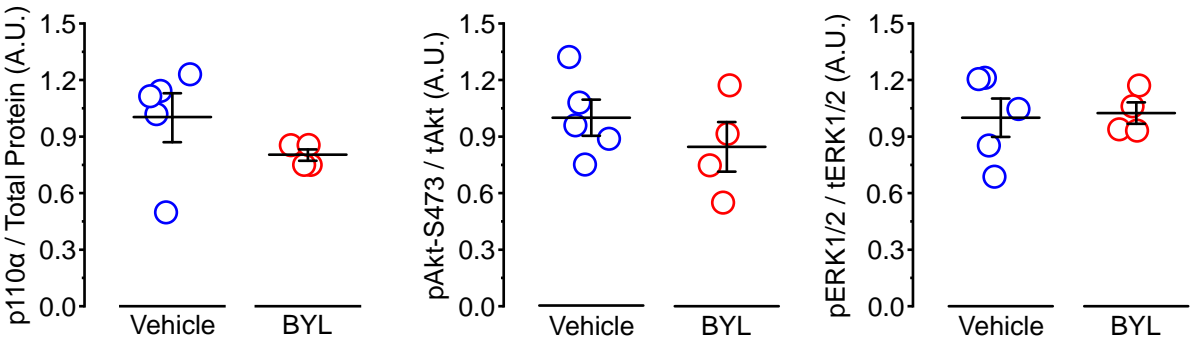


**Figure S4.** Western blots quantifications of total p110 $\alpha$  levels, phosphorylation of Akt-S473, and phosphorylation of ERK1/2 in left ventricular lysates at 7 days post MI (n=4-5 hearts/group). Data are presented as mean $\pm$ SEM.



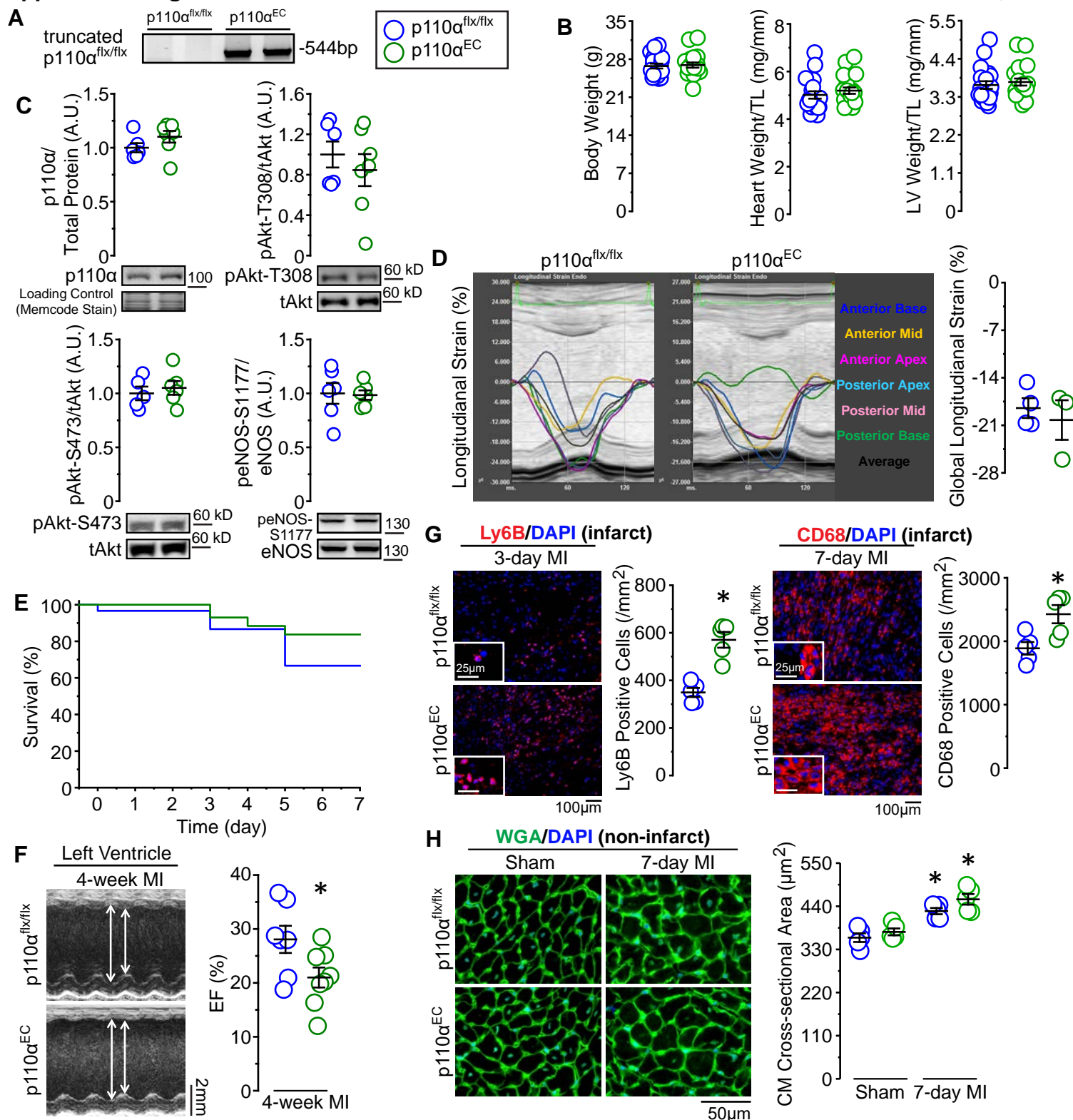


**Figure S5. (A)** Representative image of the gel showing the amplified DNA fragment with truncated *PIK3CA* allele. Genomic DNA was extracted from lung tissue. **(B)** Body weight, heart weight, and left ventricular weight from control (p110α<sup>flx/flx</sup>) and p110α<sup>EC</sup> (n=20-23 mice/group). **(C)** Western blot assessment of p110α, Akt, and eNOS protein levels from left ventricular lysates (n=6-7 hearts/group). **(D)** Left ventricular longitudinal strain analysis on p110α<sup>EC</sup> and control (p110α<sup>flx/flx</sup>) mice (n=3-4 mice/group). **(E)** Kaplan-Meier survival analysis in post-MI p110α<sup>EC</sup> and control (p110α<sup>flx/flx</sup>) mice (n=30-43 mice/group). **(F)** Echocardiography analysis at 4-week post-MI showing ejection fraction (EF) p110α<sup>EC</sup> and control (p110α<sup>flx/flx</sup>) mice (n=7-8 mice/group). **(G)** Inflammation: immunofluorescence staining for neutrophils (Ly6B, red) and macrophages (CD68, red) (n=5 hearts/group). **(H)** Cellular hypertrophy: representative immunofluorescence images of wheat germ agglutinin (WGA, green) staining to outline cardiomyocytes and quantification of cardiomyocyte cross-sectional area (n=5 hearts/group); DAPI (blue). Data are presented as mean±SEM; statistical significance is calculated using independent t-test in B-D, F, and G, log-rank test in E, two-way ANOVA with pairwise comparison in H; \*p<0.05 vs p110α<sup>flx/flx</sup> in F and G and vs sham in H.

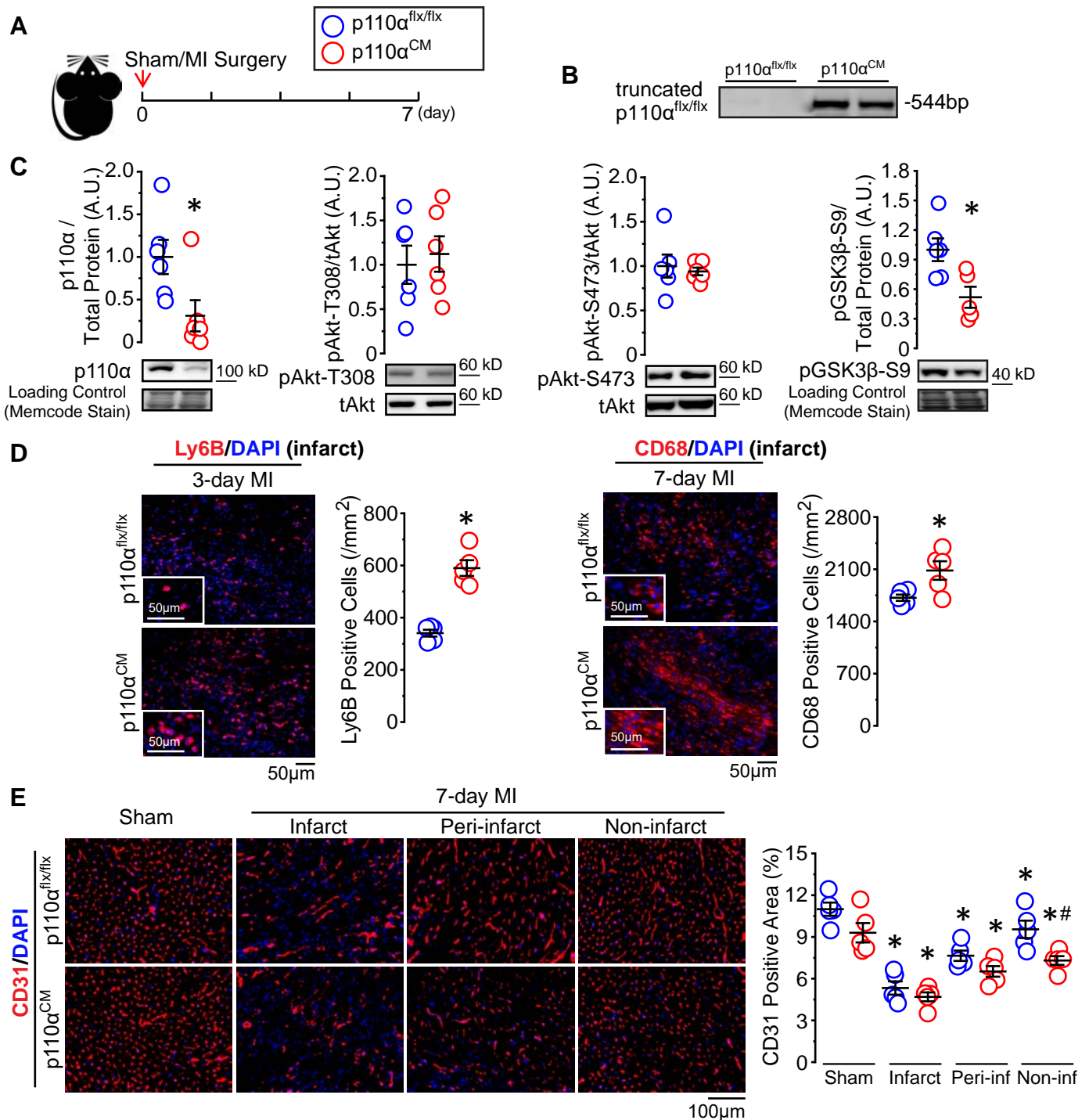


**Figure S6. (A)** Schematic of experimental design for testing the role of cardiomyocyte PI3K $\alpha$  in post-MI remodeling using cardiomyocyte-specific knock-out ( $p110\alpha^{CM}$ ) and control ( $p110\alpha^{flx/flx}$  littermates) mice. **(B)** Representative image of the gel showing the amplified DNA fragment with truncated *PIK3CA* allele. Genomic DNA was extracted from heart tissue (LV). **(C)** Western blots and quantifications of total p110 $\alpha$  levels, phosphorylation of Akt-T308, phosphorylation of Akt-S473, and phosphorylation of GSK3 $\beta$ -S9 in left ventricular lysates (n=6 hearts/group). **(D)** Inflammation: immunofluorescence staining for neutrophils (anti-Ly6B, red; representative images, left, and quantification, right) and macrophages (anti-CD68, red; representative images, left, and quantification, right); DAPI (blue); n=5 hearts/group. **(E)** Vascularization: endothelial cell immunofluorescence staining (anti-CD31, red); DAPI (blue); representative images (left) and quantification (right, n=5 hearts/group). Data are presented as mean $\pm$ SEM; statistical significance is calculated using independent t-test in C and D, two-way ANOVA with pairwise comparisons in E. \* $p$ <0.05 vs  $p110\alpha^{flx/flx}$  in C and D, vs sham in E; # $p$ <0.05 vs  $p110\alpha^{flx/flx}$  within the same treatment in E.

## Isolated Adult Mouse Cardiomyocytes

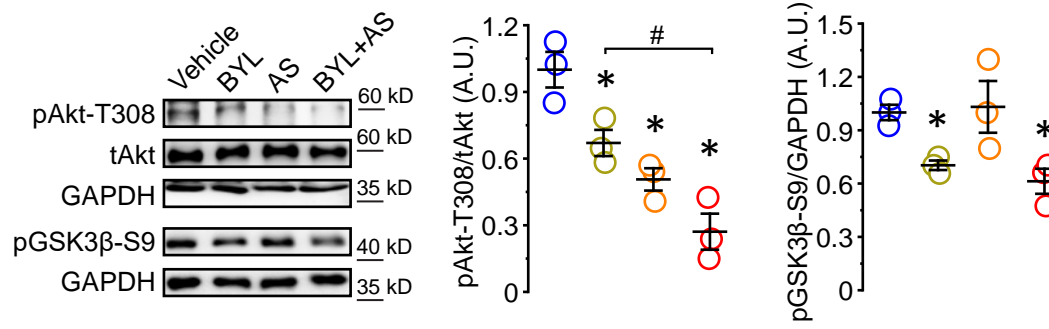
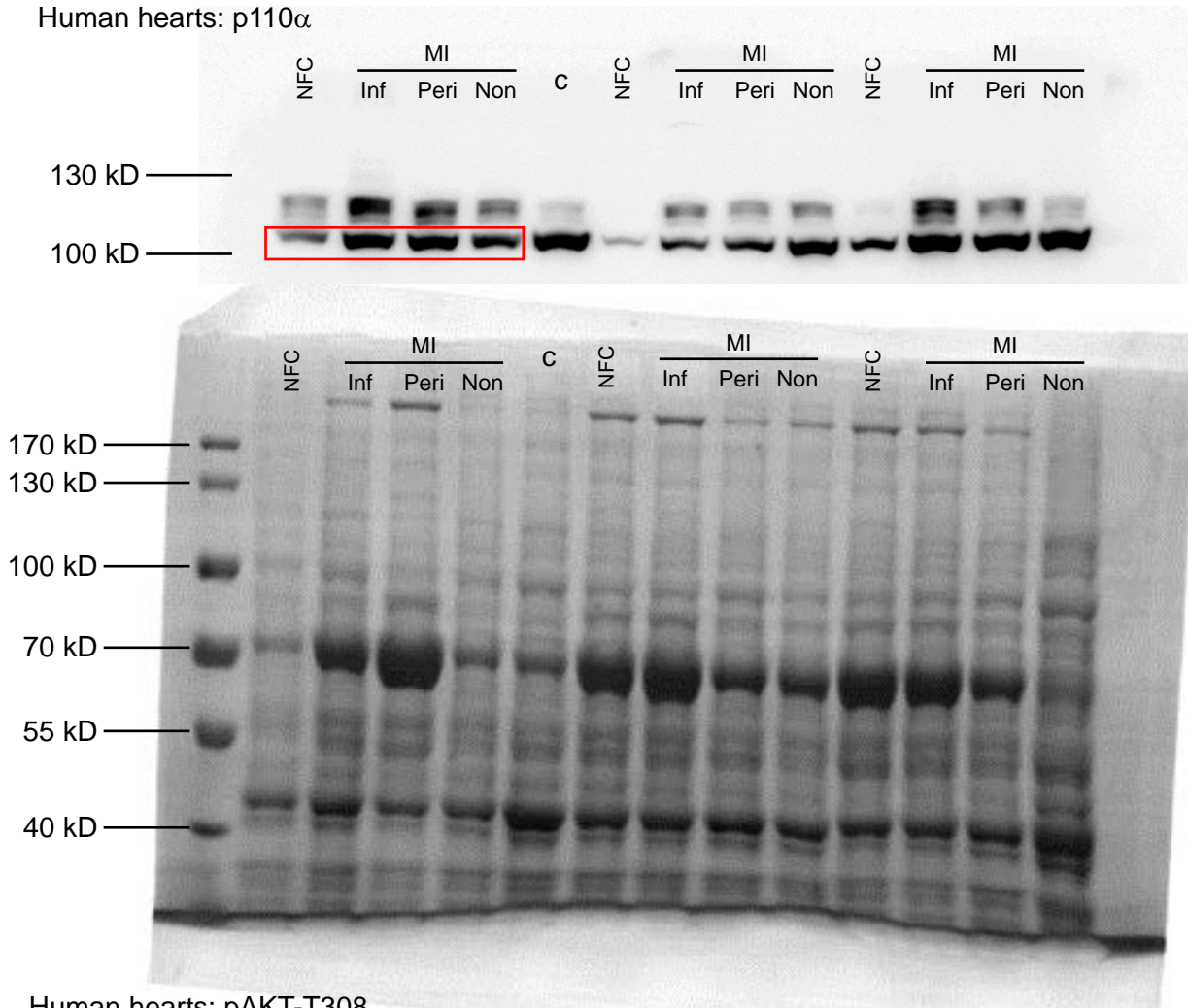


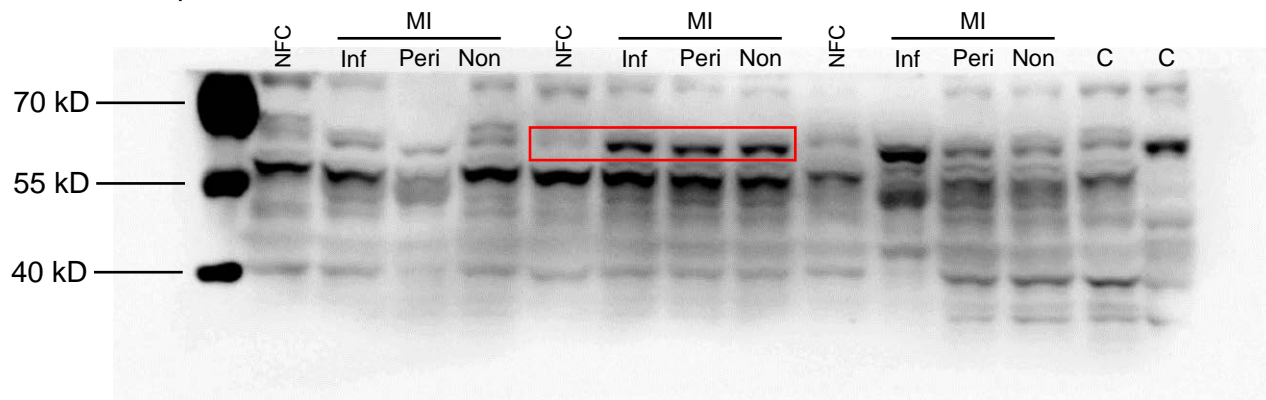
**Figure S7.** Western blots and quantifications of phosphorylation of levels of Akt-T308 and GSK3β-S9 in lysates of isolated cardiomyocytes (n=3 independent experiments); AS, PI3Kγ-specific inhibitor AS252424. Data are presented as mean±SEM; statistical significance is calculated using one-way ANOVA; \*p<0.05 vs vehicle.

## Figure 2A:

Human hearts: p110 $\alpha$



Human hearts: pAKT-T308



Human hearts: tAKT

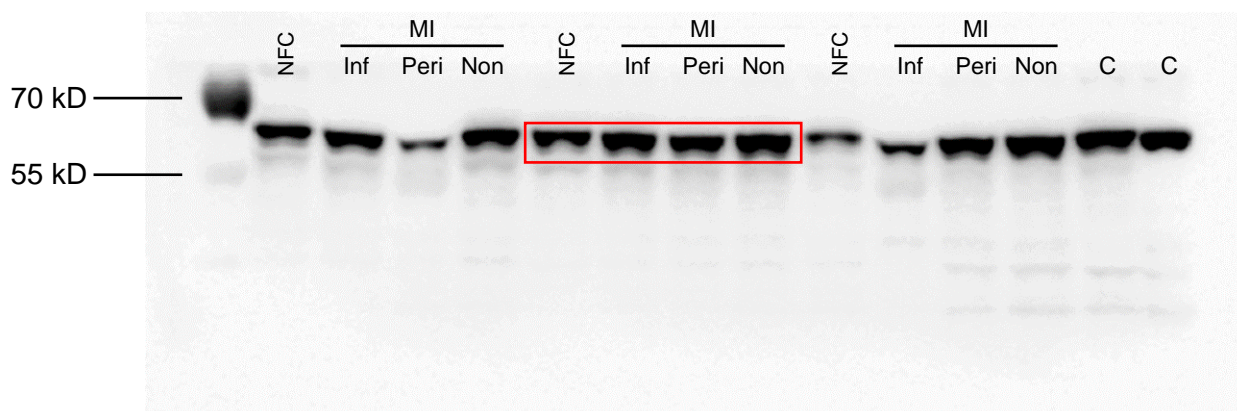
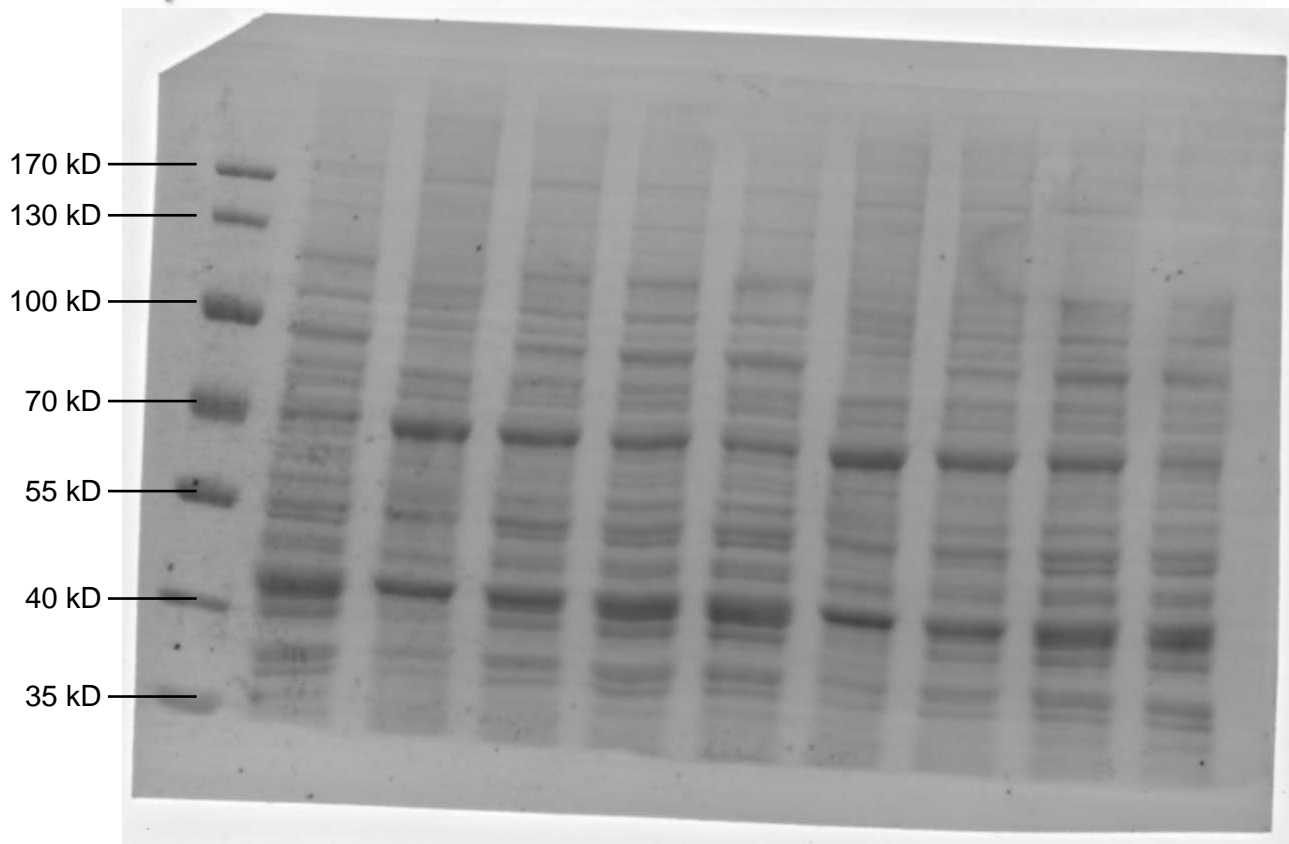
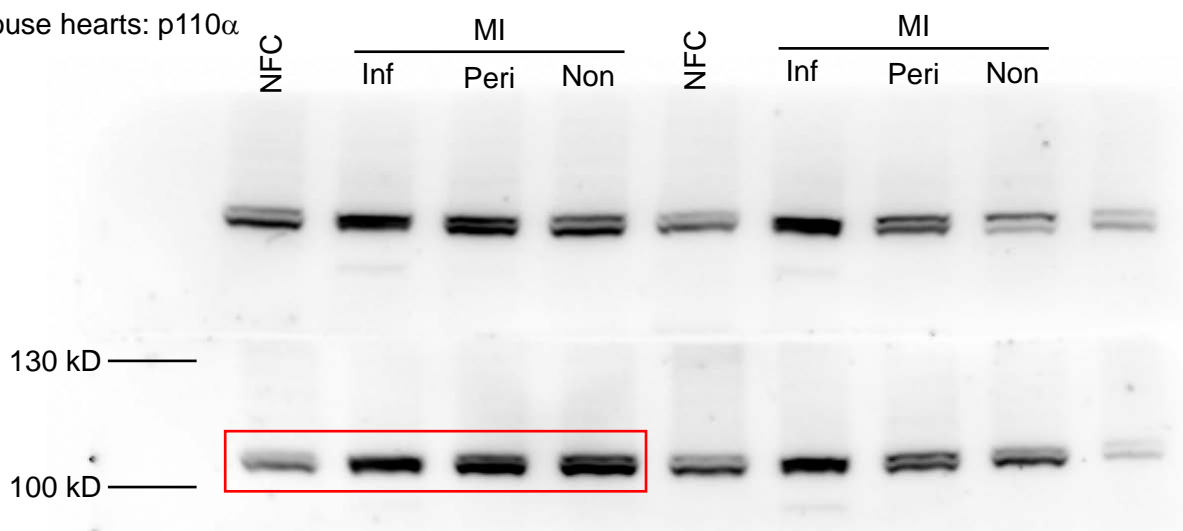


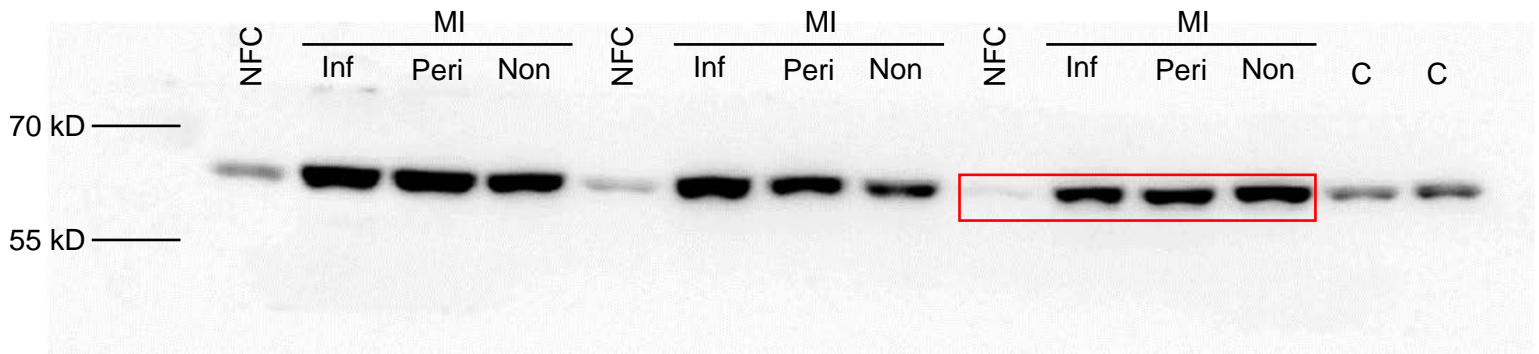
Figure 2A (continued):

Mouse hearts: p110 $\alpha$

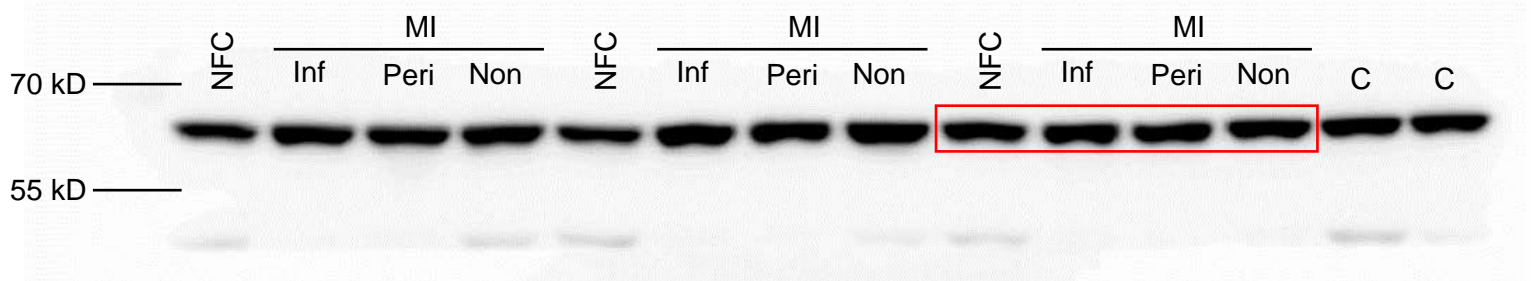


## Figure 2A (continued):

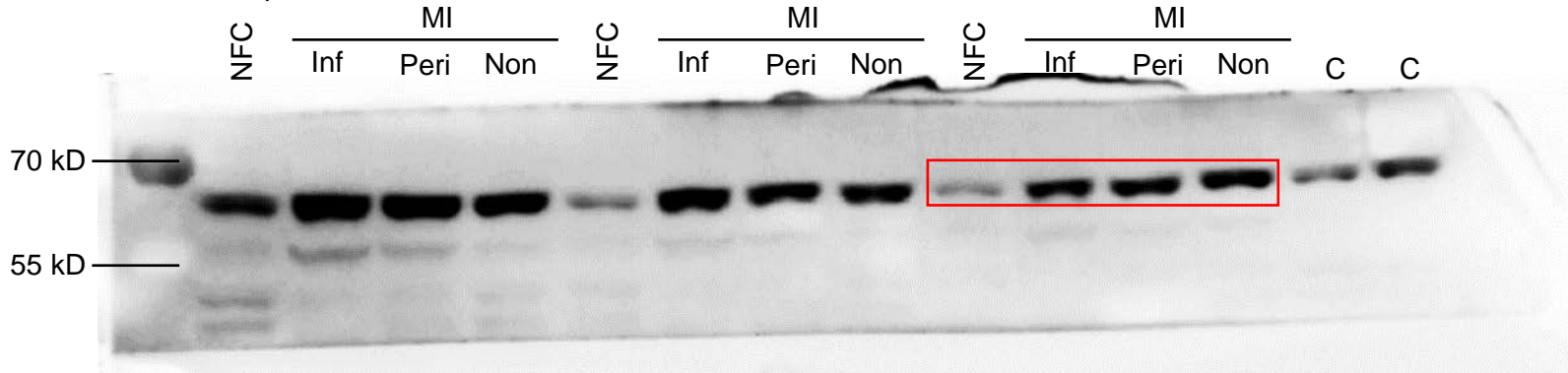
Mouse hearts: pAkt-T308



Mouse hearts: tAkt:



Mouse hearts: pAkt-S473



Mouse hearts: tAkt

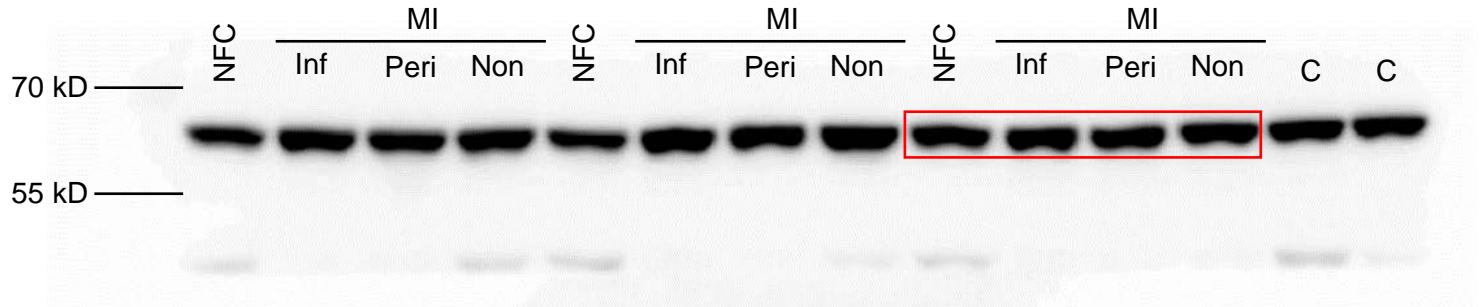
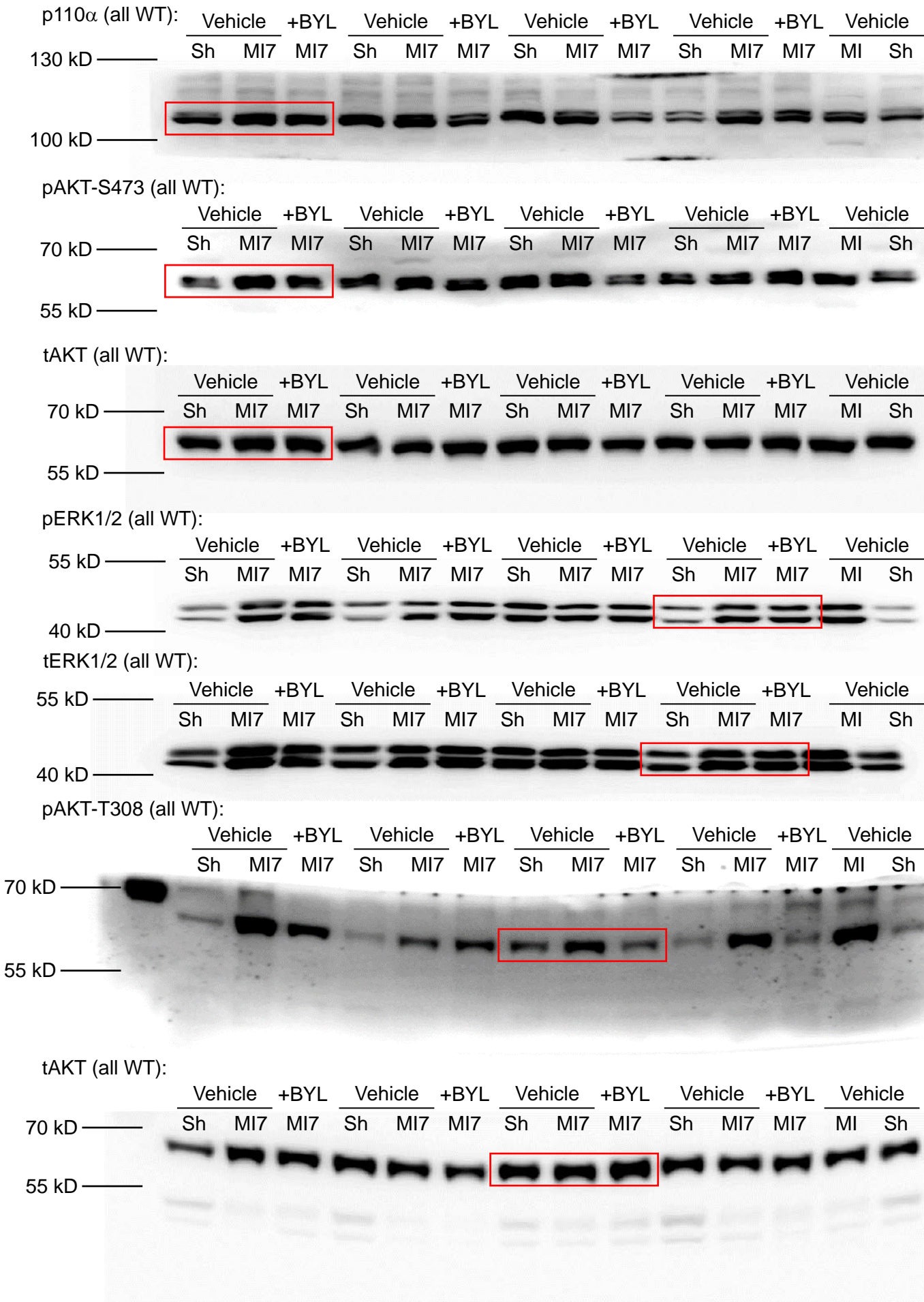


Figure 3E:

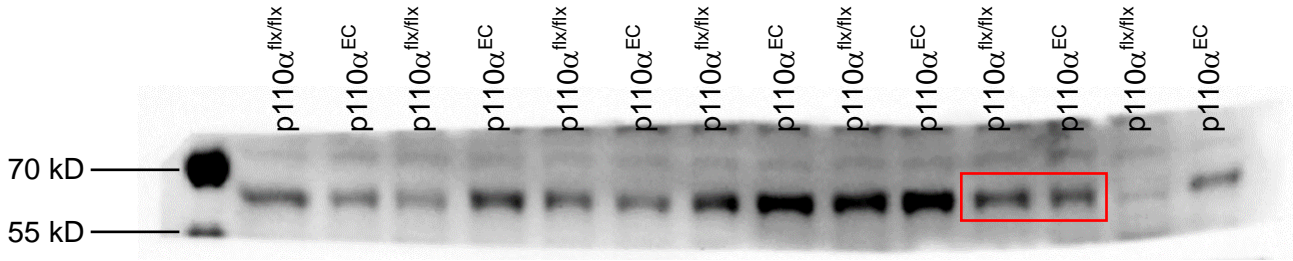




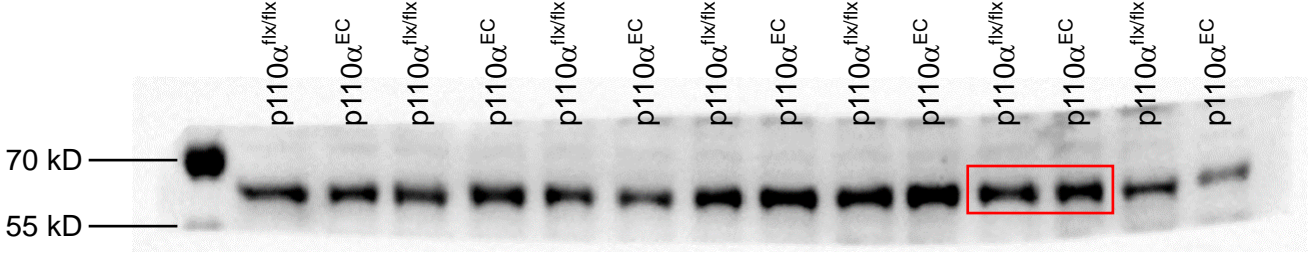


# Figure 4F:

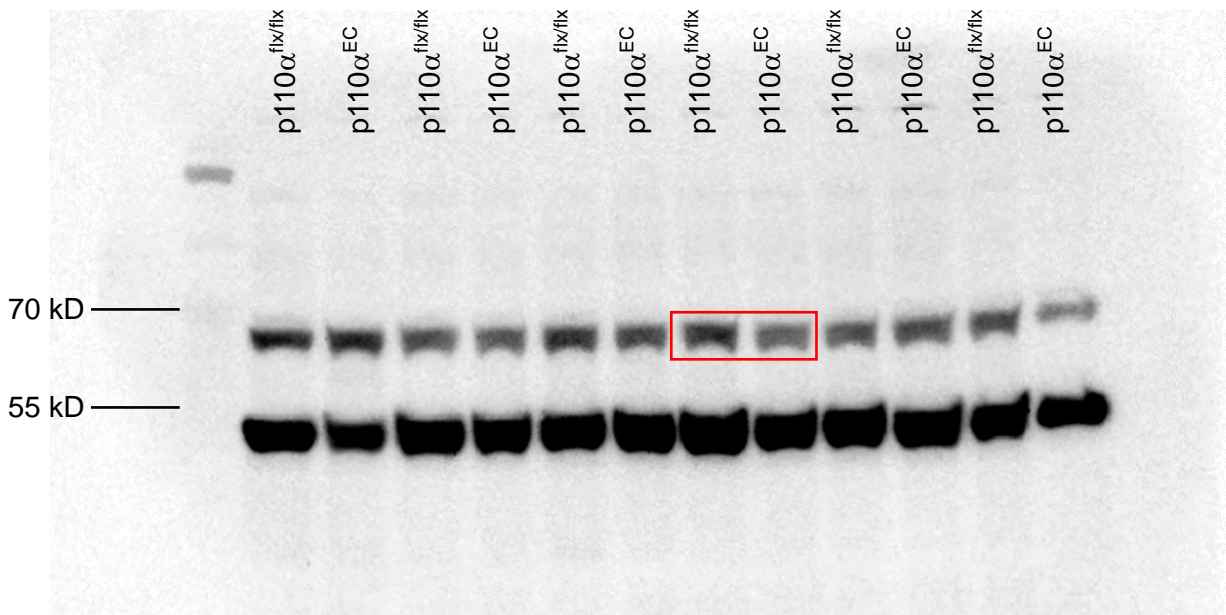
pAkt-T308 (all 7-day MI):



tAkt (all 7-day MI):



pAkt-S473 (all 7-day MI):



tAkt (all 7-day MI):

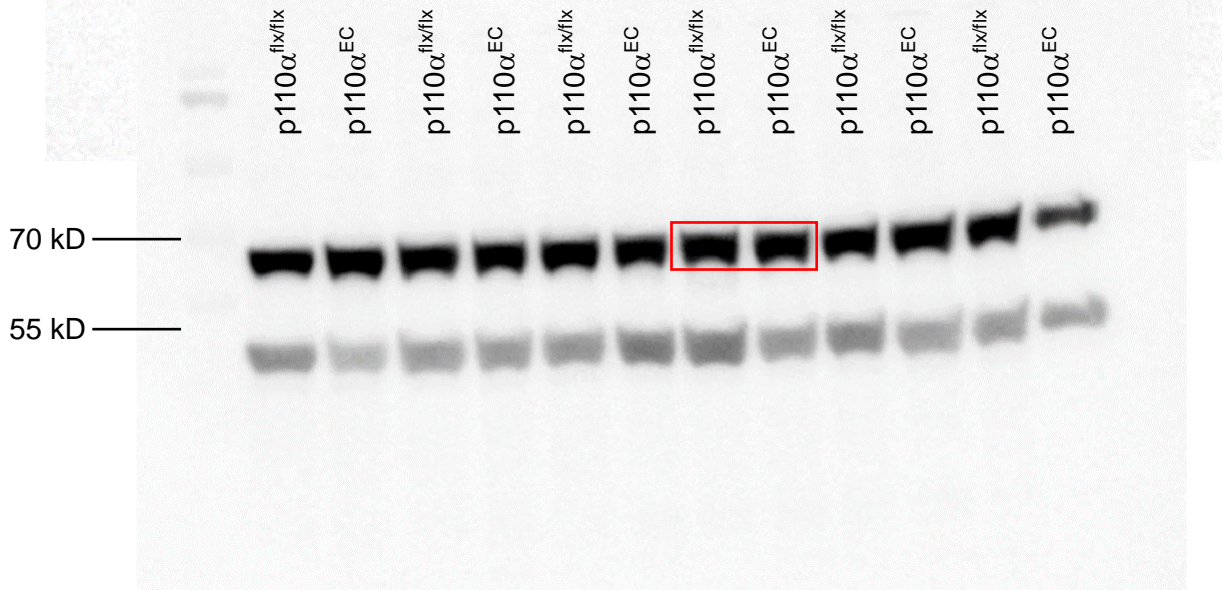
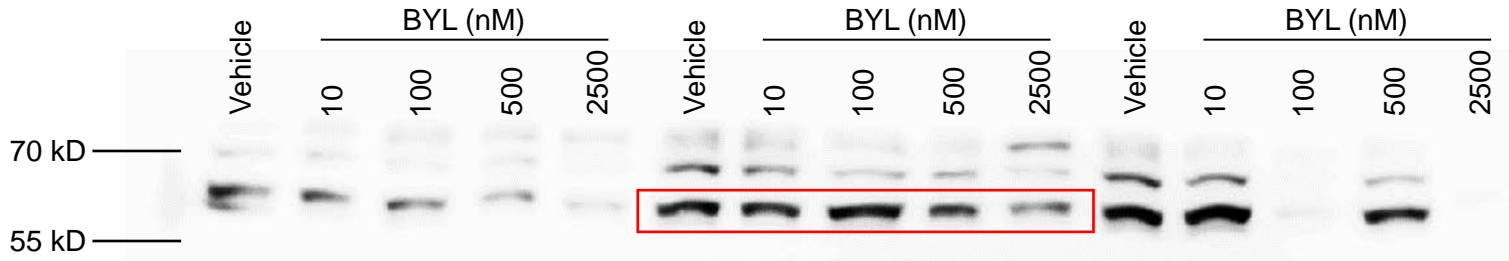
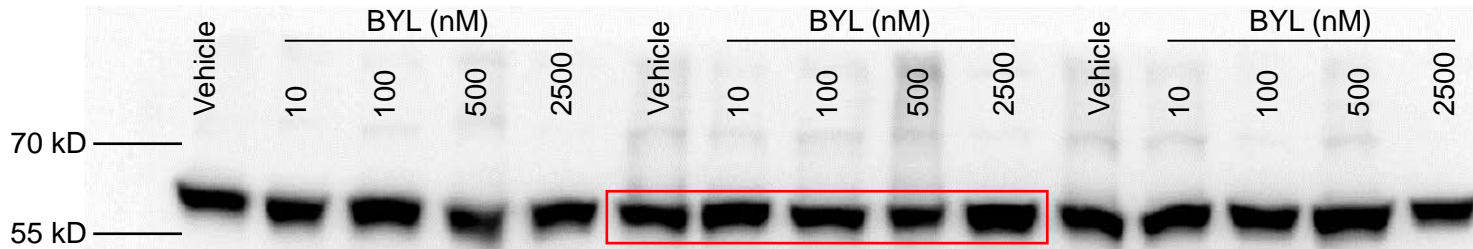


Figure 5A:

pAkt-T308 (HUVEC):



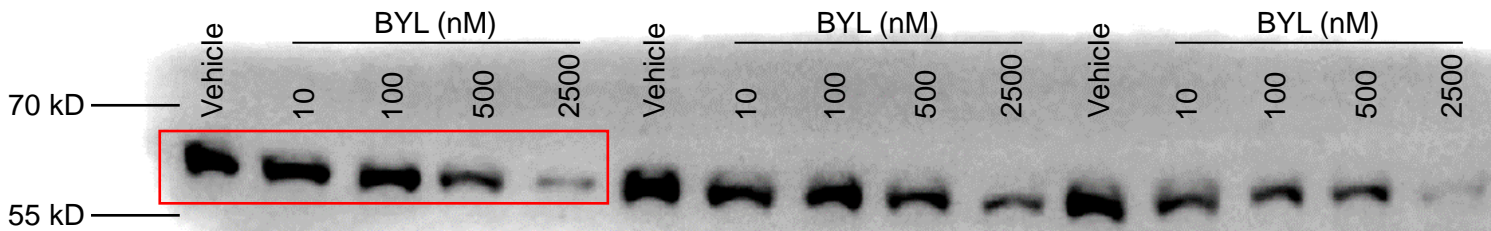
tAkt (HUVEC):



GAPDH (HUVEC):



pAkt-S473 (HUVEC):



tAkt (HUVEC):

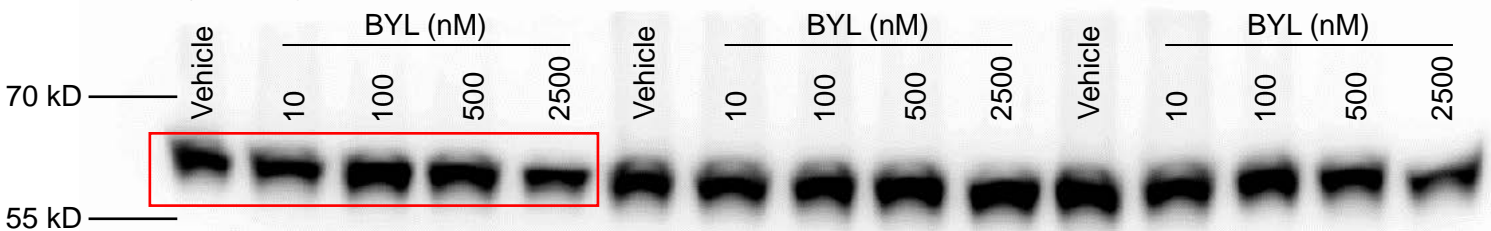
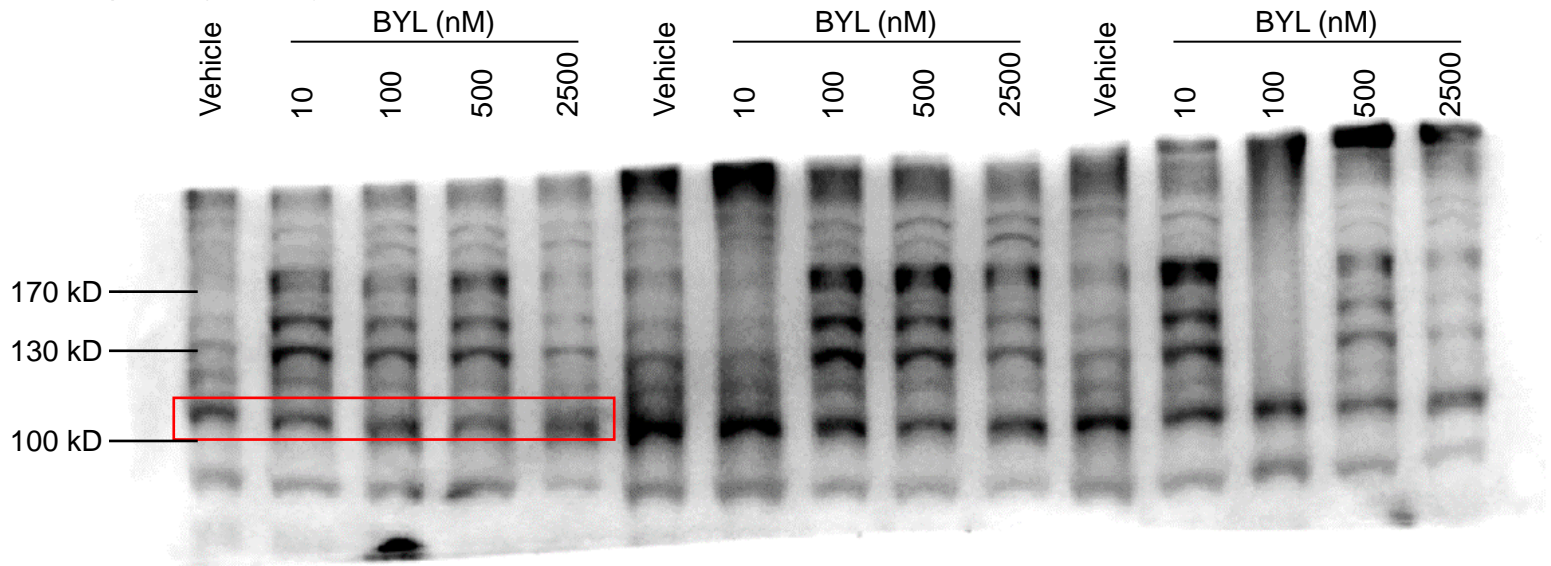
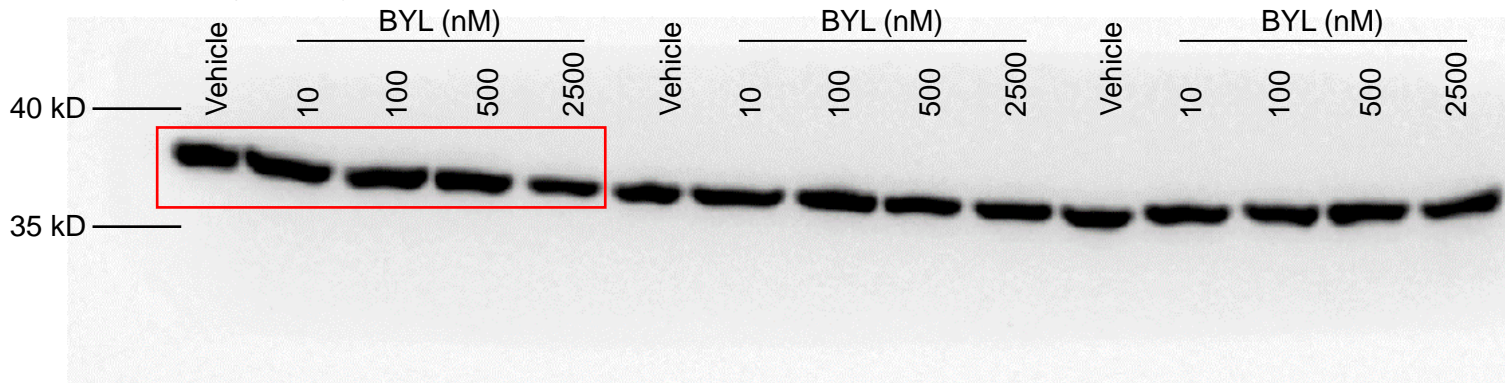


Figure 5A (continued):

p110 $\alpha$  (HUVEC):



GAPDH (HUVEC):



peNOS-S1177 (HUVEC):

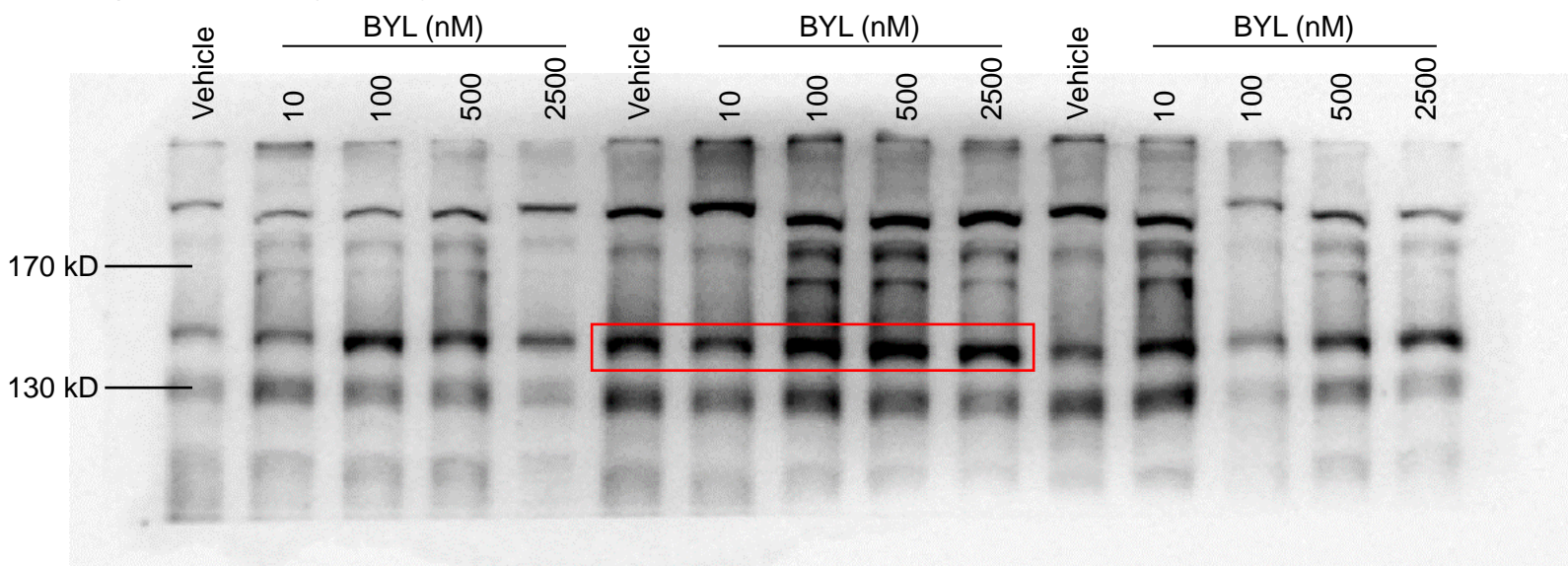
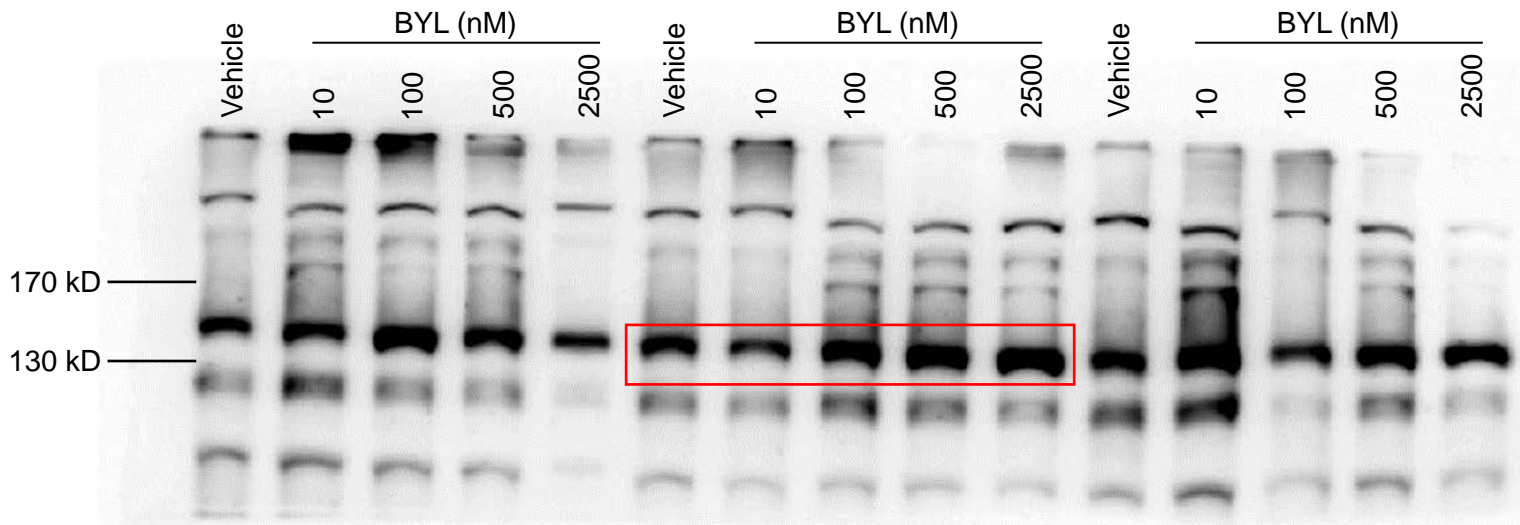


Figure 5A (continued):

eNOS (HUVEC):



GAPDH (HUVEC):

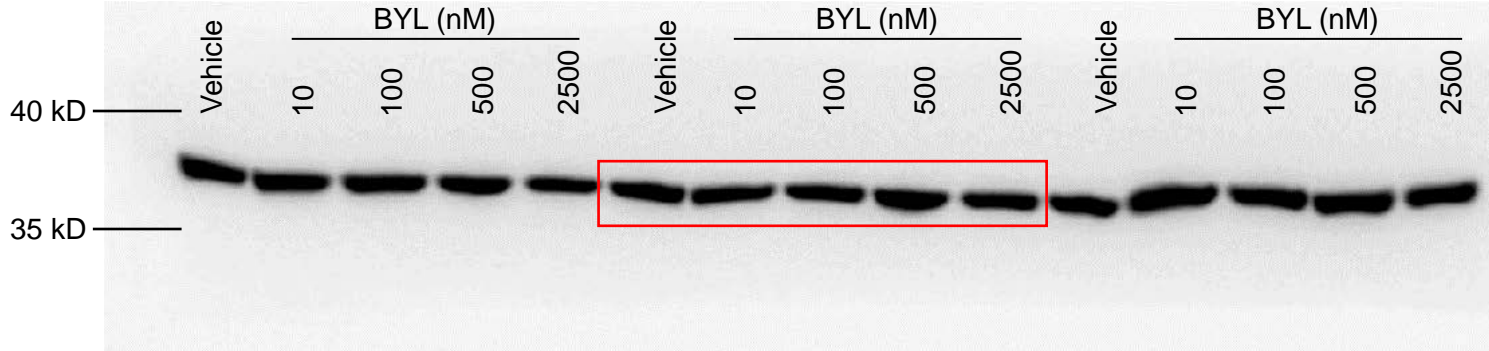


Figure 5B:

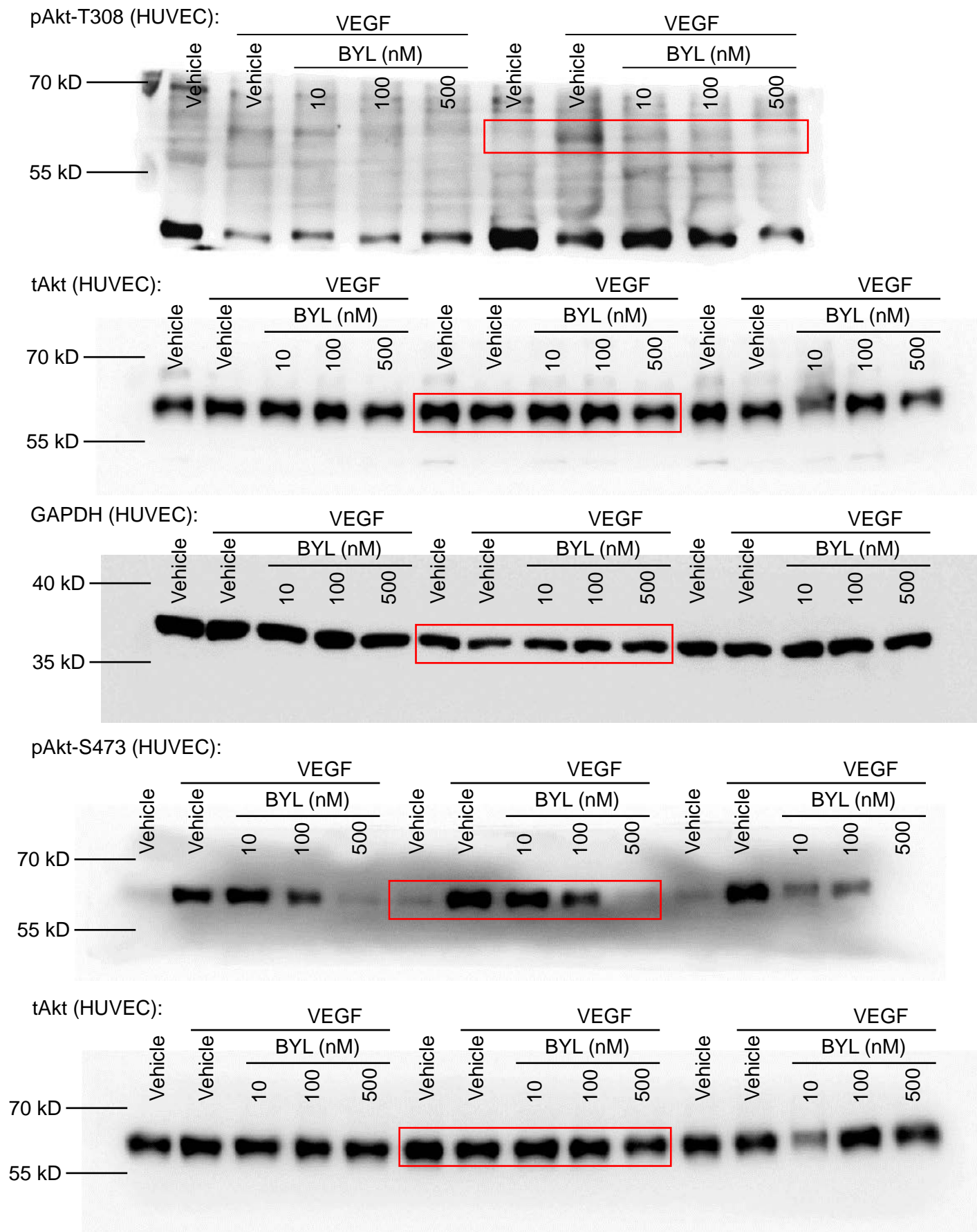
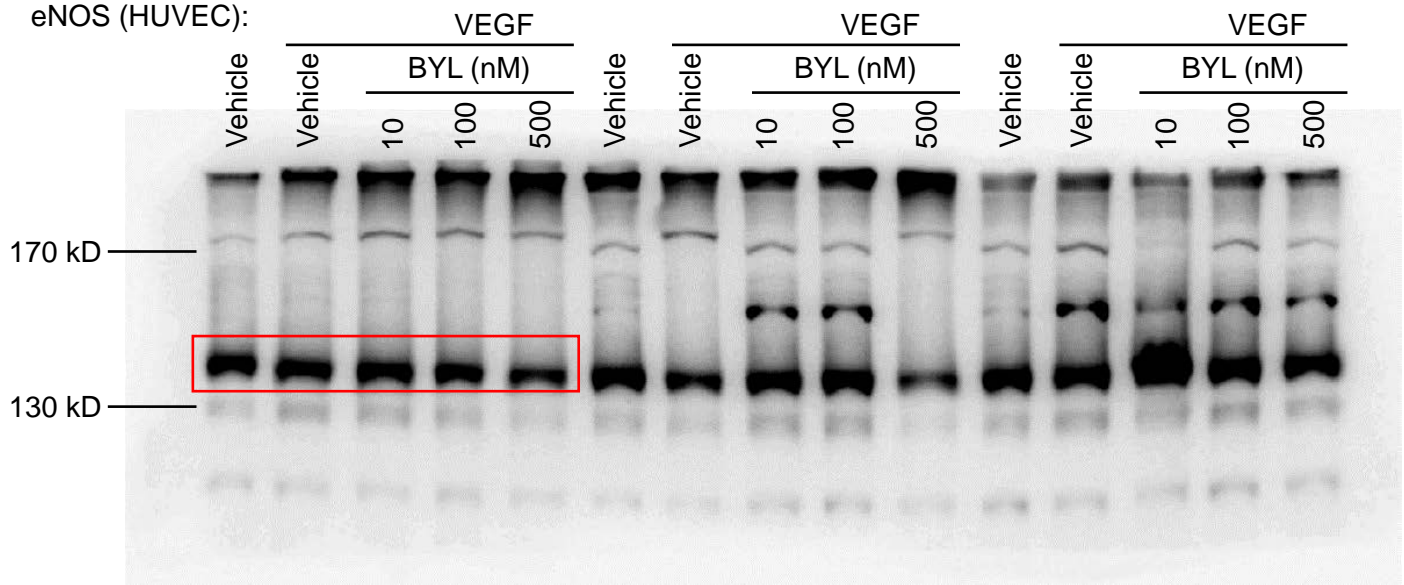




Figure 5B (continued):

eNOS (HUVEC):



GAPDH (HUVEC):

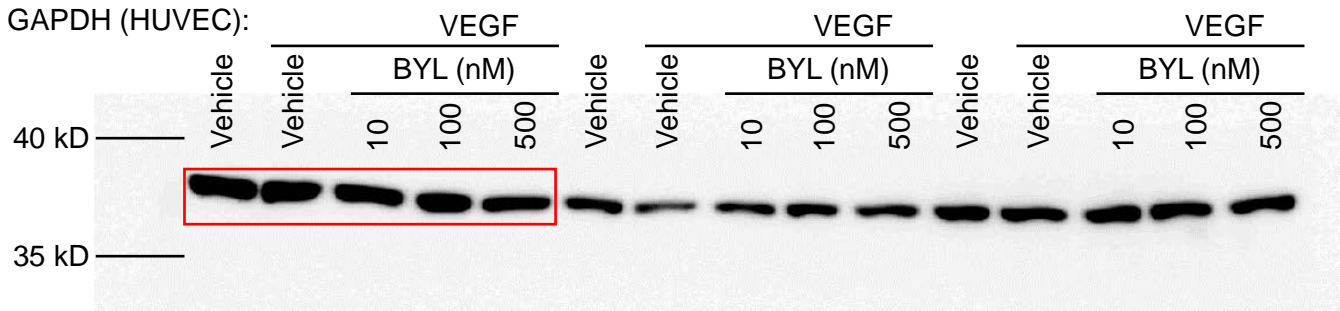
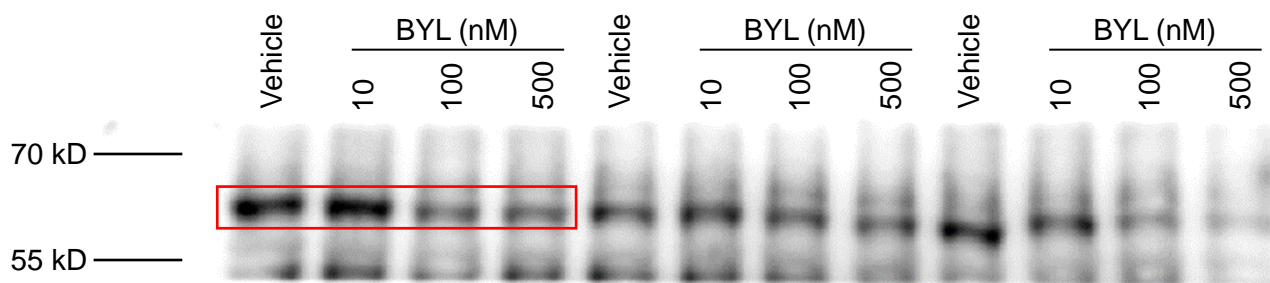
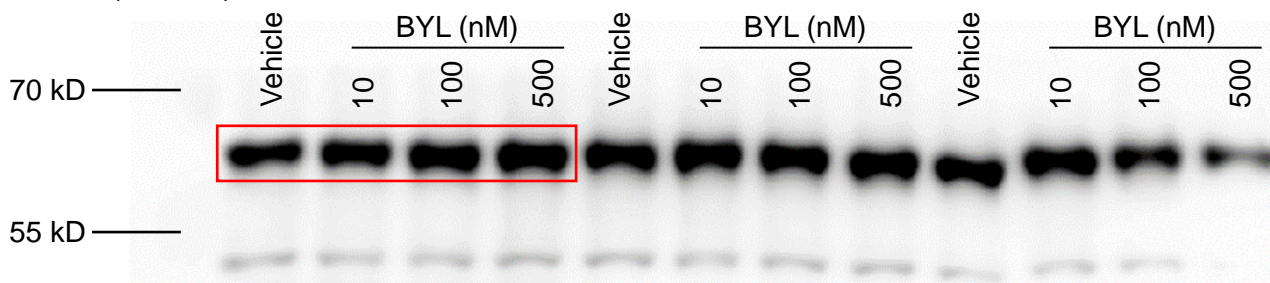


Figure 5C:

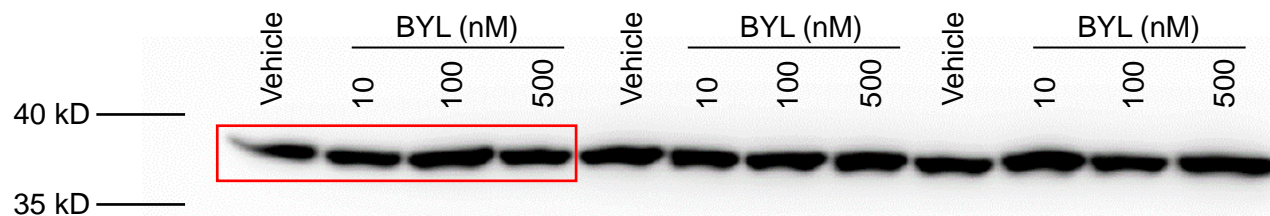
pAkt-T308 (HCAEC):



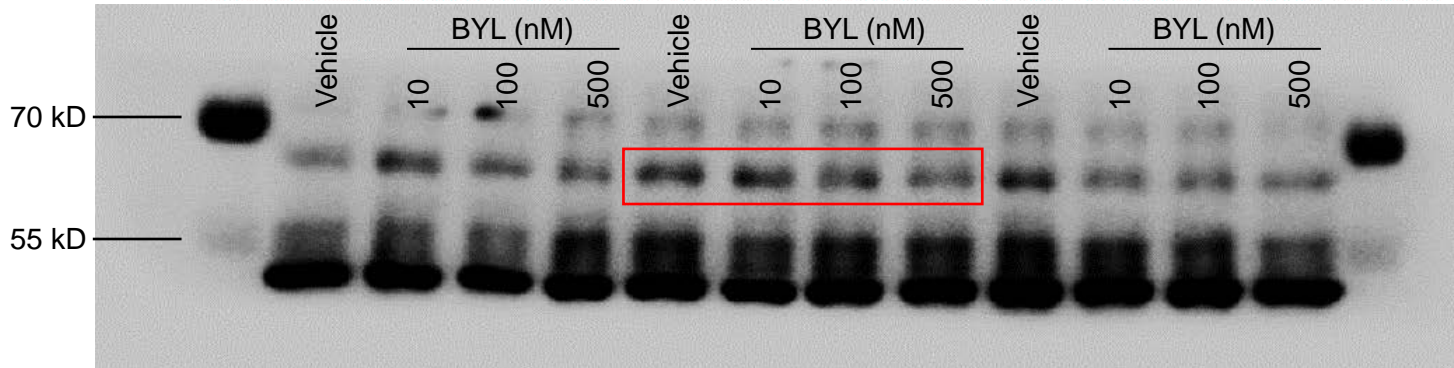
tAkt (HCAEC):



GAPDH (HCAEC):



pAkt-S473 (HCAEC):



tAkt (HCAEC):

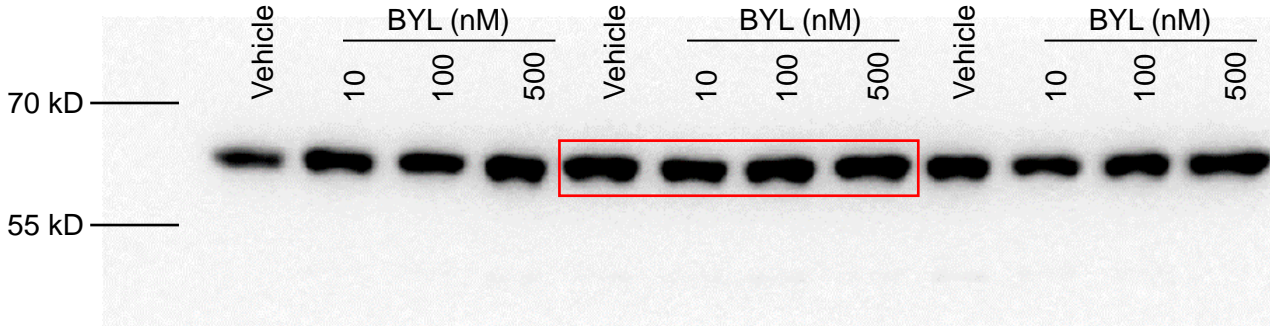
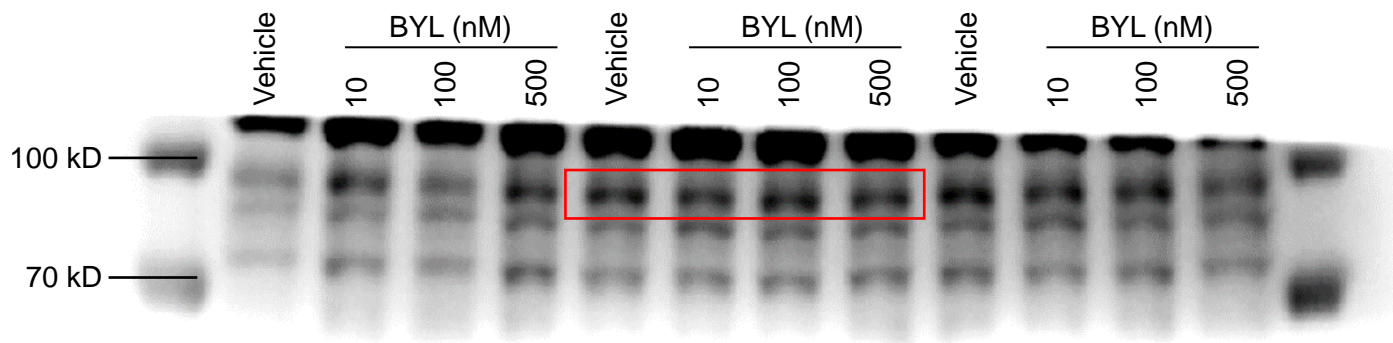


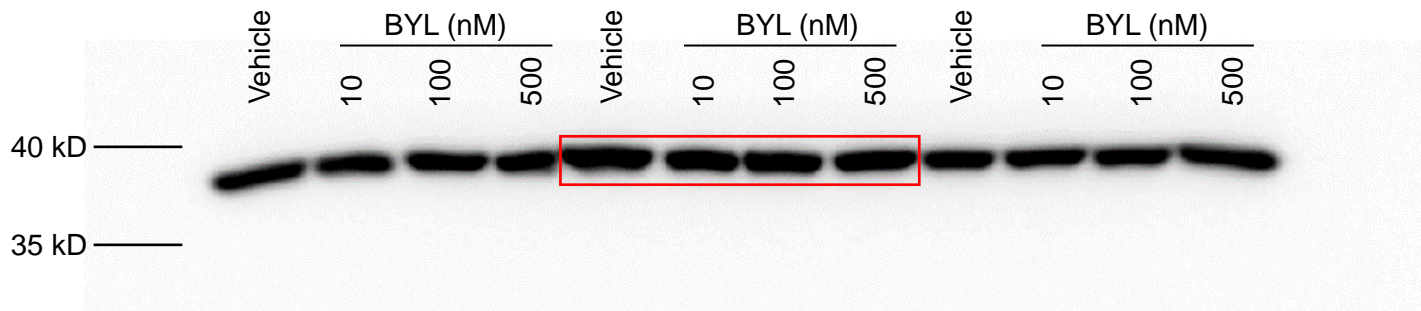


Figure 5C (continued):

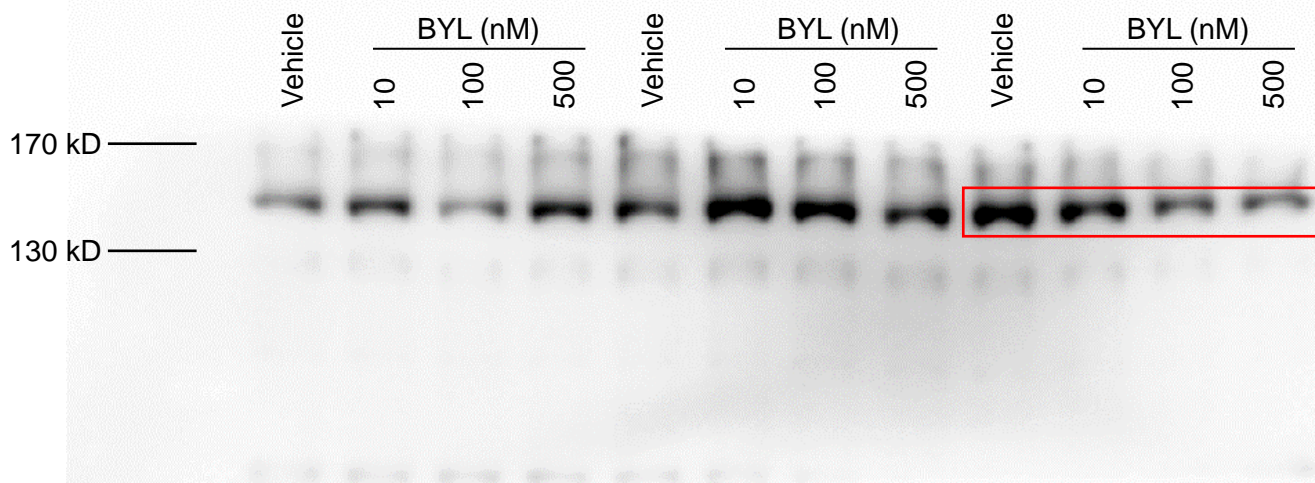
p110 $\alpha$  (HCAEC):



GAPDH (HCAEC):



peNOS-S1177 (HCAEC):



eNOS (HCAEC):

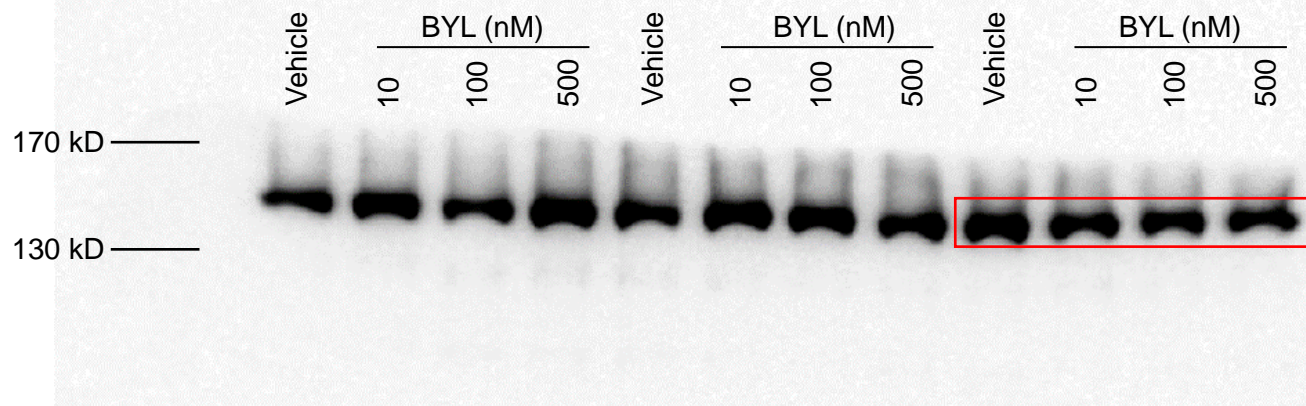


Figure 5C (continued):

GAPDH (HCAEC):

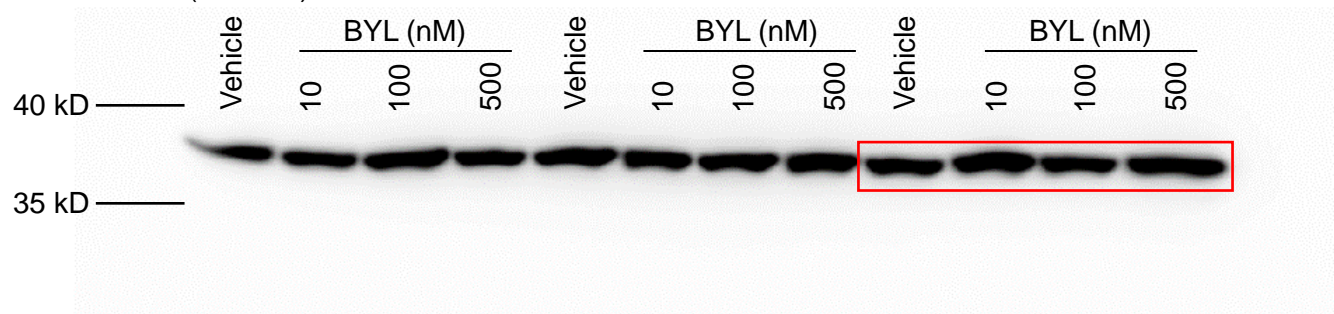


Figure 5D:

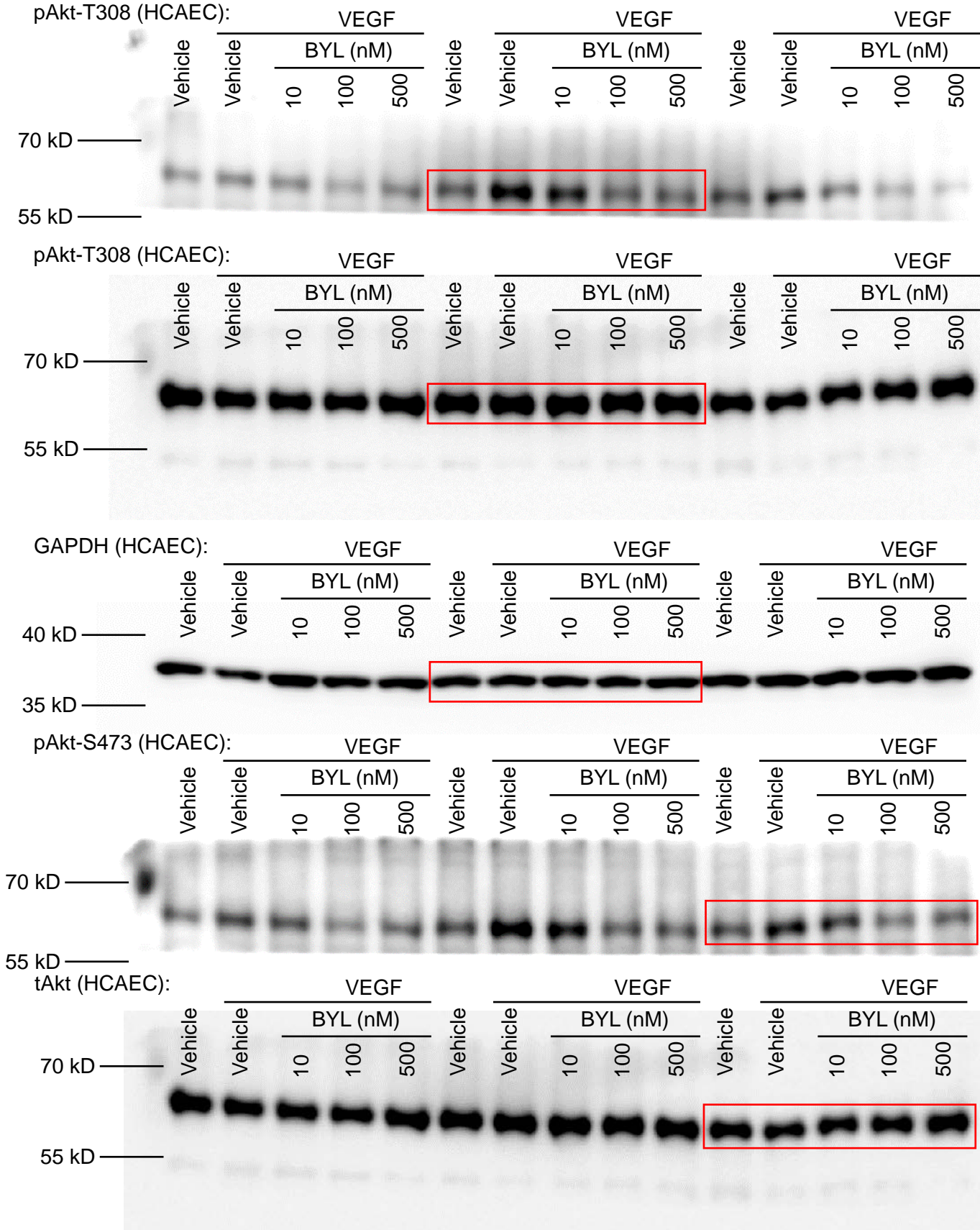


Figure 5D (continued):

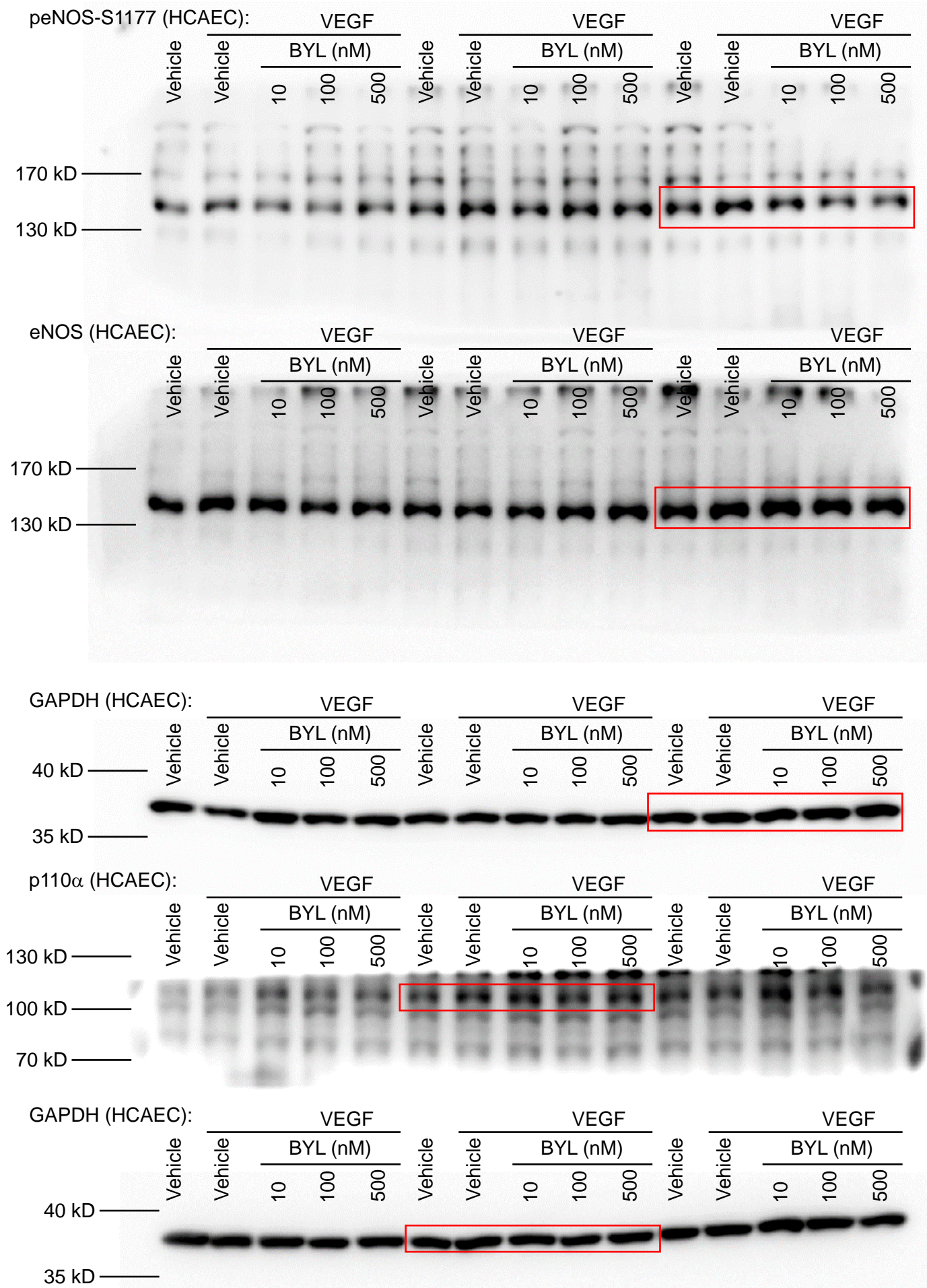
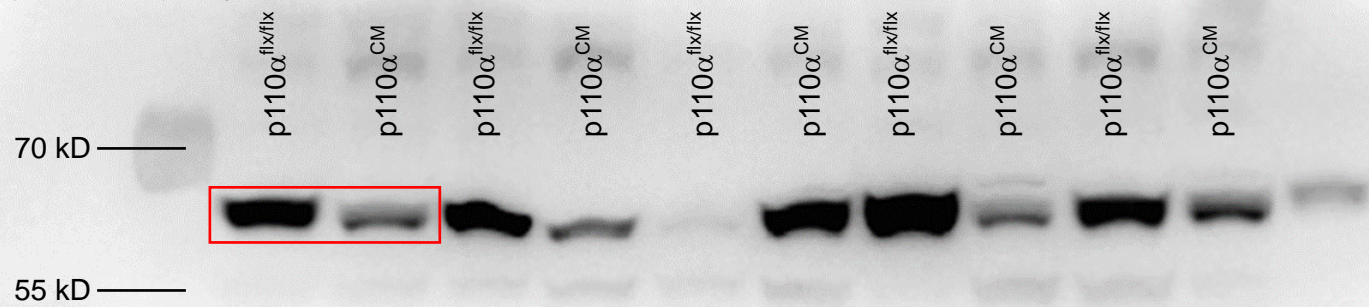
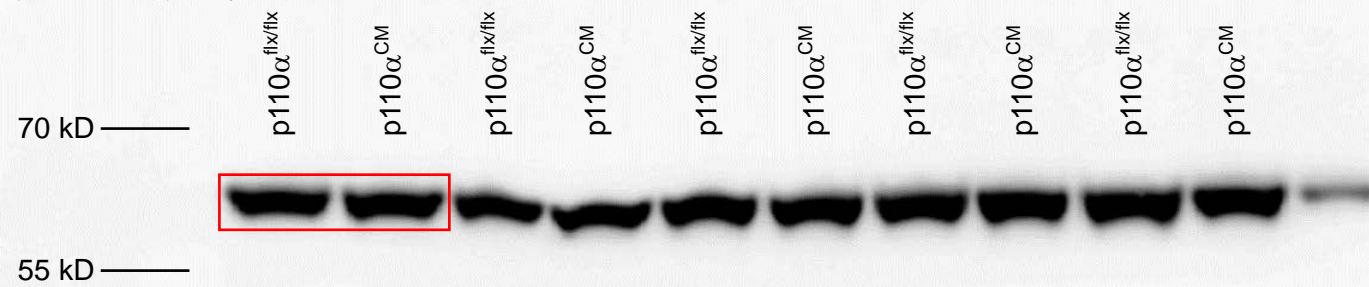


Figure 7F:

pAkt-T308 (7-day MI):

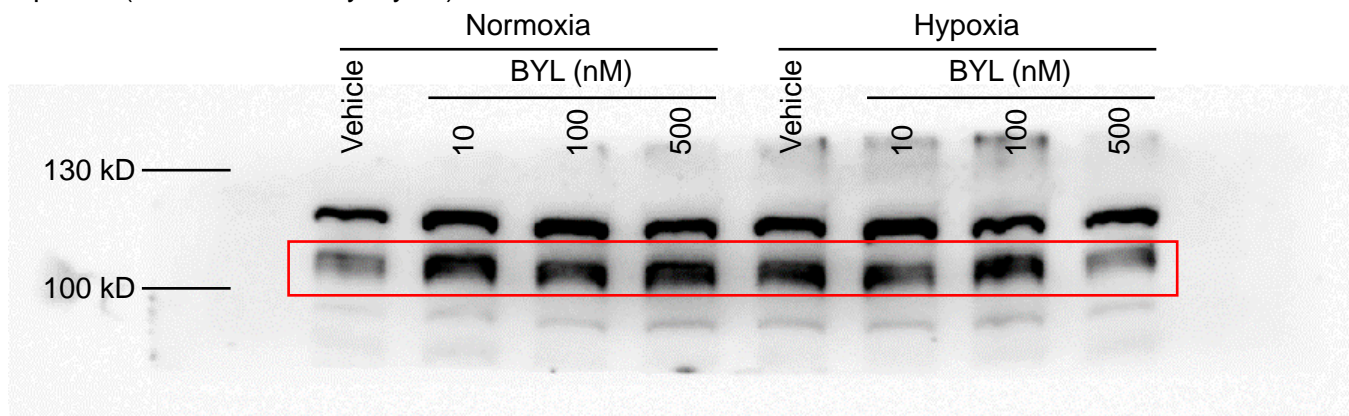


pAkt-T308 (7-day MI):

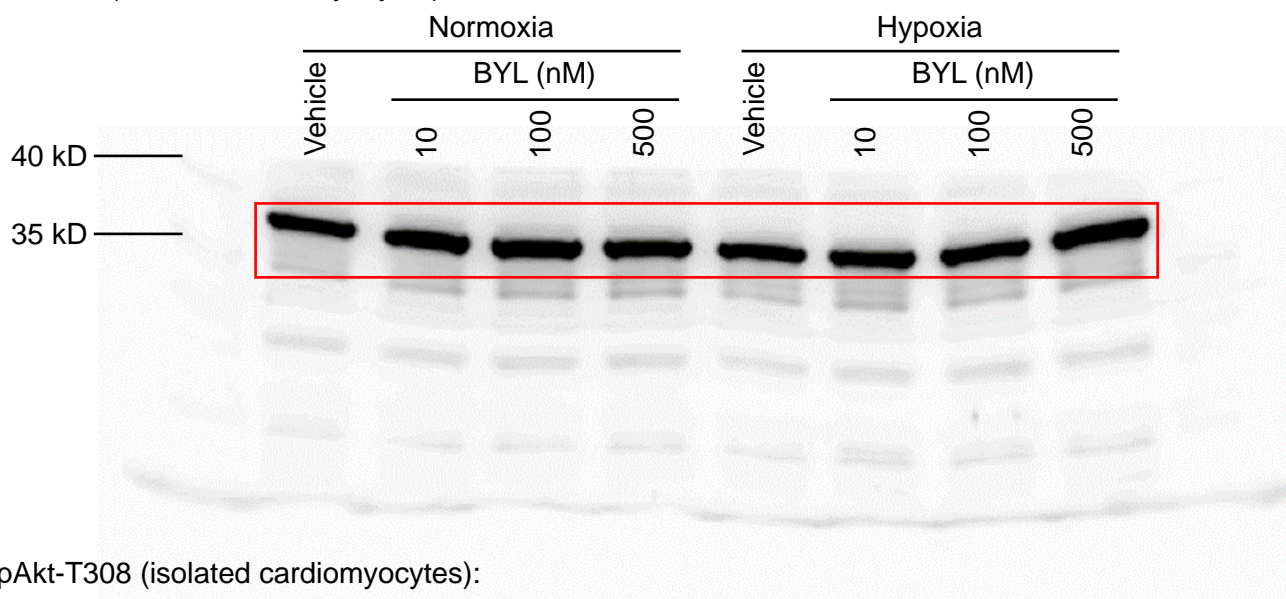


## Figure 8A:

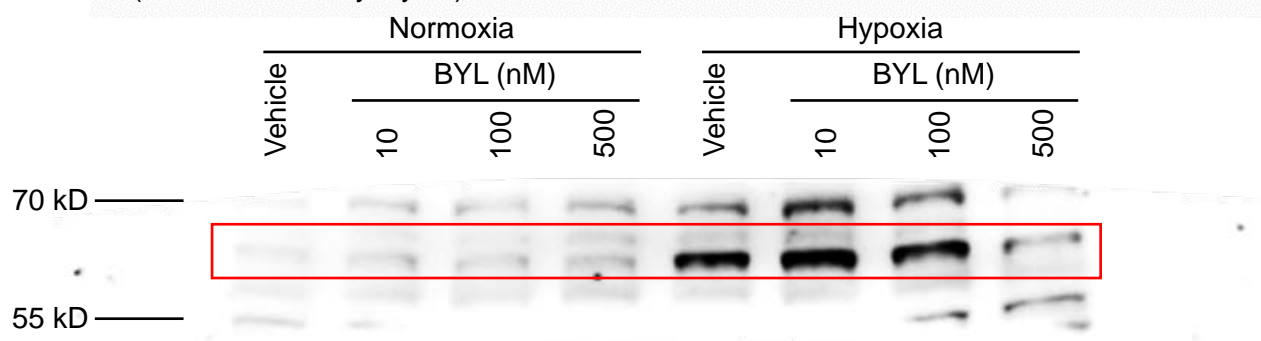
p110 $\alpha$  (isolated cardiomyocytes):



GAPDH (isolated cardiomyocytes):



pAkt-T308 (isolated cardiomyocytes):



tAkt (isolated cardiomyocytes):

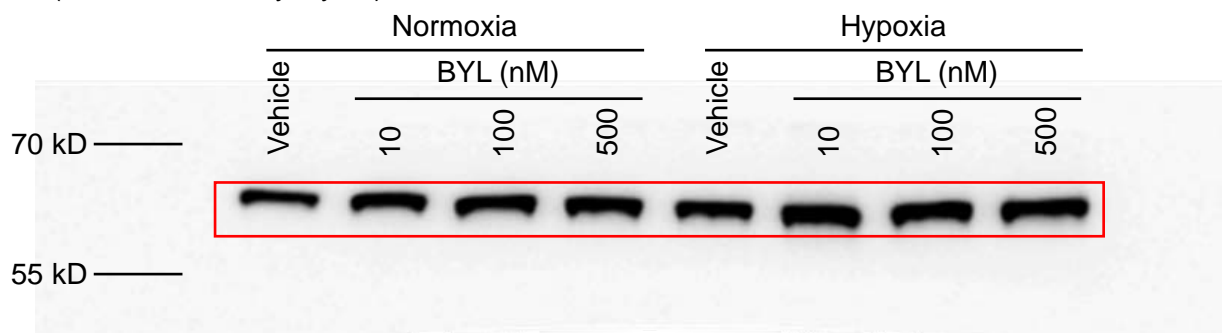
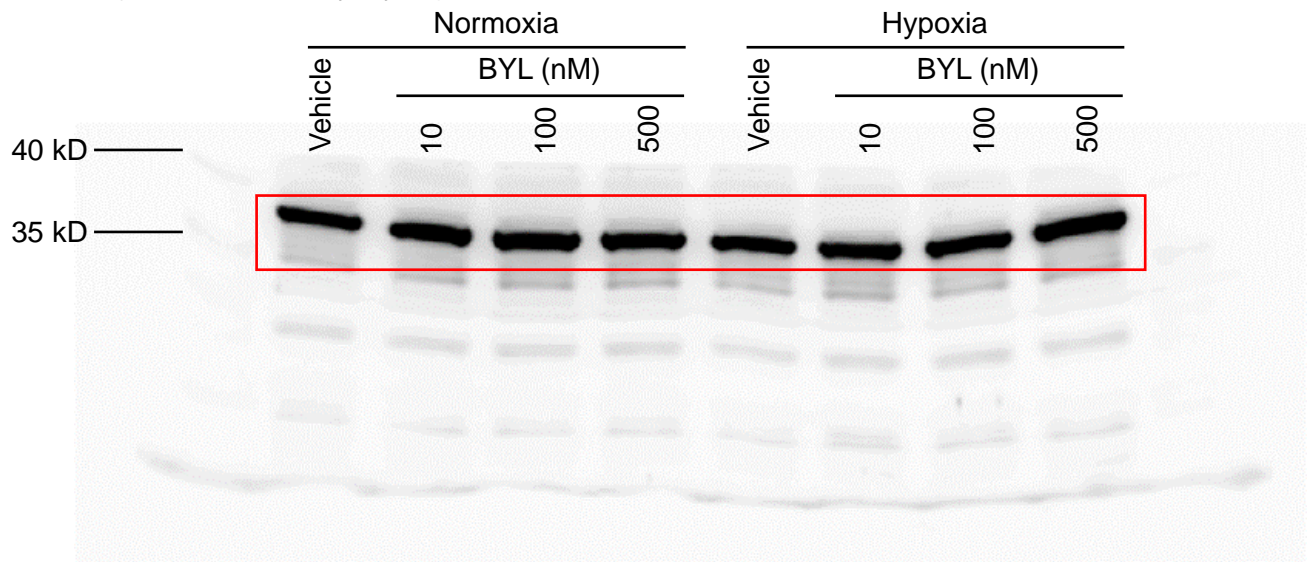
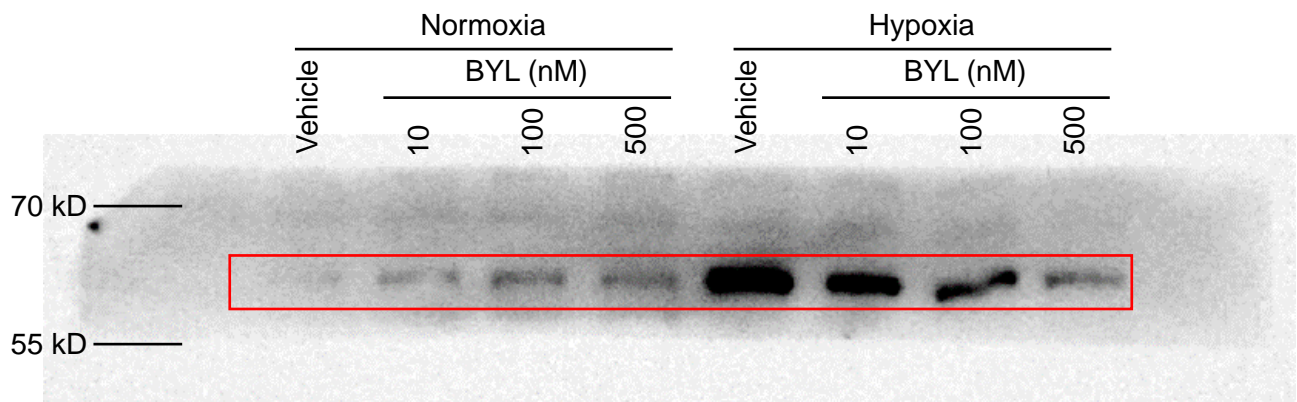


## Figure 8A (continued):

GAPDH (isolated cardiomyocytes):



pAkt-S473 (isolated cardiomyocytes):



tAkt (isolated cardiomyocytes):







Chen X *et al.*

PI3K $\alpha$  inhibition worsens heart disease

**Pharmacological and Cell-Specific Genetic PI3K $\alpha$  Inhibition  
Worsens Cardiac Remodeling After Myocardial Infarction**

Xueyi Chen<sup>1,3</sup>, Pavel Zhabyeyev<sup>1,3</sup>, Abul K. Azad<sup>1</sup>, Bart Vanhaesebroeck<sup>4</sup>,  
Chad E. Grueter<sup>5</sup>, Allan G. Murray<sup>1</sup>, Zamaneh Kassiri<sup>2,3</sup>,  
and Gavin Y. Oudit<sup>1,3,\*</sup>

<sup>1</sup>Department of Medicine, <sup>2</sup>Department of Physiology, <sup>3</sup>Mazankowski Alberta Heart Institute, University of Alberta, Edmonton, Canada; <sup>4</sup>Cancer Institute, University College London, London, UK. <sup>5</sup>Division of Cardiovascular Medicine, Department of Internal Medicine, Francois M. Abboud Cardiovascular Research Center, Fraternal Order of Eagles Diabetes Research Center, University of Iowa, Iowa City, IA, USA.

**Running title:** PI3K $\alpha$  inhibition worsens heart disease

**\*Corresponding Author:** Gavin Y. Oudit, MD, PhD, FRCP(C), Division of Cardiology, Department of Medicine, Mazankowski Alberta Heart Institute, University of Alberta, Edmonton, Alberta, T6G 2R3, Canada; Phone: (780)-407-8569, Fax: (780)-492-9753. Email: gavin.oudit@ualberta.ca.

**Category:** Research Article

**Word Count:** 9157 words; 8 Figures, 4 Supplemental Tables, and 7 Supplemental Figures.

**Abstract**

**Background:** PI3K $\alpha$  (Phosphoinositide 3-kinase  $\alpha$ ) regulates multiple downstream signaling pathways controlling cell survival, growth, and proliferation and is an attractive therapeutic target in cancer and obesity. The clinically-approved PI3K $\alpha$  inhibitor, BYL719, is in further clinical trials for cancer and overgrowth syndrome. However, the potential impact of PI3K $\alpha$  inhibition on the heart and following myocardial infarction (MI) is unclear. We aim to determine whether PI3K $\alpha$  inhibition affects cardiac physiology and post-MI remodeling and to elucidate the underlying molecular mechanisms.

**Methods and Results:** Wildtype (WT) 12-wk old male mice receiving BYL719 (daily, p.o.) for 10 days showed reduction in left ventricular longitudinal strain with normal ejection fraction, weight loss, mild cardiac atrophy, body composition alteration, and prolonged QT<sub>C</sub> interval. RNASeq analysis showed gene expression changes in multiple pathways including extracellular matrix remodeling and signaling complexes. After MI, both p110 $\alpha$  and phospho-Akt protein levels were increased in human and mouse hearts. Pharmacological PI3K $\alpha$  inhibition aggravated cardiac dysfunction and resulted in adverse post-MI remodeling, with increased apoptosis, elevated inflammation, suppressed hypertrophy, decreased coronary [blood vessel](#) density, and inhibited Akt/GSK3 $\beta$ /eNOS signaling. Selective genetic ablation of PI3K $\alpha$  in endothelial cells was associated with worsened post-MI cardiac function [and](#) reduced coronary [blood vessel](#) density. *In vitro*, BYL719 suppressed Akt/eNOS activation, cell viability, proliferation, and angiogenic sprouting in coronary and human umbilical vein endothelial cells. Cardiomyocyte-specific genetic PI3K $\alpha$  ablation resulted in mild cardiac systolic dysfunction at baseline. After MI, cardiac function markedly deteriorated with increased mortality concordant with greater

Chen X *et al.*

PI3K $\alpha$  inhibition worsens heart disease

apoptosis and reduced hypertrophy. In isolated adult mouse cardiomyocytes, BYL719 decreased hypoxia-associated activation of Akt/GSK3 $\beta$  signaling and cell survival.

**Conclusions:** PI3K $\alpha$  is required for cell survival (endothelial cells and cardiomyocytes) hypertrophic response, and angiogenesis to maintain cardiac function after MI. Therefore, PI3K $\alpha$  inhibition that is used as anti-cancer treatment, can be cardiotoxic, especially after MI.

#### Highlights

- ~~Inhibition of PI3K $\alpha$  by BYL719 worsens cardiac remodeling post myocardial infarction~~
- ~~Endothelial-specific ablation reduced coronary density~~
- ~~Cardiomyocyte-specific ablation decreased cardiac function and increased mortality~~
- ~~PI3K $\alpha$  effects are mediated via Akt/GSK3 $\beta$ /eNOS signaling~~

**Keywords:** angiogenesis / myocardial infarction / myocardial remodeling / signaling / PI3K $\alpha$

## 1. Introduction

The phosphoinositide 3-kinases (PI3Ks) are a family of conserved lipid kinases that regulate critical intracellular signaling responsible for hypertrophy, survival, proliferation, and metabolism [1, 2]. PI3K $\alpha$  is the functionally dominant PI3K isoform in many cell types and a key regulator in a wide range of cellular processes. The catalytic conversion of phosphatidylinositol-3,4-bisphosphate (PtdIns(3,4)P<sub>2</sub> or PIP<sub>2</sub>) to phosphatidylinositol-3,4,5-trisphosphate (PtdIns(3,4,5)P<sub>3</sub> or PIP<sub>3</sub>) leads to membrane recruitment of Akt, allowing the phosphorylation of an effector kinase, Akt, at Thr308 by PDK1. Subsequently, Akt phosphorylates downstream effectors and regulates various pathways, including glycogen synthase kinase 3 $\beta$  (GSK3 $\beta$ ) and endothelial nitric oxide synthase (eNOS). PI3K $\alpha$  signaling mediates cell survival, growth, electrophysiology and metabolism in different cell types [3-6][3-6].

Due to the widespread expression and diverse roles of PI3K $\alpha$ , the aberrations in PI3K $\alpha$  signaling are associated with a broad spectrum of human diseases including cancer. Gain-of-function mutations of *PIK3CA*, the gene that encodes the p110 $\alpha$  (catalytic subunit of PI3K $\alpha$ ), are frequent in many human tumors such as lung, head and neck, breast, endometrial, and cervical cancer [7-7]. In addition, disruptions of PI3K $\alpha$  signaling contribute to obesity, diabetes, and heart failure [8-10]. Currently, several PI3K $\alpha$  inhibitors are in clinical trials as cancer treatment [11-11]. One of them, BYL719 (Alpelisib), has demonstrated dose- and time-dependent PI3K $\alpha$  inhibition in both animal and human studies [12-15][12-15] and is therapeutic in *PIK3CA*-related solid tumors and overgrowth syndrome in recent clinical trials [14-16].

Heart disease is the leading cause of death followed by cancer [17,17] and both are frequently present in the same patient. Following myocardial infarction (MI), cardiac repair and remodeling, which are the result of complex interactions of cardiomyocytes and vascular endothelial cells, define cardiac recovery and patient outcomes [18]. We and others have identified PI3K $\alpha$  as a regulator of physiological hypertrophy, insulin signaling, ion channel activity, and contractility in cardiomyocytes [4, 19-21][4, 19-21] while maintaining vascular function and tone [2, 33]. However, cell-specific role of PI3K $\alpha$  on post-MI cardiac remodeling has not been elucidated and the increased use of PI3K $\alpha$  inhibitors in clinical practice as novel cancer therapies may result in cardiotoxicity due to inhibition of PI3K $\alpha$  in both cardiomyocytes and endothelial cells [22, 23][22, 23]. Indeed, very little is known about the potential cardiotoxicity with PI3K $\alpha$  inhibition.

In the present study, we showed that BYL719 administration in mice is associated with reduced global left ventricular longitudinal strain, prolonged QT interval, and altered gene expression profile. In mice receiving BYL719, post-MI vascular density was reduced, hypertrophy was suppressed, and myocardial apoptosis was increased. We also examined cell-specific effects of the loss of PI3K $\alpha$  activity in post-MI cardiac remodeling by studying post-MI remodeling in endothelial-specific (p110 $\alpha^{EC}$ ) and cardiomyocyte-specific (p110 $\alpha^{CM}$ ) PI3K $\alpha$  knockouts. We found that in endothelial cells, PI3K $\alpha$  controls endothelial survival, proliferation, and angiogenesis, while in adult cardiomyocytes, PI3K $\alpha$  is important for cell survival. Our study highlights the potential cardio-oncology issues associated with this new class of cancer therapy.

## 2. Methods

Detailed methods used in the present study and all other supporting data are available in the Data Supplement.

### 2.1 Animal Models

All animal studies were conducted according to the Canadian Council for Animal Care guidelines and approved by Animal Care and Use Committee at University of Alberta. Wild type (WT) C57BL/6 mice were purchased from Jackson Laboratory. BYL719 (50 mg/Kg/day, *p.o.*, Chemietek) or vehicle was given to 11- to 12-week-old WT mice in the morning for 10 days. Inducible endothelial-specific PI3K $\alpha$ -knockout mice (p110 $\alpha^{EC}$ ) were generated by crossing p110 $\alpha^{flx/flx}$  mice (*PIK3CA* gene with floxed 18 and 19 exons) [3][3] with tamoxifen-induced and Tie2 promoter-controlled Cre expression mice (Tie2-MerCreMer). Tamoxifen (80 mg/kg/day, Sigma-Aldrich) was given to 10-week-old mice by intraperitoneal injection for 5 days to induce endothelial-specific, floxed-exon deletion in p110 $\alpha$ ; this method has been previously shown to spare hematopoietic cells from targeted gene deletion [24, 25][24, 25]. Cardiomyocyte-specific PI3K $\alpha$ -knockout mice (p110 $\alpha^{CM}$ ) were generated by crossing p110 $\alpha^{flx/flx}$  with  $\alpha$ MHC-driven Cre expressing mice [4][4]. Homozygous littermates (p110 $\alpha^{flx/flx}$ ) of p110 $\alpha^{EC}$  and p110 $\alpha^{CM}$  mice were used as control. All mice were on the C57BL/6 background. Only male mice were used in the experiments.

The pharmacological inhibition of PI3K $\alpha$  was achieved by gavage with BYL719 (50 mg/kg by) daily for 10 days (Figure 1A). The dosing was based on studies that confirmed the therapeutic effects on PI3K $\alpha$ -driven tumors in mice (osteosarcoma, lung cancer, and

squamous cell carcinomas).[26-28] [Blood glucose measured after overnight fasting without glucose challenge.](#) Myocardial infarction was achieved by permanently ligating the proximal left anterior descending artery (LAD) of 12-week-old mice after they received 3 doses of BYL719 [\[29\]\[29\]](#). Surgery was performed by a technician who was blinded to the mouse strains and treatment. Tissue collection was performed on mice anesthetized with ketamine (100 mg/kg) and xylazine (10 mg/kg).

## 2.2 Human Explanted Hearts

Human cardiac specimens from non-failing control (NFC) and failing post-MI hearts were obtained as part of the Human Organ Procurement and Exchange program (HOPE) and Human Explanted Heart Program (HELP) respectively, approved by the Mazankowski Alberta Heart Institute and the Institutional Ethics Committee at University of Alberta [30].

## 2.3 [Body Composition Measurement, Echocardiography and Electrocardiogram](#)

[Body composition was measured in live, conscious mice using a NMR-MRI scanner \(EchoMRI\) \[31\].](#) Non-invasive transthoracic echocardiography was performed on mice anesthetized with 1.5% isoflurane using Vevo 3100 (Visualsonics). Conventional measurements and speckle-tracking strain analysis was carried out as previously described including the fractional area change (FAC) as a measure of RV systolic function [\[25\]\[25\]](#). Non-invasive electrocardiogram in lead I configuration was carried out as described [\[2020, 25\]](#).

Field Code Changed

#### 2.4 Endothelial Cell Culture, Flow Cytometry, and Bead Angiogenesis Assay

Human umbilical vein endothelial cells (HUVEC) and human coronary artery endothelial cells (HCAEC, ATCC) were used between passage 3 to 7. BYL719 was used at indicated doses. Recombinant human vascular endothelial growth factor (VEGF<sub>165</sub>, PeproTech) was added to stimulate endothelial cell responses at 50 ng/ml. Cell survival was examined on overnight vehicle- or BYL719-treated cell using flow cytometry (Attune NxT, Invitrogen) with annexin V and propidium iodide staining (Invitrogen). *In vitro* 3 dimensional (3D spheroid) angiogenesis assays were performed on HUVEC and HCAEC as previously described [25].

Field Code Changed

#### 2.5 Adult Murine Cardiomyocyte Isolation, Culture, and Stretching

Adult murine ventricular cardiomyocytes were isolated from 2% isoflurane anesthetized mice. Plated cardiomyocytes were cultured with vehicle, BYL719, or PI3K $\gamma$  inhibitor-AS252424 for 1 hour under normoxia (20% O<sub>2</sub>, 2% CO<sub>2</sub>) or hypoxia (1% O<sub>2</sub>, 2% CO<sub>2</sub>) before protein collection. Cyclical mechanical stretch of cardiomyocytes was achieved using Flexcell FX-5000 Tension System (Flexcell International Corp) at 1 Hz and 5% elongation for 3 hours in serum-free culture medium under hypoxic atmosphere [25][25]. Then, cells were collected for morphologic study.

#### 2.6 Immunofluorescence and Immunoblotting

Immunofluorescence staining was performed using established protocols [25][25]. Antibodies against CD31, Ly6B, CD68, Ki67, and BrdU were used. Intravital perfusion with fluorescein-conjugated lectin (Vectorlabs) was performed to identify the functional



vasculature. Wheat Germ Agglutinin (WGA) or phalloidin staining was performed to identify cardiomyocytes. Fragmented DNA of apoptotic cells was detected using the DeadEnd Fluorometric Terminal Deoxynucleotidyl Transferase-mediated dUTP Nick-End Labeling (TUNEL) System. Immunoblotting for various proteins was performed on left ventricular homogenates or cultured cell lysates as before [\[24, 25\]](#)[\[24, 25\]](#).

## 2.7 RNA Sequencing Analysis

RNA isolation and RNA sequencing were performed as previously described.[\[34\]](#)[\[32\]](#) Total RNAs from left ventricles (6 hearts/group) were extracted. Altered genes were defined by the boundary conditions:  $p_{\text{adj}} < 0.1$  and expression level of at least 750 TPM (transcripts per million) for either WT-vehicle or WT-BYL group (750 is 1% of 75,000 TPM, which was a maximal expression level in the dataset). Data were analyzed using WebGestalt, Protein ANalysis THrough Evolutionary Relationships (PANTHER) classification system (Pantherdb.org), and Ingenuity Pathway Analysis.

## 2.8 Statistical Analysis

Statistical analyses were carried out using SPSS Statistics 24 software, and statistical significance was defined as  $p < 0.05$  (two-sided). Continuous data were presented in scatter plots with mean  $\pm$  SEM. The differences between the two independent groups were evaluated using independent t-test or Mann-Whitney U test after normality examination. Paired t-test was carried out for two paired groups. One-way ANOVA or Kruskal-Wallis test with pairwise comparisons was used in studies with more than two groups based on the normality of the data. Two-way ANOVA was used to compare the

differences between groups with two independent variables. Repeated measures ANOVA was carried out in data with multiple measures. Categorical data were compared using Fisher exact test. Survival data were presented as the Kaplan-Meier plots, and the log-rank test was used to evaluate the statistical significance.

### **3. Results**

#### **3.1 Inhibition of PI3K $\alpha$ with BYL719 results in adverse systemic changes and altered myocardial gene expression**

BYL719 resulted in weight loss, leading to a decrease in body weight, and transiently increased blood glucose, but not fasting glucose (Figure 1A-1C). The mice displayed an increase in fat mass with a corresponding decrease in lean mass over the 10-day treatment period, associated with reduced heart and left ventricular weight (Figure 1D and 1E). Despite the preserved ejection fraction in BYL719-treated mice, stroke volume and global longitudinal strain were reduced (Table S1 and Figure 1F). The QT<sub>C</sub> interval was prolonged without alterations in the heart rate, PR interval, or QRS duration (Figure 1G and Figure S1).

To investigate the effect of pharmacological inhibition of PI3K $\alpha$  at the molecular level in the heart, we performed gene profiling of the LV tissue from mice treated with placebo or BYL719 (Data Supplement Bulk-RNAseq). A total of 292 genes were changed after BYL719 exposure, with log<sub>2</sub> FC (Fold Change) for the most genes in the approximate range of -2 to 2 (Figure 1H; heatmap of the most changed genes, Figure S2A; list of top 10 affected genes, Table S1; principle component analysis plot, Figure S3). Gene set enrichment analysis showed multiple changes in categories of biological regulation,

metabolic processes, response to stimulus (Figure S2B); membrane and nucleus, protein-containing complex, (Figure S2C); protein binding, ion binding, and nucleotide binding (Figure S2D). Kyoto Encyclopedia of Genes and Genomes (KEGG) pathway analysis showed downregulation of pathways related to structural integrity (extracellular matrix (ECM)-receptor interaction, focal adhesion) metabolism of glucose and proteins (protein digestion and absorption, AGE-RAGE signaling), and electrical activity (Figure 1I) and upregulation of metabolic pathways responsible for degradation of ketones, fatty acids, and several amino acids (Figure 1J). Taken together, these results demonstrate that PI3K $\alpha$  inhibition with BYL719 results in mild adverse systemic effects, altered myocardial gene expression and early cardiac dysfunction.

### 3.2 PI3K $\alpha$ in human and murine post MI hearts

Left ventricular specimens from post-MI patients showed markedly increased levels of p110 $\alpha$ , the catalytic subunit of PI3K $\alpha$ , in the infarct and peri-infarct regions. This increase correlated with enhanced Akt phosphorylation in these regions compared with non-failing human hearts (Figure 2A). We observed similar changes in PI3K $\alpha$ /Akt signaling in post-MI murine hearts (Figure 2A) showing a conserved response in humans and mice. These changes suggest that the PI3K $\alpha$  pathway is upregulated in response to MI and may have an adaptive role. To investigate this possibility, we induced MI by LAD ligation in mice treated with either vehicle or BYL719 (Figure 2B). BYL719 treatment decreased post-MI survival due to increase in non-rupture related deaths (Figure 2C). Echocardiographic analyses showed exacerbation of systolic dysfunction in BYL719 versus vehicle-treated post-MI mice, characterized by decreased ejection fraction, enlarged left ventricular

chamber, and worsened wall motion index (Figure 2D and Table S2). Interestingly, right ventricular fractional area change, a measure of RV systolic function, was also further compromised in the post-MI setting in response to BYL719 (Figure 2D and Table S2).

Because myocardial apoptosis determines the severity of myocardial ischemic injury, we evaluated apoptosis using TUNEL staining. One-day post-MI, BYL719-treatment increased myocardial apoptosis and elevated inflammatory cell infiltration compared with vehicle-treated controls (Figure 3A and 3B). In addition, BYL719 treatment suppressed post-MI cardiomyocyte hypertrophy and reduced coronary vascular density in the peri-infarct area without affecting cardiomyocyte size or vascular density of sham-operated groups (Figure 3C and 3D). Phosphorylation of myocardial Akt (Thr308), GSK3 $\beta$  (Ser9), and eNOS (Ser1177) were reduced in BYL719-treated mice in comparison with vehicle-treated day 7 post-MI (Figure 3E), but levels of p110 $\alpha$ , phospho-Akt at Ser473, and phospho-ERK were not altered (Figure S4). These results indicate that systemic PI3K $\alpha$  inhibition is detrimental in the post-MI setting by curtailing protective signaling pathways, resulting in increased apoptosis, impaired hypertrophy, and reduced vascular density.

### 3.3 Endothelial-specific PI3K $\alpha$ Ablation Worsens Post-MI Remodeling

We next examined the cell-specific role of PI3K $\alpha$  signaling in endothelial cells and cardiomyocytes in myocardial ischemic injury. We used mice with endothelial-specific PI3K $\alpha$  ablation (p110 $\alpha^{EC}$ ) (Figure 4A) ~~[25, 32, 33]~~[25, 33, 34]. Successful ablation in endothelial cells was confirmed by the presence of truncated *PIK3CA* in the DNA extracted from lungs of p110 $\alpha^{EC}$  mice (Figure S5A). Mice with endothelial-PI3K $\alpha$  ablation

showed comparable body weight, heart weight, and myocardial levels of p110 $\alpha$ , phospho-Akt, and phospho-eNOS compared to p110 $\alpha^{\text{flx/flx}}$  littermate controls at baseline (Figure S5B-C). Systolic function and global longitudinal strain were similar in p110 $\alpha^{\text{EC}}$  and p110 $\alpha^{\text{flx/flx}}$  hearts (Figure 4B, Figure S5D, and Table S3).

Following MI, deterioration in systolic function worsened at 7-day and 4-week post-MI in p110 $\alpha^{\text{EC}}$  hearts compared with sham; however, post-MI survival was similar (Figure 4B, Figure S5E-F, and Table S3). Inflammatory cell infiltration was increased post-MI in p110 $\alpha^{\text{EC}}$  hearts compared with controls (Figure S5G) without altering the increase in cardiomyocyte size post-MI (Figure S5H). Since endothelial survival and angiogenesis is critical in post-infarct recovery, and PI3K $\alpha$  is highly expressed in endothelial cells, we performed immunostaining to examine apoptosis, proliferation, and vascular density. We detected a higher number of apoptotic endothelial cells at day 1, decreased number of proliferating endothelial cells at day 3, lower vascular density, and reduced functional vasculature at day 7 post-MI in p110 $\alpha^{\text{EC}}$  mice (Figure 4C-4E). Whole-heart phospho-Akt levels were lower post-MI in p110 $\alpha^{\text{EC}}$  hearts (Figure 4F). These results indicate that endothelial PI3K $\alpha$  is required in the infarct and peri-infarct regions of the heart to maintain cardiac function by supporting endothelial survival, proliferation, and angiogenesis.

### 3.4 Inhibition of PI3K $\alpha$ Impairs Angiogenesis

To further delineate the impact of PI3K $\alpha$  inhibition on endothelial cells, we examined the effects of BYL719 on human umbilical vein endothelial cells (HUVEC), commonly used primary endothelial cells, and human coronary artery endothelial cells (HCAEC), human coronary primary endothelial cells. We first tested the effect of BYL719 on primary

endothelial cells in response to VEGF. BYL719 concentration range 10-500 nmol/L was selected because 500 nmol/L is the lowest concentration in the plasma of patients with continuous BYL719 treatment [14]. In HUVEC without VEGF stimulation, BYL719 suppressed Akt activity without affecting phospho-eNOS or p110 $\alpha$  protein levels (Figure 5A) while VEGF-induced Akt phosphorylation decreased in response to BYL719 treatment in a dose-dependent manner (Figure 5B). Meanwhile, VEGF-induced eNOS phosphorylation was only partially suppressed by 500 nmol/L BYL719 (Figure 5B). In HCAEC and in the absence of VEGF, 100 nmol/L and 500 nmol/L exerted a small inhibition of Akt/eNOS signaling (Figure 5C) while in response to VEGF stimulation, BYL719 at 100 nmol/L and 500 nmol/L abolished VEGF-induced Akt activation, with partial inhibitory effect on eNOS phosphorylation (Figure 5D).

BYL719 inhibition in HUVEC decreased the number of viable cells, increased apoptosis, and reduced proliferation (Figure 6A and 6B). The majority of HUVEC underwent cell death through apoptosis, not necrosis. BYL719 treatment reduced angiogenic sprouting illustrated by reduced number of sprouts and cumulative sprout length (Figure 6C). In HCAEC, both 100 nmol/L and 500 nmol/L BYL719 decreased cell viability, increased apoptosis, and decreased cell proliferation (Figure 6D and 6E) with survival analyses of HCAECs showing cell death patterns similar to HUVEC. Angiogenic sprouting (number of sprouts and cumulative sprout length) was inhibited by BYL719 (Figure 6F) in HCAEC. Collectively, these results suggest that endothelial PI3K $\alpha$  activity is required to maintain Akt/eNOS signaling in ECs, survival, proliferation, and angiogenesis.

### 3.5 Cardiomyocyte PI3K $\alpha$ Protects Against Ischemic Injury by Inhibiting Apoptosis and Supporting Hypertrophy

We next investigated the role of PI3K $\alpha$  in the cardiomyocytes during MI was investigated using mice with cardiomyocyte-specific p110 $\alpha$  ablation (p110 $\alpha^{\text{CM}}$ ) (Figure S6A). The p110 $\alpha^{\text{CM}}$  mice express truncated *PIK3CA* gene (Figure S6B). These mice had unchanged body weight and displayed reduced heart weight and left ventricular weight compared to p110 $\alpha^{\text{flx/flx}}$  littermates (Figure 7A), consistent with similar to the findings from BYL719-treated WT mice. p110 $\alpha^{\text{CM}}$  hearts showed marked reduction in p110 $\alpha$  and basal phospho-GSK3 $\beta$  levels without differences in basal phospho-Akt level (Figure S6C). Cardiomyocyte-specific PI3K $\alpha$  deficiency exacerbated post-MI systolic dysfunction, enlargement of the left ventricle, and increased mortality due to cardiac rupture (Figure 7B, 7C, and Table S4). Although p110 $\alpha^{\text{CM}}$  hearts showed no apoptosis at baseline, the number of apoptotic cells detected in p110 $\alpha^{\text{CM}}$  hearts at day 1 post-MI was considerably larger than in p110 $\alpha^{\text{flx/flx}}$  (Figure 7D). p110 $\alpha^{\text{CM}}$  hearts also displayed an increase in inflammatory responses after MI as shown by increased infiltration by neutrophils and macrophages (Figure S6D). Post-MI myocardial hypertrophy and vascular density in the non-infarct area was compromised in p110 $\alpha^{\text{CM}}$  hearts (Figure 7E and Figure S6E). Furthermore, Akt phosphorylation was lower in p110 $\alpha^{\text{CM}}$  hearts after MI (Figure 7F). These results suggest that (i) under normal physiological conditions, cardiomyocyte PI3K $\alpha$  plays a role in maintaining normal cardiac function and (ii) in the post-MI setting, cardiomyocyte PI3K $\alpha$  controls cell survival and hypertrophy.

To elucidate acute effects of the PI3K $\alpha$  activity on cardiomyocyte survival, adult mouse cardiomyocytes were isolated from WT mice, and treated with BYL719 in normoxic

and hypoxic conditions. While BYL719 had no effect on Akt activity under normoxic condition, it inhibited hypoxia-induced Akt activation and GSK3 $\beta$  phosphorylation in a dose-dependent manner (Figure 8A). This effect could not be attributed to potential role of PI3K $\gamma$  since using AS252424, a specific inhibitor of PI3K $\gamma$ , caused further inhibition of Akt phosphorylation without a differential effect on GSK3 $\beta$  phosphorylation (Figure S7). These results confirm that lowered GSK3 $\beta$  phosphorylation in the p110 $\alpha^{\text{CM}}$  hearts and in cells treated with BYL719 is directly link to decrease in PI3K $\alpha$  signaling. Subjecting cultured isolated cardiomyocytes to 3-hr mechanical stretching under hypoxia to simulate *in vivo* conditions revealed increased cardiomyocyte apoptosis (Figure 8B). BYL719 treatment also blunted the hypoxia-triggered increase in F/G-actin ratio (Figure 8C), a key control mechanism for PI3K $\alpha$  [9][9], rendering cells more vulnerable to biomechanical stress. Taken together, PI3K $\alpha$  activity plays a role in post-MI hypertrophy, cytoskeletal response to biomechanical stress, and cell survival by protecting against hypoxia-induced apoptosis.

#### **4. Discussion**

Cardiovascular disease (CVD) and cancer are the two leading causes of death worldwide [34, 35][35, 36] and are closely linked illustrated by cancer patients having a higher incidence of ischemic heart disease, and vice versa [36, 37][37, 38], which has been attributed to shared risk factors and, importantly, the consequence of cancer therapy having detrimental effects on the cardiovascular system [22, 23, 38, 39][22, 23, 39, 40]. Since PI3K $\alpha$  is emerging as a major target for cancer therapies [12-16][12-16], knowledge



of PI3K $\alpha$  function in healthy and post-MI hearts is critical for optimization of treatment of ischemic heart disease and cancer care.

-Activation of the PI3K $\alpha$ /Akt signaling pathway contributes to cancer development and progression as PI3K $\alpha$  activity is frequently activated in a variety of common human tumors [7-7]. Use of PI3K $\alpha$ -specific inhibitors, such as alpelisib (BYL719) and serabelisib, has achieved initial success on advanced solid tumors especially in combination with standard anti-cancer therapy [14, 15, 40, 41][41, 42]. ~~In this study, we found that BYL719 also leads to lean mass reduction and fat mass increase, which are associated with poor outcomes in CVD [42, 43].~~ The major toxic effects of PI3K $\alpha$  inhibitors reported in clinical trials are hyperglycemia, cutaneous reactions, and gastrointestinal discomfort [44]. ~~We used BYL719 concentration of 500 nmol/L for our *in vitro* studies as this is the lowest plasma concentration in patients with continuous BYL719 treatment [43].~~ In this study, we used the dose of 50 mg/kg because it produces robust anti-tumor response in mouse models [44][12, 26-28]. ~~In our study, prolonged treatment with BYL719 resulted in transient hyperglycemia, comparable to the antitumor effects and burden of hyperglycemia seen in humans [14, 44].~~ In our study, we found that BYL719 also leads to transient hyperglycemia associated with lean mass reduction and fat mass increase, which are associated with poor outcomes in CVD [31, 45]. Treatment with BYL719 also resulted in reduced cardiac size, prolonged QT<sub>c</sub> interval, and compromised LV global longitudinal strain. Both prolonged QT<sub>c</sub> interval and lower global longitudinal strain have been associated with a higher risk of cardiovascular morbidity and mortality in patients [45, 46][46, 47]. BYL719-mediated prolongation of QT<sub>c</sub> interval is due to the inhibition of the late sodium current in cardiomyocytes, which increases the

risk of ventricular arrhythmias [11, 20][11, 20]. BYL719 also resulted in transcriptome changes in the heart characterized by (i) disruptions in pathways responsible for metabolism of glucose, fatty acids, and amino acids; (ii) downregulation of the pathways responsible for structural integrity (ECM-receptor interactions and focal adhesion); and (iii) disruptions in excitability. Taken together, our study demonstrates that the systemic (e.g., hyperglycemia) and cardiac-specific effects of PI3K $\alpha$  inhibition predispose the heart to ~~higher~~greater cardiovascular risks.

We found that the PI3K $\alpha$  inhibitor, BYL719, has detrimental effects on cardiac health and post-MI cardiac repair, suggesting that both endothelial and cardiomyocyte PI3K $\alpha$  plays an important role in cardiac recovery after MI (Figure 8D). In both human and murine hearts, p110 $\alpha$  and Akt phosphorylation were upregulated after MI suggesting that PI3K $\alpha$ /Akt signaling is required for compensatory post-MI ventricular remodeling and revascularization (Figure 8D, green paths). Pharmacological inhibition of PI3K $\alpha$  (Figure 8D, red paths) inhibits both cardiomyocyte and endothelial PI3K $\alpha$  leading to increased apoptotic cell death, decreased cardiomyocyte hypertrophy, and diminished angiogenesis. Reduced number of cardiomyocytes, disrupted compensatory hypertrophy, and diminished re-vascularization resulted in exacerbated cardiac dysfunction and a tendency to increased mortality after MI. Importantly, post-MI biventricular dysfunction was exacerbated by inhibition of PI3K $\alpha$  signaling. Our findings are corroborated by the increased risk of heart failure in patients treated with sunitinib, a tyrosine kinase inhibitor with antitumor and antiangiogenic activities [47][48] and are likely to translate to other types of chemotherapy such as anthracycline where cell protective signaling plays a dominant role [43, 48][31, 49].

Endothelial PI3K $\alpha$  signaling is required to maintain vascular function under physiologic conditions with endothelial cells under unstressed physiologic conditions. Post-MI, endothelial-specific PI3K $\alpha$  ablation resulted in (i) unchanged mortality, (ii) increased apoptosis and inflammation, (iii) reduced angiogenesis in infarct and peri-infarct areas, and (iv) worsened cardiac dysfunction. Reduced angiogenesis in response to PI3K $\alpha$  inhibition was also observed *in vitro* and was mediated via Akt/eNOS signaling consistent with a key role of eNOS in increasing capillary density post-MI and attenuating heart failure [49, 50][50, 51]. We observed that the cardiomyocyte PI3K $\alpha$  is required to maintain heart weight, and normal cardiac function. Cardiomyocyte-specific PI3K $\alpha$  ablation lead to considerable increase in mortality and was associated with enhanced myocardial apoptosis and inflammation, suppressed adaptive hypertrophy, reduced angiogenesis in non-infarct area, and worsened cardiac dysfunction. The cardioprotective effects seen with increased cardiac PI3K $\alpha$  activity further corroborate our results [54][52].

*Clinical implications of PI3K $\alpha$  inhibition.* Our results suggest (i) a therapeutic potential of upregulation of cardiac PI3K $\alpha$  to enhance post-MI cardiac repair by improving cell survival and angiogenesis; (ii) a concern of cardiotoxicity of PI3K $\alpha$  inhibitors in healthy and MI hearts. Patients receiving these drugs in clinical trials need close monitoring especially in patients with preexisting cardiovascular disease. Further research is needed into the development of strategies to counteract cardiotoxic effects of PI3K $\alpha$  inhibition for healthy and MI hearts.

### **Acknowledgments**

#### **Funding**

This work was supported by operating grants from the Canadian Institutes for Health Research (CIHR) and Heart and Stroke Foundation to GY Oudit. Ms. Xueyi Chen was funded by Li Ka Shing Sino-Canadian Exchange Program.

#### **Author contributions**

XC performed experiments, analyzed data, drafted the manuscript; PZ, CEG performed experiments, analyzed data, revised the manuscript; AKA performed experiments, analyzed data; BV, AGM, ZK, revised manuscript; GYO, revised manuscript, funding, supervision.

#### **Conflict of interest Disclosures**

B.V. is a consultant for Karus Therapeutics (Oxford, UK), iOnctura (Geneva, Switzerland) and Venthera (Palo Alto, CA, USA) and has received speaker fees from Gilead Sciences (Foster City, US). The other authors have no competing interests.

#### **References**

- [1] B. Vanhaesebroeck, L. Stephens, P. Hawkins, PI3K signalling: the path to discovery and understanding, *Nature reviews. Molecular cell biology* 13(3) (2012) 195-203.
- [2] G.Y. Oudit, H. Sun, B.G. Kerfant, M.A. Crackower, J.M. Penninger, P.H. Backx, The role of phosphoinositide-3 kinase and PTEN in cardiovascular physiology and disease, *Journal of molecular and cellular cardiology* 37(2) (2004) 449-71.

- [3] M. Graupera, J. Guillermet-Guibert, L.C. Foukas, L.K. Phng, R.J. Cain, A. Salpekar, ~~W. Pearce, S. Meek, J. Millan, P.R. Cutillas, A.J. Smith, A.J. Ridley, C. Ruhrberg, H. Gerhardt, B. Vanhaesebroeck, et al.~~ Angiogenesis selectively requires the p110 $\alpha$  isoform of PI3K to control endothelial cell migration, *Nature* 453(7195) (2008) 662-6.
- [4] B.A. McLean, P. Zhabyeyev, V.B. Patel, R. Basu, N. Parajuli, J. DesAulniers, ~~A.G. Murray, Z. Kassiri, B. Vanhaesebroeck, G.Y. Oudit, et al.~~ PI3K $\alpha$  is essential for the recovery from Cre/tamoxifen cardiotoxicity and in myocardial insulin signalling but is not required for normal myocardial contractility in the adult heart, *Cardiovascular research* 105(3) (2015) 292-303.
- [5] B.A. McLean, P.C. Kienesberger, W. Wang, G. Masson, P. Zhabyeyev, J.R. Dyck, ~~G.Y. Oudit, et al.~~ Enhanced recovery from ischemia-reperfusion injury in PI3K $\alpha$  dominant negative hearts: investigating the role of alternate PI3K isoforms, increased glucose oxidation and MAPK signaling, *Journal of molecular and cellular cardiology* 54 (2013) 9-18.
- [6] K.C. Yang, Y.T. Tseng, J.M. Nerbonne, Exercise training and PI3K $\alpha$ -induced electrical remodeling is independent of cellular hypertrophy and Akt signaling, *Journal of molecular and cellular cardiology* 53(4) (2012) 532-41.
- [7] P. Liu, H. Cheng, T.M. Roberts, J.J. Zhao, Targeting the phosphoinositide 3-kinase pathway in cancer, *Nature reviews. Drug discovery* 8(8) (2009) 627-44.
- [8] X. Huang, G. Liu, J. Guo, Z. Su, The PI3K/AKT pathway in obesity and type 2 diabetes, *International journal of biological sciences* 14(11) (2018) 1483-1496.
- [9] V.B. Patel, P. Zhabyeyev, X. Chen, F. Wang, M. Paul, D. ~~Fan, B.A. McLean, R. Basu, P. Zhang, S. Shah, J.F. Dawson, W.G. Pyle, M. Hazra, Z. Kassiri, S. Hazra, B. Vanhaesebroeck, C.A. McCulloch, G.Y. Oudit, Fan, et al.~~ PI3K $\alpha$ -regulated gelsolin activity is a critical determinant of cardiac cytoskeletal remodeling and heart disease, ~~Nat Commun~~[Nature communications](#) 9(1) (2018) 5390.
- [10] R.R. Madsen, B. Vanhaesebroeck, R.K. Semple, Cancer-Associated PIK3CA Mutations in Overgrowth Disorders, *Trends in molecular medicine* 24(10) (2018) 856-870.

- [11] C. Sadasivan, P. Zhabyeyev, D. Labib, J.A. White, D.I. Paterson, G.Y. Oudit, Cardiovascular toxicity of PI3K $\alpha$  inhibitors, [Clinical science Clin Sci \(Lond\)](#) 134(19) (2020) 2595-2622.
- [12] C. Fritsch, A. Huang, C. Chatenay-Rivauday, C. Schnell, A. Reddy, M. [Liu, A. Kauffmann, D. Guthy, D. Erdmann, A. De Pover, P. Furet, H. Gao, S. Ferretti, Y. Wang, J. Trappe, S.M. Brachmann, S.M. Maira, C. Wilson, M. Boehm, C. Garcia-Echeverria, P. Chene, M. Wiesmann, R. Cozens, J. Lehar, R. Schlegel, G. Caravatti, F. Hofmann, W.R. Sellers, Liu, et al.](#), Characterization of the novel and specific PI3K $\alpha$  inhibitor NVP-BYL719 and development of the patient stratification strategy for clinical trials, [Mol Cancer TherMolecular cancer therapeutics](#) 13(5) (2014) 1117-29.
- [13] A. Mizrahi, Y. Shamay, J. Shah, S. Brook, J. Soong, V.K. Rajasekhar, [J.L. Humm, J.H. Healey, S.N. Powell, J. Baselga, D.A. Heller, A. Haimovitz-Friedman, M. Scaltriti, et al.](#), Tumour-specific PI3K inhibition via nanoparticle-targeted delivery in head and neck squamous cell carcinoma, *Nature communications* 8 (2017) 14292.
- [14] D. Juric, J. Rodon, J. Tabernero, F. Janku, H.A. Burris, J.H.M. Schellens, [M.R. Middleton, J. Berlin, M. Schuler, M. Gil-Martin, H.S. Rugo, R. Seggewiss-Bernhardt, A. Huang, D. Bootle, D. Demanase, L. Blumenstein, C. Coughlin, C. Quadl, J. Baselga, et al.](#), Phosphatidylinositol 3-Kinase  $\alpha$ -Selective Inhibition With Alpelisib (BYL719) in PIK3CA-Altered Solid Tumors: Results From the First-in-Human Study, *Journal of clinical oncology : official journal of the American Society of Clinical Oncology* 36(13) (2018) 1291-1299.
- [15] F. Andre, E. Ciruelos, G. Rubovszky, M. Campone, S. Loibl, H.S. Rugo, [H. Iwata, P. Conte, I.A. Mayer, B. Kaufman, T. Yamashita, Y.S. Lu, K. Inoue, M. Takahashi, Z. Papai, A.S. Longin, D. Mills, C. Wilke, S. Hirawat, D. Juric, et al.](#), Alpelisib for PIK3CA-Mutated, Hormone Receptor-Positive Advanced Breast Cancer, *The New England journal of medicine* 380(20) (2019) 1929-1940.

- [16] Q. Venot, T. Blanc, S.H. Rabia, L. Berteloot, S. Ladraa, J.P. Duong, ~~E. Blanc, S.C. Johnson, C. Huguin, O. Boccara, S. Sarnacki, N. Boddaert, S. Pannier, F. Martinez, S. Magassa, J. Yamaguchi, B. Knebelmann, P. Merville, N. Grenier, D. Joly, V. Cormier-Daire, C. Michot, C. Bole-Feysot, A. Picard, V. Soupre, S. Lyonnet, J. Sadoine, L. Slimani, C. Chaussain, C. Laroche-Raynaud, L. Guibaud, C. Broissand, J. Amiel, C. Legendre, F. Terzi, G. Canaud, et al.~~, Targeted therapy in patients with PIK3CA-related overgrowth syndrome, *Nature* 558(7711) (2018) 540-546.
- [17] G.B.D. ~~Diseases, C. Injuries, D. Collaborators~~, ~~Global burden of 369 diseases, regional, and injuries in 204 countries and territories, 1990-2019 national age-sex specific mortality for 264 causes of death, 1980-2016~~: a systematic analysis for the Global Burden of Disease Study 2019 ~~2016~~, *Lancet* ~~396(10258) (2020) 1204-1222~~ (London, England) ~~390(10100) (2017) 1151-1210~~.
- [18] S.D. Prabhu, N.G. Frangogiannis, The Biological Basis for Cardiac Repair After Myocardial Infarction: From Inflammation to Fibrosis, *Circ Res* 119(1) (2016) 91-112.
- [19] J.R. McMullen, T. Shioi, L. Zhang, O. Tarnavski, M.C. Sherwood, P.M. Kang, ~~S. Izumo, et al.~~, Phosphoinositide 3-kinase(p110 $\alpha$ ) plays a critical role for the induction of physiological, but not pathological, cardiac hypertrophy, *Proceedings of the National Academy of Sciences of the United States of America* 100(21) (2003) 12355-60.
- [20] P. Zhabyeyev, B. McLean, X. Chen, B. Vanhaesebroeck, G.Y. Oudit, Inhibition of PI3Kinase- $\alpha$  is pro-arrhythmic and associated with enhanced late Na(+) current, contractility, and Ca(2+) release in murine hearts, *Journal of molecular and cellular cardiology* 132 (2019) 98-109.
- [21] M.A. Crackower, G.Y. Oudit, I. Kozieradzki, R. Sarao, H. Sun, T. Sasaki, ~~E. Hirsch, A. Suzuki, T. Shioi, J. Irie Sasaki, R. Sah, H.Y. Cheng, V.O. Rybin, G. Lembo, L. Fratta, A.J. Oliveira dos Santos, J.L. Benovic, C.R. Kahn, S. Izumo, S.F. Steinberg, M.P. Wymann, P.H.~~

- [Backx, J.M. Penninger, et al.](#), Regulation of myocardial contractility and cell size by distinct PI3K-PTEN signaling pathways, *Cell* 110(6) (2002) 737-49.
- [22] U. Campia, J.J. Moslehi, L. Amiri-Kordestani, A. Barac, J.A. Beckman, D.D. Chism, [P. Cohen, J.D. Groarke, J. Herrmann, C.M. Reilly, N.L. Weintraub, et al.](#), Cardio-Oncology: Vascular and Metabolic Perspectives: A Scientific Statement From the American Heart Association, *Circulation* 139(13) (2019) e579-e602.
- [23] C.G. Lenneman, D.B. Sawyer, Cardio-Oncology: An Update on Cardiotoxicity of Cancer-Related Treatment, [Circulation research](#)*Circ Res* 118(6) (2016) 1008-20.
- [24] M. Shen, M. Hu, P.W.M. Fedak, G.Y. Oudit, Z. Kassiri, Cell-Specific Functions of ADAM17 Regulate the Progression of Thoracic Aortic Aneurysm, [Circulation research](#)*Circ Res* 123(3) (2018) 372-388.
- [25] X. Chen, P. Zhabyeyev, A.K. Azad, W. Wang, R.A. Minerath, J. DesAulniers, [C.E. Grueter, A.G. Murray, Z. Kassiri, B. Vanhaesebrouck, G.Y. Oudit, et al.](#), Endothelial and cardiomyocyte PI3K $\beta$  divergently regulate cardiac remodelling in response to ischaemic injury, *Cardiovascular research* 115(8) (2019) 1343-1356.
- [26] E. Castellano, C. Sheridan, M.Z. Thin, E. Nye, B. Spencer-Dene, M.E. Diefenbacher, [G. Moore, M.S. Kumar, M.M. Murillo, E. Gronroos, F. Lassailly, G. Stamp, J. Downward, et al.](#), Requirement for interaction of PI3-kinase p110 $\alpha$  with RAS in lung tumor maintenance, *Cancer cell* 24(5) (2013) 617-30.
- [27] B. Gobin, M.B. Huin, F. Lamoureux, B. Ory, C. Charrier, R. Lanel, [S. Battaglia, F. Redini, F. Lezot, F. Blanchard, D. Heymann, et al.](#), BYL719, a new  $\alpha$ -specific PI3K inhibitor: single administration and in combination with conventional chemotherapy for the treatment of osteosarcoma, *International journal of cancer* 136(4) (2015) 784-96.
- [28] M. Elkabets, E. Pazarentzos, D. Juric, Q. Sheng, R.A. Pelossof, S. [Brook, A.O. Benzaken, J. Redon, N. Morse, J.J. Yan, M. Liu, R. Das, Y. Chen, A. Tam, H. Wang, J. Liang, J.M. Gorski, D.A. Kerr, R. Rosell, C. Teixido, A. Huang, R.A. Gosssein, N. Rosen, T.G. Bivona, M. Scaltriti,](#)



~~J. Baselga, Brook, et al.~~, AXL mediates resistance to PI3K $\alpha$  inhibition by activating the EGFR/PKC/mTOR axis in head and neck and esophageal squamous cell carcinomas, *Cancer cell* 27(4) (2015) 533-46.

[29] W. Wang, S.M. McKinnie, V.B. Patel, G. Haddad, Z. Wang, P. ~~Zhabyeyev, S.K. Das, R. Basu, B. McLean, V. Kandalam, J.M. Penninger, Z. Kassiri, J.C. Vederas, A.G. Murray, G.Y. Oudit, Zhabyeyev, et al.~~, Loss of Apelin exacerbates myocardial infarction adverse remodeling and ischemia-reperfusion injury: therapeutic potential of synthetic Apelin analogues, *Journal of the American Heart Association* 2(4) (2013) e000249.

[30] M. Litvinukova, C. Talavera-Lopez, H. Maatz, D. Reichart, C.L. Worth, E.L. Lindberg, ~~M. Kanda, K. Polanski, M. Heinig, M. Lee, E.R. Nadolmann, K. Roberts, L. Tuck, E.S. Fasouli, D.M. DeLaughter, B. McDonough, H. Wakimoto, J.M. Gorham, S. Samari, K.T. Mahbubani, K. Saeb-Parsy, G. Patone, J.J. Boyle, H. Zhang, H. Zhang, A. Viveiros, G.Y. Oudit, O. Bayraktar, J.G. Seidman, C.E. Seidman, M. Nosedá, N. Hubner, S.A. Teichmann, et al.~~, Cells of the adult human heart, *Nature* doi: 10.1038/s41586-020-2797-4. (2020).

[31] B.A. McLean, V.B. Patel, P. Zhabyeyev, X. Chen, R. Basu, F. Wang, et al., PI3K $\alpha$  Pathway Inhibition With Doxorubicin Treatment Results in Distinct Biventricular Atrophy and Remodeling With Right Ventricular Dysfunction, *Journal of the American Heart Association* 8(9) (2019) e010961.

[32] D.D. Hall, J.M. Ponce, B. Chen, K.M. Spitler, A. Alexia, G.Y. Oudit, ~~L.S. Song, C.E. Grueter, et al.~~, Ectopic expression of Cdk8 induces eccentric hypertrophy and heart failure, *JCI insight* 2(15) (2017) e92476.

[33] J. Guillemet-Guibert, K. Bjorklof, A. Salpekar, C. Gonella, F. Ramadani, A. Bilancio, ~~S. Meek, A.J. Smith, K. Okkenhaug, B. Vanhaesebroeck, et al.~~, The p110 $\beta$ p110beta isoform of phosphoinositide 3-kinase signals downstream of G protein-coupled receptors and is functionally redundant with p110 $\gamma$ p110gamma, *Proceedings of the National Academy of Sciences of the United States of America* 105(24) (2008) 8292-7.

- [3334] W. Wang, M. Shen, C. Fischer, R. Basu, S. Hazra, P. Couvineau, ~~M. Paul, F. Wang, S. Toth, D.S. Mix, M. Peglitsch, N.P. Gerard, M. Bouvier, J.C. Vederas, J.M. Penninger, Z. Kassiri, G.Y. Oudit, et al.~~, Apelin protects against abdominal aortic aneurysm and the therapeutic role of neutral endopeptidase resistant apelin analogs, *Proceedings of the National Academy of Sciences of the United States of America* 116(26) (2019) 13006-13015.
- [3435] C.W. Duarte, V. Lindner, S.A. Francis, D. Schoormans, Visualization of Cancer and Cardiovascular Disease Co-Occurrence With Network Methods, *JCO clinical cancer informatics* 1 (2017) 1-12.
- [3536] L. Vincent, D. Leedy, S.C. Masri, R.K. Cheng, Cardiovascular Disease and Cancer: Is There Increasing Overlap?, *Current oncology reports* 21(6) (2019) 47.
- [3637] B. Zoller, J. Ji, J. Sundquist, K. Sundquist, Risk of coronary heart disease in patients with cancer: a nationwide follow-up study from Sweden, *European journal of cancer (Oxford, England : 1990)* 48(1) (2012) 121-8.
- [3738] T. Hasin, Y. Gerber, S.A. Weston, R. Jiang, J.M. Killian, S.M. Manemann, ~~J.R. Gerhan, V.L. Roger, et al.~~, Heart Failure After Myocardial Infarction Is Associated With Increased Risk of Cancer, *Journal of the American College of Cardiology* 68(3) (2016) 265-271.
- [3839] R.J. Koene, A.E. Prizment, A. Blaes, S.H. Konety, Shared Risk Factors in Cardiovascular Disease and Cancer, *Circulation* 133(11) (2016) 1104-14.
- [3940] W.C. Meijers, M. Maglione, S.J.L. Bakker, R. Oberhuber, L.M. Kieneker, S. de Jong, ~~B.J. Haubner, W.B. Nagengast, A.R. Lyon, B. van der Vegt, D.J. van Veldhuisen, B.D. Westenbrink, P. van der Meer, H.H.W. Sillje, R.A. de Boer, et al.~~, Heart Failure Stimulates Tumor Growth by Circulating Factors, *Circulation* 138(7) (2018) 678-691.
- [4041] I.A. Mayer, A. Prat, D. Egle, S. Blau, J.A.P. Fidalgo, M. Gnant, ~~P.A. Fasching, M. Colleoni, A.C. Wolff, E.P. Winer, C.F. Singer, S. Hurvitz, L.G. Estevez, P.A. van Dam, S. Kummel, C. Mundhenke, F. Holmes, N. Babbar, L. Charbonnier, I. Diaz-Padilla, F.D. Vogl, D. Sellami, C.L. Arteaga, et al.~~, A Phase II Randomized Study of Neoadjuvant Letrozole Plus

Chen X *et al.*

PI3K $\alpha$  inhibition worsens heart disease

Alpelisib for Hormone Receptor-Positive, Human Epidermal Growth Factor Receptor 2-Negative Breast Cancer (NEO-ORB), *Clinical cancer research : an official journal of the American Association for Cancer Research* 25(10) (2019) 2975-2987.

[442] D. Juric, F. Janku, J. Rodon, H.A. Burris, I.A. Mayer, M. Schuler, ~~R. Seggewiss-Bernhardt, M. Gil Martin, M.R. Middleton, J. Baselga, D. Bootle, D. Demanse, L. Blumenstein, K. Schumacher, A. Huang, C. Quadt, H.S. Rugo, et al.~~, Alpelisib Plus Fulvestrant in PIK3CA-Altered and PIK3CA-Wild-Type Estrogen Receptor-Positive Advanced Breast Cancer: A Phase 1b Clinical Trial, *JAMA oncology* ~~(20185(2) (2019) e184475.~~

~~[42][43] P. Srikanthan, T.B. Horwich, C.H. Tseng, Relation of Muscle Mass and Fat Mass to Cardiovascular Disease Mortality, *The American journal of cardiology* 117(9) (2016) 1355-60.~~

[43] B.A. McLean, V.B. Patel, P. Zhabyeyev, X. Chen, R. Basu, F. Wang, S. Shah, B. Vanhaesebroeck, G.Y. Oudit, PI3K $\alpha$  Pathway Inhibition With Doxorubicin Treatment Results in Distinct Biventricular Atrophy and Remodeling With Right Ventricular Dysfunction, *Journal of the American Heart Association* 8(9) (2019) e010961.

[44] A. Esposito, G. Viale, G. Curigliano, Safety, Tolerability, and Management of Toxic Effects of Phosphatidylinositol 3-Kinase Inhibitor Treatment in Patients With Cancer: A Review, *JAMA oncology* (2019).

[44] Y. Ando, S. Iwasa, S. Takahashi, H. Saka, T. Kakizume, K. Natsume, et al., Phase I study of alpelisib (BYL719), an alpha-specific PI3K inhibitor, in Japanese patients with advanced solid tumors, *Cancer Sci* 110(3) (2019) 1021-1031.

[45] P. Srikanthan, T.B. Horwich, C.H. Tseng, Relation of Muscle Mass and Fat Mass to Cardiovascular Disease Mortality, *The American journal of cardiology* 117(8) (2016) 1355-60.

[4546] J.B. Nielsen, C. Graff, P.V. Rasmussen, A. Pietersen, B. Lind, M.S. Olesen, ~~J.J. Struijk, S. Haunso, J.H. Svendsen, L. Køber, T.A. Gørdes, A.G. Holst, et al.~~, Risk prediction of cardiovascular death based on the QTc interval: evaluating age and gender differences in a large primary care population, *European heart journal* 35(20) (2014) 1335-44.

[4647] T. Biering-Sorensen, S.R. Biering-Sorensen, F.J. Olsen, M. Sengelov, P.G. Jorgensen, R. Mogelvang, ~~A.M. Shah, J.S. Jensen, et al.~~, Global Longitudinal Strain by Echocardiography Predicts Long-Term Risk of Cardiovascular Morbidity and Mortality in a Low-Risk General Population: The Copenhagen City Heart Study, *Circulation. Cardiovascular imaging* 10(3) (2017).

[4748] C.J. Richards, Y. Je, F.A. Schutz, D.Y. Heng, S.M. Dallabrida, J.J. Moslehi, ~~T.K. Choueiri, et al.~~, Incidence and risk of congestive heart failure in patients with renal and nonrenal cell carcinoma treated with sunitinib, *Journal of clinical oncology : official journal of the American Society of Clinical Oncology* 29(25) (2011) 3450-6.

[4849] J. Li, P.Y. Wang, N.A. Long, J. Zhuang, D.A. Springer, J. Zou, ~~Y. Lin, C.K.E. Block, J.H. Park, J.G. Kang, P.M. Hwang, et al.~~, p53 prevents doxorubicin cardiotoxicity independently of its prototypical tumor suppressor activities, *Proceedings of the National Academy of Sciences of the United States of America* 116(39) (2019) 19626-19634.

[4950] S.P. Jones, J.J. Greer, R. van Haperen, D.J. Duncker, R. de Crom, D.J. Lefer, Endothelial nitric oxide synthase overexpression attenuates congestive heart failure in mice, *Proceedings of the National Academy of Sciences of the United States of America* 100(8) (2003) 4891-6.

[5051] L. Chen, Y. Zhang, L. Tao, Z. Yang, L. Wang, Mesenchymal Stem Cells with eNOS Over-Expression Enhance Cardiac Repair in Rats with Myocardial Infarction, *Cardiovasc Drugs Ther* 31(1) (2017) 9-18.

[5452] K.C. Yang, P.Y. Jay, J.R. McMullen, J.M. Nerbonne, Enhanced cardiac PI3K $\alpha$  signalling mitigates arrhythmogenic electrical remodelling in pathological hypertrophy and heart failure, *Cardiovascular research* 93(2) (2012) 252-62.

**Figure Legends**

**Figure 1. Systemic effects and changes in the transcriptome with BYL719 treatment.** **A.** Schematic of experimental design for 10-day BYL719 administration in WT mice. **B.** Time course of body weight changes during BYL treatment (left: n=10-11 mice/group) and body weight after 10-day treatment with vehicle or BYL719 (right: n=17-18 mice/group). **C.** Blood glucose level in mice treated with vehicle or BYL719 (n=9-13 mice/group) at 3 and 10 days. **D.** Alteration of body composition in mice after 10-day treatment with vehicle or BYL719 (n=9 mice/group). **E.** Heart weight and left ventricular weight in mice after 10-day treatment with vehicle or BYL719 (n=16 mice/group). **F.** Representative M-mode images, ejection fraction (EF) (n=10 mice/group), and left ventricular longitudinal strain analysis (n=7 mice/group) in mice after 10-day treatment with vehicle or BYL719. **G.** QTc interval in mice treated with BYL719 on Day 0 (before administration), Day 3, and Day 10 (n=11 mice). **H.** Volcano plot of gene expression changes due 10-day treatment with BYL719. Blue symbols: altered genes defined by the boundary conditions ( $p < 0.1$  and expression levels for WT-vehicle or WT-BYL of at least 1% of maximal expression level, 75,000 TPM). Grey symbols: genes that did not satisfy boundary conditions. **I.** Over-representation analysis of upregulated genes within KEGG (Kyoto Encyclopedia of Genes and Genomes) pathways displayed as an enrichment ratio (x axis). **J.** Over-representation analysis of downregulated genes within KEGG pathways displayed as an enrichment ratio (X-axis). Data are presented as mean $\pm$ SEM; statistical significance is calculated using repeated measures ANOVA with pairwise test in B and G; independent t-test in B, D, E, and F; one-way ANOVA in C. \* $p < 0.05$  vs WT-Vehicle

group in B and D-F, vs fasting in C, and vs day 0 in F; # $p < 0.05$  vs WT-Vehicle (1 h post treatment) in C.

**Figure 2. Alterations in PI3K $\alpha$  pathway in human and murine hearts post MI and the effect of BYL719 on post-MI mortality and cardiac function.** **A.** Protein levels of p110 $\alpha$  and phosphorylation levels of Akt in control (non-failing control (NFC) or Sham) and post-MI hearts (n=4-5 hearts/group). **B.** Schematic of experimental design for testing the effect of BYL719 treatment on post-MI remodeling. **C.** Kaplan-Meier survival curve (left) and distribution of causes of death (right) in post-MI mice treated with vehicle or BYL719 (n=26 mice/group) ( $p=0.065$ ). **D.** Echocardiographic assessment of cardiac function at 7 days post MI: representative M-mode images, left ventricular ejection fraction (EF), right ventricular fractional area change (FAC), left ventricular end-systolic volume (LVESV), left ventricular end-diastolic volume (LVEDV), and wall motion score index (WMSI) in mice treated with vehicle or BYL719 (n=10-14 mice/group). Data are presented as mean $\pm$ SEM; statistical significance is calculated using one-way ANOVA in A, log-rank test and fisher exact test in C, and two-way ANOVA with pairwise test in D; \* $p < 0.05$  vs NFC or sham, # $p < 0.05$  vs WT-Vehicle 7-day MI.

**Figure 3. BYL719 and post-MI ventricular remodeling.** **A.** Apoptosis: terminal deoxynucleotidyl transferase-mediated dUTP nick-end labeling (TUNEL, green) and DAPI (blue) staining of the sections of 1-day post-MI hearts; representative images (left) and quantification (right, n=5 hearts/group). **B.** Inflammation: immunofluorescence staining for neutrophils (anti-Ly6B, red; top: representative images, left, and

quantification, right) and macrophages (anti-CD68, red; bottom: representative images, left, and quantification, right); DAPI (blue); n=5 hearts/group. **C.** Cellular hypertrophy: wheat germ agglutinin (WGA) staining (green) to outline cardiomyocyte; DAPI (blue); representative images (left) and quantification (right, n=5 hearts/ group). **D.** Vascularization: endothelial cell immunofluorescence staining (anti-CD31, red); DAPI (blue); representative images (left) and quantification (right, n=5 hearts/group). **E.** Western blots and quantifications of phosphorylation levels of Akt-T308, GSK3 $\beta$ -S9, and eNOS-S1177 in left ventricular lysates (n=4-5 hearts/group). Data are presented as mean $\pm$ SEM; statistical significance is calculated using two-way ANOVA with pairwise comparison in A, C, and D, independent t-test in B, and one-way ANOVA in E; \*p<0.05 vs sham, #p<0.05 vs WT-Vehicle MI.

**Figure 4. Endothelial PI3K $\alpha$  is required for preservation of cardiac function and angiogenesis after MI.** **A.** Schematic of experimental design for testing the role of endothelial PI3K $\alpha$  in post-MI remodeling using conditional knock-out (p110 $\alpha^{EC}$ ) and control (p110 $\alpha^{flx/flx}$  littermates) mice. **B.** Echocardiographic assessment of cardiac function at 7 days post MI: representative M-mode images, ejection fraction (EF), left ventricular end-systolic volume (LVESV), left ventricular end-diastolic volume (LVEDV), and wall motion score index (WMSI) (n=10 mice/group). **C.** Endothelial apoptosis: immunofluorescence staining of endothelial cells (ECs) (CD31, red), TUNEL (green), and DAPI (blue): representative images (left, white arrows indicate red-green co-localization) and quantification (right, n=5 hearts/group). **D.** Endothelial proliferation: immunofluorescence staining for ECs (CD31, green), immunofluorescence staining of

proliferating ECs (Ki67, red), and DAPI (blue): representative images (left, white arrows indicate red-green co-localization) and quantification (right, n=5 hearts/group). **E.** Vascularization: immunofluorescence staining of ECs (CD31, red; top), lectin (green; middle) *in vivo* perfusion, and quantifications (bottom, n = 5 hearts/group). **F.** Western blots and quantification of Akt phosphorylation in 7-day post-MI hearts (n=4-7 hearts/group). Data are presented as mean $\pm$ SEM; statistical significance is calculated using two-way ANOVA with pairwise comparisons in B-E, and independent t-test in F; \*p<0.05 vs sham in B and E, vs infarct in C and D, vs indicated group in F, #p<0.05 vs p110 $\alpha^{flx/flx}$  within the same treatment.

**Figure 5. PI3K $\alpha$  activity is required to maintain Akt/eNOS signaling in endothelial**

**cells.** **A.** Inhibition of PI3K $\alpha$  by BYL719 and Akt/eNOS signaling in cultured human umbilical vein endothelial cells (HUVEC) (no VEGF; n=3 independent experiments). **B.** Effect of inhibition of PI3K $\alpha$  by BYL719 on vascular endothelial growth factor (VEGF)-induced Akt/eNOS activation in HUVEC (n=3 independent experiments). **C.** Inhibition of PI3K $\alpha$  by BYL719 and Akt/eNOS signaling in human coronary artery endothelial cells (HCAEC) (no VEGF, n=4 independent experiments). **D.** Effect of inhibition of PI3K $\alpha$  by BYL719 on VEGF-stimulated Akt/eNOS signaling in HCAEC (n=4 independent experiments). Data are presented as mean $\pm$ SEM; statistical significance is calculated using one-way ANOVA; \*p<0.05 vs vehicle without VEGF, #p<0.05 vs vehicle with VEGF.

**Figure 6. PI3K $\alpha$  activity is required for endothelial cell survival, proliferation, and**

**angiogenesis.** **A.** Effect of BYL719 (500 nmol/L) on cell survival of HUVEC: flow



cytometry images and quantification of staining with annexin V and propidium iodide (n=6 independent experiments). **B.** Effect of BYL719 (500 nmol/L) on proliferation rate of HUVEC: BrdU (red) and DAPI (blue) staining (n=8 independent experiments). **C.** Effects of BYL719 (500 nmol/L) on angiogenic sprouting in HUVEC (n=4 independent experiments). **D.** Effect of BYL719 (500 nmol/L) on cell survival of HCAEC: flow cytometry images and quantification of staining with annexin V and propidium iodide (n=5 independent experiments). **E.** Effects of BYL719 (500 nmol/L) on proliferation rate of HCAEC: BrdU (red) and DAPI (blue) staining (n=6 independent experiments). **F.** Effects of BYL719 (500 nmol/L) on angiogenic sprouting in HCAEC (n=4 independent experiments). Data are presented as mean $\pm$ SEM; statistical significance is calculated using independent t-test in A-C, one-way ANOVA in D-F; \*p<0.05 vs vehicle.

**Figure 7. Role of cardiomyocyte PI3K $\alpha$  at baseline and in post-MI cardiac remodeling.** **A.** Heart/body weight, heart weight, and left ventricular weight in cardiomyocyte-specific knockout (p110 $\alpha^{CM}$ ) and control (littermates, p110 $\alpha^{flx/flx}$ ) mice (n=9-14 mice/group). **B.** Echocardiographic assessment of cardiac function at 7 days post MI: representative M-mode images, left ventricular ejection fraction (EF), right ventricular fractional area change (FAC), left ventricular end-systolic volume (LVESV), and left ventricular end-diastolic volume (LVEDV) (n=10 mice/group). **C.** Kaplan-Meier survival analysis for survival rate (top) and cardiac rupture incidence (bottom) (n=13-30 mice/group). **D.** Apoptosis: TUNEL (green) and DAPI (blue) staining: representative images (left) and quantification (right, n=4 hearts/group). **E.** Cellular hypertrophy: WGA (green) staining to outline cardiomyocytes: representative images (left) and quantification

(right, n=5 hearts/group). **F.** Western blots and quantification for Akt in left ventricle lysates from post-MI p110 $\alpha^{\text{CM}}$  and p110 $\alpha^{\text{flx/flx}}$  hearts (n=4-5 hearts/group). Data are presented as mean $\pm$ SEM; statistical significance is calculated using independent t-test in A and F, two-way ANOVA with pairwise comparison in B, D, and E, and log-rank test in C; \*p<0.05 vs p110 $\alpha^{\text{flx/flx}}$  in A, C, and F, vs sham in B, D, and E, #p<0.05 vs p110 $\alpha^{\text{flx/flx}}$  MI.

**Figure 8. Effects BYL719 on isolated adult mouse cardiomyocytes under hypoxia and schematic of the roles of PI3K $\alpha$  in cardiomyocytes and endothelial cells at baseline and post MI.** **A.** Western blots and quantification of Akt/GSK3 $\beta$  signaling in lysates from cardiomyocytes cultured under normoxic and hypoxic condition (n=6 hearts, 3 independent experiments). **B.** Representative images (left) and quantification of apoptotic cell death (right) of isolated cardiomyocyte under hypoxic condition with cyclic mechanical stretch (right, n=8 hearts, 4 independent experiments). **C.** Representative images of F-actin (green), G-actin (red), and DAPI (blue) staining (left) and quantification of F/G-actin ratio (right, n=8 hearts, 4 independent experiments). **D.** Schematic of the roles of PI3K $\alpha$  in cardiomyocytes and endothelial cells at baseline and post-MI: in cardiomyocyte, PI3K $\alpha$  regulates survival and adaptive hypertrophy; in endothelial cells, PI3K $\alpha$  regulates survival and angiogenesis to maintain vascular distribution in response to MI. Data are presented as mean $\pm$ SEM; statistical significance is calculated using one-way ANOVA in A and B, two-way ANOVA with pairwise comparison in C; \*p<0.05 vs normoxia in A and C, vs vehicle in B, #p<0.05 vs hypoxia-vehicle in A and C.